CHARACTERISATION OF CARDIOMYOCYTE PLASTICITY AND THE ROLE OF FIBROBLASTS DURING ZEBRAFISH HEART REGENERATION

HÉCTOR SÁNCHEZ IRANZO

MADRID, 2018

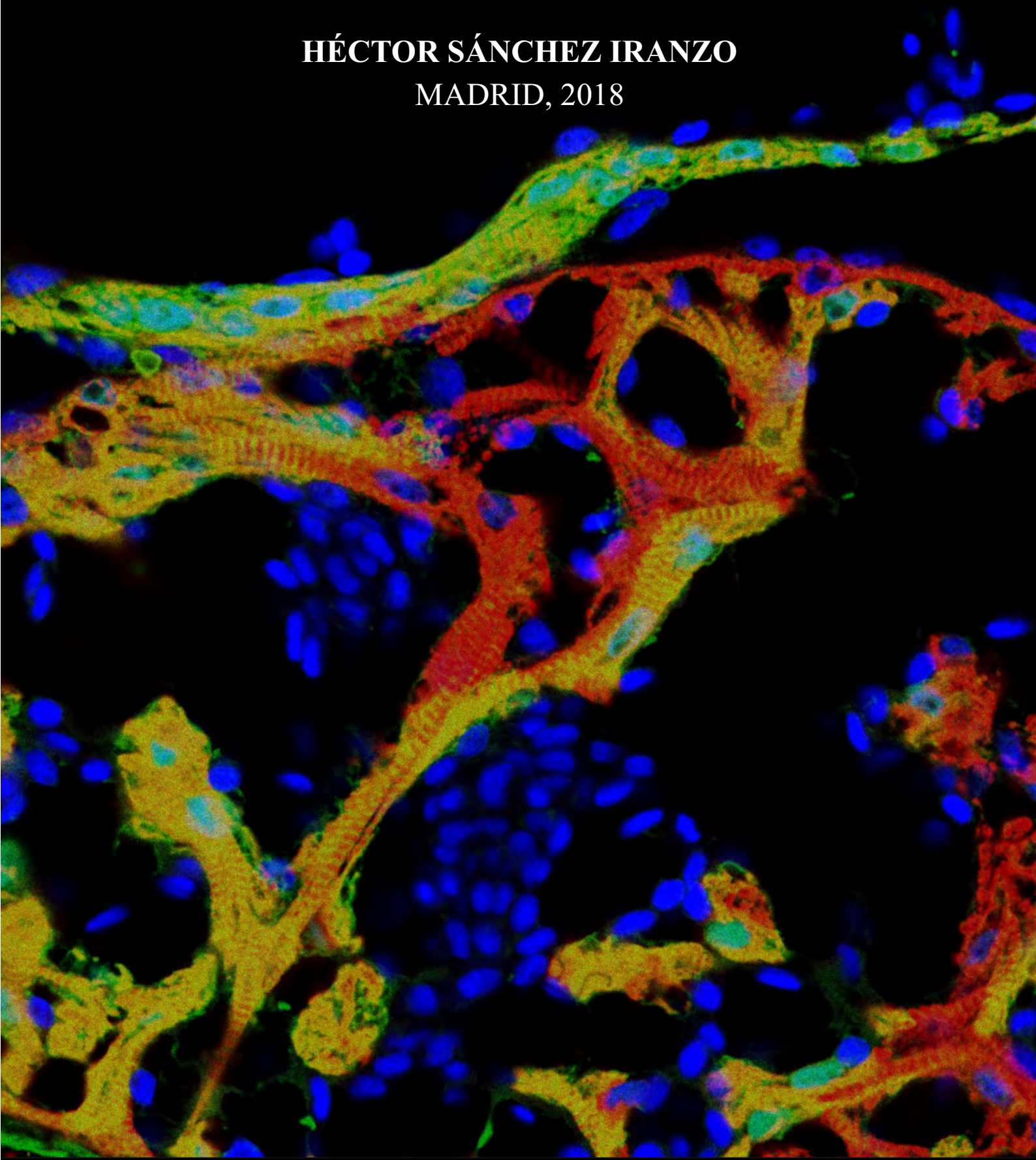

Universidad Autónoma de Madrid
Departamento de Biología Molecular

Universidad Autónoma de Madrid

Programa de Doctorado en Biociencias Moleculares

Tesis doctoral

Characterisation of cardiomyocyte plasticity and the role of fibroblasts during zebrafish heart regeneration

Héctor Sánchez Iranzo

Madrid 2018
Facultad de Ciencias

Universidad Autónoma de Madrid

Characterisation of cardiomyocyte plasticity and the role of fibroblasts during zebrafish heart regeneration

Doctorando:

Héctor Sánchez Iranzo
Licenciado en Farmacia y Bioquímica

Madrid 2018

Directora de Tesis:
Nadia Mercader Huber

Dr. **Nadia Mercader Huber**, Principal Investigator of the group "Epicardium Development and its Role in Regeneration" at the National Center for Cardiovascular Research (CNIC-ISCIII), warrants that this work was performed in her Laboratory and supports the defense of the thesis entitled:

"Characterisation of cardiomyocyte plasticity and the role of fibroblasts during zebrafish heart regeneration"

During this period Héctor Sánchez Iranzo was supported by a PhD Fellowhip FPU12/03007

Madrid, 25 de octubre de 2017

Nadia Mercader Huber

ABSTRACT

ABSTRACT

The zebrafish is an established model organism to study heart regeneration, in which pre-existing cardiomyocytes (CMs) proliferate to replace the lost myocardium. During development, mesodermal progenitors from the first heart field (FHF) form a primitive cardiac tube, to which cells from the second heart field (SHF) are added. Here we investigated whether FHF and SHF derivatives in the zebrafish give rise to distinct CM populations, and examined the degree of cell fate plasticity of SHF derivatives during heart regeneration. Using *tbx5a*-lineage tracing we found that the adult zebrafish heart is also composed of CM populations from the FHF and SHF. Furthermore, ablation of FHF-derived CMs in the embryo is compensated by expansion of SHF-derived cells. *tbx5a* lineage-tracing was also employed to investigate the fate of trabecular CMs during adult heart regeneration. While previous clonal analysis suggested that the different myocardial layers are rebuilt by CMs within each layers, we describe that trabecular CMs can switch their fate and differentiate into cortical myocardium. Heart regeneration is preceded by a fibrotic response. Thus, fibrosis and regeneration are not mutually exclusive responses. Upon cardiac cryoinjury, collagen and other extracellular matrix (ECM) components accumulate at the injury site. Unlike the situation in mammals, fibrosis in zebrafish is transient and its regression is concomitant with regrowth of the myocardial wall. We describe that during fibrosis regression, fibroblasts are not fully eliminated and become inactivated. Unexpectedly, limiting the fibrotic response by genetic ablation of *col1a2*-expressing cells not only failed to enhance regeneration but also impaired CMs proliferation. We conclude that zebrafish regeneration is a process that requires CM plasticity, and involves ECM-producing cells that become inactive and promote CMs proliferation.

RESUMEN

RESUMEN

El pez cebra es un organismo modelo ampliamente usado para estudiar la regeneración de corazón, en el que los cardiomiocitos preexistentes proliferan y reemplazan el miocardio perdido. Durante el desarrollo, los progenitores mesodérmicos del campo cardiaco primario forman un tubo cardiaco, al cual se añaden las células del campo cardiaco secundario. Aquí investigamos si los derivados de ambos campos en el pez dan lugar a distintas poblaciones de cardiomiocitos, y el grado de plasticidad durante la regeneración. El trazado de linaje de las células *tbx5a*-positivas también nos permitió investigar el destino de los cardiomiocitos durante la regeneración en adulto. Mientras que los análisis de trazado de linaje previos sugirieron que cada capa de cardiomiocitos es derivada de la misma capa, aquí describimos que los cardiomiocitos de las trabéculas pueden cambiar su especificación y diferenciarse en miocardio cortical. La regeneración del corazón está precedida de una respuesta fibrótica. Por lo tanto, fibrosis y regeneración no son respuestas mutuamente excluyentes. Tras una criolesión, colágeno y otras proteínas de matriz extracelular se acumulan en el lugar del daño. A diferencia de lo que ocurre en mamíferos, la fibrosis es una respuesta transitoria y simultánea a la regeneración de la nueva pared miocárdica. Aquí describimos que durante la regresión de la fibrosis, los fibroblastos no son completamente eliminados, sino que se inactivan. Sorprendentemente, limitar la respuesta fibrótica por ablación de las células que expresan *col1a2* no estimuló la regeneración, sino que disminuyó la proliferación de cardiomiocitos. Concluimos que la regeneración del corazón de pez cebra es un proceso en el que hay una gran plasticidad de cardiomiocitos, y las células que producen matriz extracelular y se inactivan, promueven la proliferación de cardiomiocitos.

INDEX

INDEX

ABBREVIATIONS

ABREVIATIONS

4-OHT: 4-hydroxy-tamoxifen

α-SMA: α Smooth Muscle Actin

Amp: Ampicillin resistance gene

AHF: Anterior Heart Field

BAC: Bacterial artificial chromosome

BDM: 2,3-Butanedione 2-monoxime

bmp2b: *bone morphogenetic protein 2b (*zebrafish gene)

bmp4: *bone morphogenetic protein 4* (zebrafish gene)

BrdU: Bromodeoxyuridine

cmlc2: *cardiac myosin light chain 2* (zebrafish gene, current official name *myl7*)

Col1a1: Collagen, type I, alpha 1 (zebrafish protein)

Col1a1: *Collagen, type I, alpha 1* (mouse gene)

col1a1a: *collagen, type I, alpha 1a* (zebrafish gene)

col1a1b: *collagen, type I, alpha 1b* (zebrafish gene)

col12a1a: *collagen, type XII, alpha 1a* (zebrafish gene)

CreER^{T2}: Cre Estrogen Receptor T2

ctgfa: *connective tissue growth factor a* (zebrafish gene)

DAPI: 4',6-diamidino-2-phenylindole

drl: *draculin* (zebrafish gene)

dpf: days post fertilisation

dpi: days post injury

DTA: Diphtheria toxin A

E: Embryonic day

ECM: Extracellular matrix

EMT: Epithelial to Mesenchymal Transition

EPDC: Epicardial derived cells.

FBS: Fetal bovine serum

Fgf: *Fibroblast growth factor* (mouse gene)

Fgf10: *Fibroblast growth factor 10* (mouse gene)

FHF: First Heart Field

fli1a: *Fli-1 proto-oncogene, ETS transcription factor a* (zebrafish gene)

fn1a: *fibronectin 1a* (zebrafish gene)

fpkm: fragments per kilobase of exon per million fragments mapped

FSP-1: Fibroblast specific protein 1 (mouse protein)

Fstl1: *Follistatin-like 1* (mouse gene)

FVS: Fractional volume shortening

Gata4: *GATA binding protein 4* (mouse gene)

GFP: Green Fluorescent Protein

hand2: *heart and neural crest derivatives expressed 2* (zebrafish gene)

hey2: *hes-related family bHLH transcription factor with YRPW motif 2* (zebrafish gene)

hhip: *hedgehog interacting protein* (zebrafish gene)

hpf: hours post fertilisation

igf1: *insulin-like growth factor 1* (zebrafish gene)

Isl1: *Islet 1* (mouse gene)

ISH: *in situ* hybridization

kdrl: *kinase insert domain receptor like* (zebrafish gene)

lama5: *laminin, alpha 5* (zebrafish gene)

loxl2b: *lysyl oxidase-like 2b* (zebrafish gene)

ltbp3: *lateng TGF-beta binding protein 3* (zebrafish gene)

Mef2c: *Myocyte enhancer factor 2c* (mouse gene)

Mesp1: *Mesoderm posterior 1* (mouse gene)

MHC: Myosin heavy chain

mmp2: matrix metallopeptidase 2 (zebrafish gene)

mmp11a: *matrix metallopeptidase 11a* (zebrafish gene)

mmp14a: *matrix metallopeptidase 14a* (zebrafish gene)

MI: Myocardial infarction

Mtz: Metronidazole

myl7: *myosin, light chain 7, regulatory* (zebrafish gene)

nppa: *natriuretic peptide A* (zebrafish gene)

NTR: Nitroreductase

PBS: Phosphate buffered saline

Postn: *Periostin* (mouse gene)

postnb: periostin b (zebrafish gene)

PFA: Paraformaldehyde

raldh2: *Aldehyde dehydrogenase 1 family, member A2* (*aldh1a2*, zebrafish gene)

rspo1: *R-spondin 1* (zebrafish gene)

Scn5a: *Sodium channel, voltage-gated, type V, alpha* (mouse gene)

Scn10a: *Sodium channel, voltage-gated, type X, alpha* (mouse gene)

PTU: N-Phenylthiourea

RNA-Seq: Ribonucleic acid sequencing

SHF: Second Heart Field

Tbx1: *T-box 1* (mouse gene)

Tcf21: *Transcription factor 21* (mouse gene)

tcf21: *transcription factor 21* (zebrafish gene)

tbx2b: *T-box 2b* (zebrafish gene)

Tbx5: *T-box 5* (mouse gene)

TBX5: T-box 5 (mouse protein)

tbx5a: *T-box 5a* (zebrafish gene)

tbx5b: *T-box 5b* (zebrafish gene)

tgf-β: *transforming growth factor, beta* (group of zebrafish genes)

TUNEL: Terminal deoxynucleotidyl transferase dUTP nick end labelling

ubb: *ubiquitin b* (zebrafish gene)

vcana: *versican a* (zebrafish gene)

wnt5a: *wingless-type MMTV integration site family, member 5A* (zebrafish gene)

wnt16: *wingless-type MMTV integration site family, member 16* (zebrafish gene)

wpf: weeks post fertilisation

wt1a: *wilms tumor 1a* (zebrafish gene)

wt1b: *wilms tumor 1b* (zebrafish gene)

INTRODUCTION

INTRODUCTION

I Mammalian and zebrafish heart development

I.1 Heart development and heart fields

The heart is the first organ to develop in the embryo. Its early function is essential to provide nutrients and to remove waste from cells when the embryo reaches a size that makes passive diffusion no longer efficient (Vincent and Buckingham, 2010).

In mouse and birds, precursor cells from the splanchnic mesoderm beneath the head folds form the cardiac crescent, which subsequently fuses at the midline to form the primitive cardiac tube. This “peristaltic pump”, rapidly begins to pump blood (Kirby, 2007; Lawson et al., 1991; Tam et al., 1997). Cells from the cardiac crescent express the transcription factor *Mesp1*, which is one of the first markers distinguishing cardiac progenitor cells from other mesodermal derivatives (Saga et al., 1999). These early progenitors are known as the First Heart Field (FHF), and mostly contribute to the myocardium of the left ventricle and parts of the atria. According to some studies, once the early heart tube is formed, there is limited proliferation, and its increase in size partly depends on addition of progenitor cells (Dyer and Kirby, 2009; Soufan et al., 2006; van den Berg et al., 2009).

Later, new progenitor cells are added to the early heart tube, constituting the Second Heart Field (SHF) which expand the anterior and posterior poles of the cardiac tube. Cells added at the anterior (arterial) pole express *Fgf8*, *Fgf10* (Kelly et al., 2001), *Tbx1* (Xu et al., 2004) and can be distinguished by the activity of a *Mef2c* enhancer (*Mef2c*-Anterior Heart Field) (Dodou et al., 2004).

A *mef2c-AHF-Cre* transgenic mouse line was used to lineage trace the anterior SHF derived cells, helping to identify that they give rise to endothelial and myocardial components of the outflow tract, right ventricle and ventricular septum (Verzi et al., 2005).

Cells from the SHF added at the posterior (venous pole) express *Isl1*. These cells contribute to parts of the atria and the atrio-ventricular canal (Cai et al., 2003; Galli et al., 2008).

In mammals, coincident with the addition of SHF progenitors, the cardiac tube loops, converting the original anterior-posterior polarity into the right-left polarity seen in the adult organism (Gilbert, 2010; Männer et al., 2010). At the end of the looping process, specialised cardiomyocyte (CM) called trabeculae grow towards the lumen of the ventricle, where they function to increase the surface area and boost nutrition and oxygen uptake, and providing more contractile force

(Lindsey et al., 2014; Samsa et al., 2013). Subsequently, the compact layer is formed and replaces the trabeculae as the providers of the main contractile force (Wessels and Sedmera, 2003). The atria and ventricle are septated to transform the heart into a four-chambered organ (van den Berg et al., 2009).

In the mature vertebrate heart, the myocardium is covered by the epicardium, the outermost cardiac epithelium that envelops the surface of the heart. During development, epicardial cells derive from the proepicardial organ, a cell cluster close to the venous pole of the heart tube (Männer et al., 2005; Virágh and Challice, 1981) expressing *Wt1* (Carmona et al., 2001), *Tbx18* (Haenig and Kispert, 2004; Tanaka and Tickle, 2004) and *Tcf21* (Robb et al., 1998). Epicardial-derived cells (EPDCs) give rise to smooth muscle of the coronary blood vessels and cardiac fibroblasts (Cai et al., 2008; Zhou et al., 2008).

In addition to mesodermal derivatives, the neural crest also contributes to the developing heart and large vessels. Neural crest-derived cells contributes to form the endothelium of the aortic arch arteries and to the septum between the aorta and the pulmonary artery (Waldo et al., 1998). They also participate in the formation of the valves and the conduction system (Gorza et al., 1988; Jain et al., 2011).

While there are good markers available for the SHF, specific FHF markers have remained elusive. A marker that has traditionally been used is *Tbx5*. It belongs to the T-box family, which was named after the founding member, T, encoding the transcription factor Brachyury (Herrmann et al., 1990). Whereas the expression of *Tbx5* is excluded from the derivatives of the anterior SHF, which give rise to the mammalian right ventricle (Devine et al., 2014), it is expressed in all the progenitors that will give rise to the atria, including posterior heart field derivatives (Bruneau et al., 1999). This evidence supports *Tbx5* as a good marker for FHF-derived ventricular CMs.

In contrast to the mammalian heart, the cardiac chambers in the zebrafish are not septated and its heart is instead formed by a single ventricle and a single atrium. Despite this simpler cardiac architecture, zebrafish hearts are formed in a manner similar to that of avian and mammalian hearts. A primordial heart tube is first formed from FHF-derived cells to which SHF derived cells are added. This was first discovered using double transgenic *myl7:EGFP;myl7:nucDsRed2* zebrafish, in which two different fluorescent proteins are expressed under the *myl7* specific promoter (de Pater et al., 2009). The assay was based on the different folding kinetics of the EGFP and nucDsRed2 fluorescent proteins. As the EGFP folds much faster than the nucDsRed2, the presence of $EGFP^{+}$/$nucDsRed2^{-}$ CMs indicated that they had recently differentiated. By this way, they identified the addition of new CMs to both the arterial and venous pole.

Some markers have been also identified for the zebrafish heart fields, including *latent tgf-β binding protein 3* (*ltbp3*) as a marker for the SHF (Zhou et al. 2011) and *draculin* (*drl*) for the

FHF (Mosimann et al., 2015). However, none of them have been studied in mammals, which impedes the direct comparison of the described zebrafish FHF and SHF to its mammalian counterparts. Importantly, when the SHF mammalian maker *Isl1* was used in the zebrafish model, it was found not to label the SHF, but instead labelled the precursors of the pacemaker (Tessadori et al., 2012).

I.2 Tbx5 function and expression pattern during heart development

The expression pattern of *Tbx5* is conserved across evolution. It is expressed in the neural retina of the developing eye and in the forelimb bud in mouse, chick, Xenopus and zebrafish (Chapman et al., 1996; Gibson-Brown et al., 1998; Horb and Thomsen, 1999; Pi-Roig et al., 2014; Showell et al., 2006).

In the mouse heart, *Tbx5* becomes abundantly expressed throughout the cardiac crescent around embryonic day (E) 8.0 (Bruneau et al., 1999). At E8.5 E9.0, when the heart undergoes looping, *Tbx5* is expressed in the entire future left ventricle. This pattern persists; by E11.5 very little expression is found in the right ventricle or outflow tract but significant expression is found in the left ventricle (Bruneau et al., 1999). During development of the mouse ventricular chambers, *Tbx5* expression becomes restricted to the trabeculae on the left side of the ventricular septum (Bruneau et al., 1999; Takeuchi et al., 2003). Suppression of this differential expression by overexpressing *Tbx5* in the precursors of both ventricular chambers or by deleting this gene, abrogates ventricular septum formation (Koshiba-Takeuchi et al., 2009), thus highlighting the importance of *Tbx5* for the development of a septated ventricle in mammalian hearts.

Mutations in the coding region or splice regulatory sequences of *Tbx5* were described to be the cause of 70% of Holt-Oram syndrome cases (Debeer et al., 2007; McDermott et al., 2005). Holt-Oram syndrome is an autosomal dominant disorder that affects 1 in 100,000-135,000 live births in European populations (Barisic et al., 2014) and is characterised by upper-limb and heart defects. Structural abnormalities of the heart can include secundum-type atrial septal defects, primum-type atrial septal defects, and/or ventricular septal defects. Conduction system defects manifest on electrocardiography as a long PR interval, atrio-ventricular block, bundle branch block, bradycardia, sick sinus syndrome, and atrial fibrillation (Basson et al., 1994; Holt and Oram, 1960; Newbury-Ecob et al., 1996). Interestingly, a homozygous single-base-pair mutation within a *cis*-regulatory element controlling TBX5 was recently identified in a patient, raising the possibility that some of the remaining 30% of Holt-Oram syndrome cases are caused by mutations in *cis*-regulatory elements (Smemo et al., 2012).

In mice, *Tbx5* is required for the regulation of the critical conduction system ion channels, *Gja5* (*Connexin 40*) *Scn5a* and *Scn10a*, and ablation of *Tbx5* from the adult ventricular conduction system results in loss of these ion channels and in an altered ventricular conduction system function (Arnolds et al., 2012; Bruneau et al., 2001; Moskowitz et al., 2004; van den Boogaard et al., 2012; van Weerd et al., 2014).

Furthermore, together with *Mef2c* and *Gata4*, *Tbx5* is one of the three cardiac transcription factors that are sufficient to directly reprogram fibroblasts to CMs (Ieda et al., 2010), illustrating its importance during CM development and maturation.

The teleost genome underwent a duplication event during fish evolution (Taylor et al., 2001; Wittbrodt et al., 1998). As a consequence, most of the mammalian genes that are conserved have two homologs in zebrafish, usually designated as "a" and "b". This is the case for *Tbx5*, which has two orthologs in zebrafish: *tbx5a* and *tbx5b*. While *tbx5a* reproduces the expression pattern described in mouse and chick embryos, *tbx5b* is expressed robustly only in eye and heart (Albalat et al., 2010; Parrie et al., 2013).

The classic *tbx5a* zebrafish *heartstrings* mutant was found during a screen for recessive lethal mutations affecting cardiac function. Zebrafish with this mutation do not develop pectoral fins and display heart looping and chamber maturation defects (Ahn et al., 2002; Garrity et al., 2002). Nonetheless, *tbx5b* knockdown does not result in patterning defects observed either in *tbx5a* mutants or after knockdown experiments. Moreover, known direct targets of mammalian TBX5 or zebrafish *tbx5a*, such as *bmp4*, *nppa*, *tbx2b* and *hey2* were not disrupted after *tbx5b* knockdown. The only defects observed in heart development upon *tbx5b* knockdown were the abnormal expansion of *hand2* and *vcana* (Parrie et al., 2013). Overall, these results suggest that while there is some functional redundancy between the two paralogs, *tbx5a* appears to play a dominant role during zebrafish heart development.

Despite its importance in human health and heart development, the expression pattern and dynamics of *tbx5a* during zebrafish development and regeneration have not been studied in detail.

I.3 Zebrafish cardiomyocyte subtypes and their developmental origin

The zebrafish heart initially develops as a cardiac tube in which there is a single layer of CMs lined with endocardium towards the lumen. This first myocardial layer is known as the primordial layer. At 3 days postfertilisation (dpf), some of these CMs delaminate to form the trabeculae (Gupta and Poss, 2012; Staudt et al., 2014). At later stages during development, around 8 weeks postfertilisation (wpf), the trabeculae breach the primordial layer and form the cortical layer covering the primordial layer (Gupta and Poss, 2012) (Fig. 1).

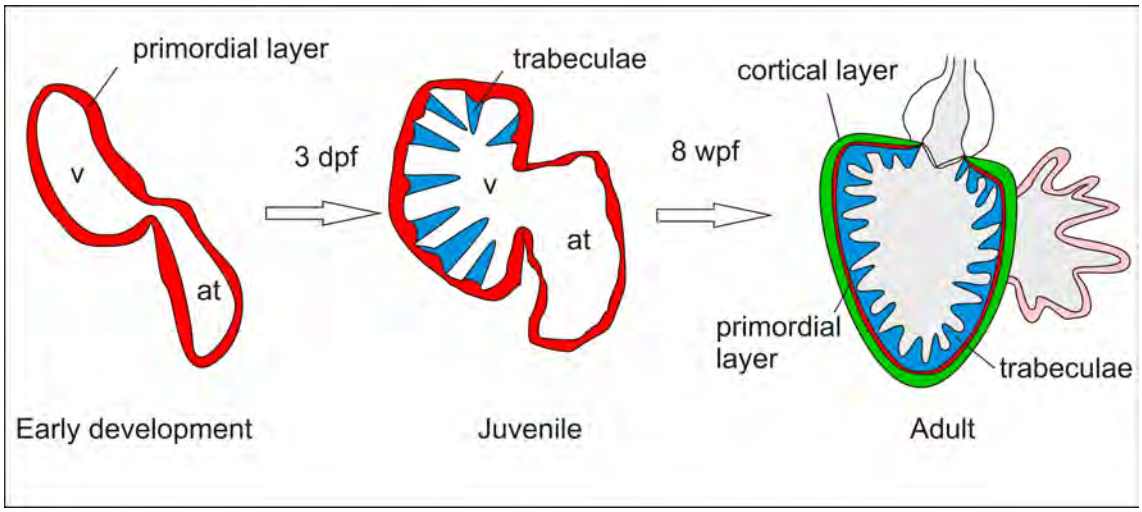

Figure 1. Cardiomyocyte subtypes in the zebrafish heart. The heart initially develops as a single layered tube. At 3 dpf, trabecular CMs delaminate from the primordial layer. At 8 wpf, the cortical layer is formed derived from the trabecular CMs. Red, primordial layer; Blue, trabeculae; Green, cortical layer.

II Zebrafish heart regeneration

Cardiovascular diseases are the major cause of death in humans (Benjamin et al., 2017; Bui et al., 2011). The most common presentation of them is myocardial infarction (MI), in which part of the heart is damaged by a lack of oxygen (ischemia). As the capacity for CM proliferation is very low in mammals (Bergmann et al., 2009; Bergmann et al., 2015; Senyo et al., 2013), the injured myocardium cannot be recovered, and in the long term, this can lead to heart failure.

Contrary to what is observed in mammals, some vertebrates including zebrafish have the capacity to regenerate their heart upon injury (Poss et al., 2002). Clearly, from a translational perspective, it is very important to determine the fate of different cell types during this process, and to develop different injury models to examine this repair mechanism.

II.1 The Cre-lox system to analyse lineage tracing

One of the best ways to trace the fate of cells is the Cre-lox system. The Cre enzyme is a recombinase derived from the P1 bacteriophage that specifically recognises loxP sites (Abremski and Hoess, 1984). When two loxP sites are present in the same linear DNA molecule, Cre binds the two sites together and excises the sequence between them, which leads to the re-ligation of the flanking ends. As this causes a change in the DNA sequence of the cell, it will be permanent and transmitted to the progeny of those cells. Spatial specificity can be achieved by expressing the Cre enzyme under a tissue specific promoter. This system has been complemented by fusing

the Cre enzyme to an ER^{T2} domain that drives the translocation of the Cre enzyme to the nucleus upon 4-hydroxy-tamoxifen (4-OHT) administration. This elegant system provides a method to activate and temporally control the recombination process (Feil et al., 1997).

The Cre system will be used during this thesis to permanently label cells with fluorescent proteins in order to follow its fate (Mosimann et al., 2011) (Fig. 2 A).

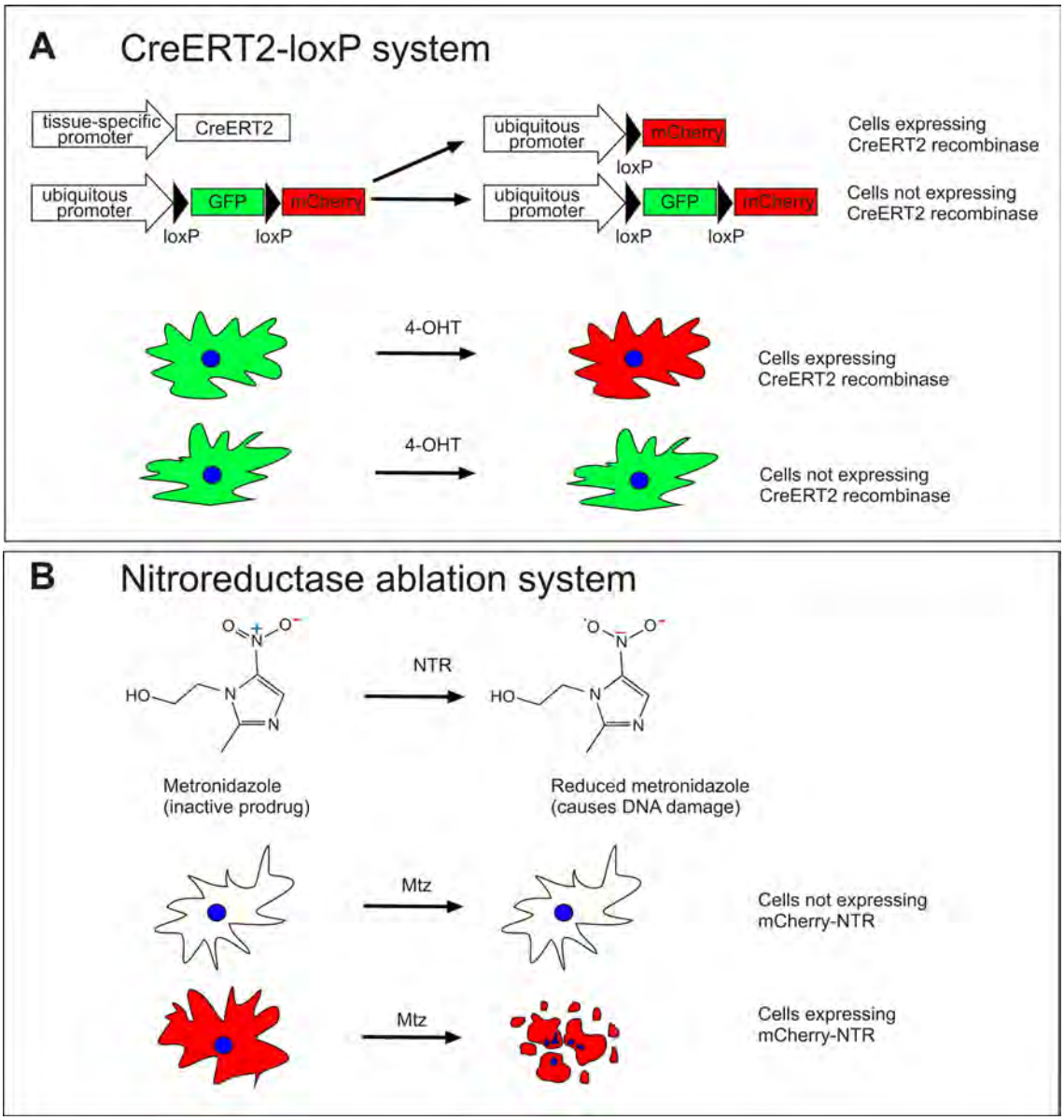

Fig. 2. Cre-lox and nitroreductase systems. A, $CreER^{T2}$ enzyme recombines the sequence between the two loxP sites, leading to permanent changes in the DNA. B, Nitroreductase (NTR) reduces Mtz to its active form. Cells that express this enzyme die when Mtz is administered.

II.2 Heart regeneration discovery, injury models and cell ablation

The first evidence of vertebrate heart regeneration was obtained some years ago from studying amphibians, in which ventricular injury induced CM proliferation in frogs, newts and axolotls (Flink, 2002; Oberpriller and Oberpriller, 1971; Oberpriller and Oberpriller, 1974; Piatkowski et al., 2013; Rumyantsev, 1966; Rumyantsev, 1973; Witman et al., 2011).

Heart regeneration in the zebrafish was described later, in 2002 (Poss et al., 2002). After amputation of the cardiac ventricle apex, a blood clot was formed, which was then replaced by fibrin, and by day 60, the resected cardiac tissue including the myocardium had regenerated. Interestingly, in this model, only small deposits of collagen were found at 14 days post amputation. This result is in contrast to the mammalian reaction to injury, in which an extensive fibrotic response occurs (Travers et al., 2016). This finding suggested that fibrosis could be one of the factors that inhibits heart regeneration in mammals. Nevertheless, while this model system proves that heart regeneration is possible in the zebrafish, it does not mimic human MI, where the dead tissue remains at the injury site.

Subsequently, a zebrafish injury model that better resembles human MI was developed simultaneously by three laboratories (Chablais et al., 2011; González-Rosa et al., 2011; Schnabel et al., 2011). The model is based on freezing the apex of the ventricle using a copper probe previously cooled in liquid nitrogen and is known as the cryoinjury model. In contrast to the amputation model described above, cryoinjury induces an extensive scar formation that does not impede regeneration. In this case, the period of time necessary for regeneration is increased to 130 days. During this thesis, I will use the cryoinjury model for the bulk of experimental approaches, as it best reproduces human MI, where a coronary artery is occluded and CMs die because of the generated hypoxia.

A third injury model was reported in the same year that the zebrafish cryoinjury model was described (Wang et al. 2011). In this case, the model was based on a genetic strategy whereby a myocardial specific *myl7:CreER*^{T2} zebrafish line was crossed into a *β-actin2:loxP-mCherry-loxP-DTA* line. Upon 4-OHT administration, some CMs expressed diphtheria toxin A (DTA) and died. As the system is not totally efficient, 60 % of CMs were found to be ablated and complete regeneration was achieved after 30 days.

A more efficient and versatile alternative to cell ablation by DTA is the use of the nitroreductase (NTR) enzyme form *E. coli* (Curado et al., 2007; Curado et al., 2008). NTR catalyses the conversion of the non-toxic pro-drug metronidazole (Mtz) into a DNA interstrand cross-linking agent (Anlezark et al., 1992; Edwards, 1993; Lindmark and Müller, 1976) that causes apoptosis and death of cells expressing NTR at the time of Mtz administration (Fig. 2 B). An advantage of

this system is that NTR expression does not produce cell ablation *per se*, allowing a more precise temporal control through the administration of Mtz.

In this thesis, these advanced ablation strategies will be used with two objectives: (1) as an injury model and (2) to study the role of a cell type during regeneration.

II.3 Origin of the new cardiomyocytes

Since the discovery that the zebrafish can regenerate its heart, many studies have attempted to find the source of the newly generated myocardium. Along this line, the first strategy was the use of *myl7:nuc-dsRed2* transgenic line to monitor CM differentiation (Lepilina et al., 2006). Because these authors identified CMs with low levels of nuc-dsRed2 at the regenerating area, it was suggested that these CMs were differentiating from another cell type, such as cardiac stem cells or the epicardium.

Then, in 2010, the Cre recombinase technology was used by two independent groups to identify that the source of the new CMs are pre-existent CMs that activate *gata4* regulatory sequences in response to injury (Jopling et al., 2010; Kikuchi et al., 2010). However, as they used *cmlc2* (currently known as *myl7*) and it labels all the CMs and *gata4* regulatory sequences that are only activated after injury, it was not possible to differentiate the contribution of different CMs subtypes to regeneration.

Later, in 2011, work based on *tcf21* as an epicardial marker (Kikuchi et al., 2011b) and an unbiased pan-epicardial lineage tracing strategy (González-Rosa et al., 2012), the possibility of epicardium-to-myocardium transdifferentiation was definitively ruled out.

A clonal analysis system was later developed to lineage-trace individual CMs (Gupta and Poss, 2012; Tekeli et al., 2017). Results from these studies suggested that each myocardial layer contributed to its own myocardial subtype. By using the *ctgfa* enhancer element as a marker for the primordial layer of CMs, a very recent study has shown that this layer does contribute to the regenerated myocardium (Pfefferli and Jaźwińska, 2017).

II.4 Dynamics of zebrafish heart regeneration

Aside from CMs, the heart is formed by a diversified set of non-muscle cell types. In the adult zebrafish, the surface of the heart is covered by the epicardium, while its luminal side is covered by the endocardium. In addition to this, there are blood vessels, such as the main descending coronary artery, which are covered by smooth muscle. This cellular composition strongly resembles that of the mammalian heart.

In zebrafish, heart injury is quickly followed by an initial inflammatory response; indeed, expression of proinflammatory cytokines can be detected at 3 hours post injury. This inflammatory response has been shown to be important for CM proliferation (de Preux Charles et al., 2016; Huang et al., 2013b).

Shortly after injury, there is also an organ-wide response of the endocardium, wherein endocardial cells become rounded, and activate some genes such as the retinoic acid biosynthetic gene *raldh2* (Kikuchi et al., 2011a). This response is quickly restricted to the injury area.

The epicardium also becomes activated at this time and reexpresses embryonic genes such as *raldh2*, *tbx18* and *wt1b* upon injury (González-Rosa et al., 2011; Lepilina et al., 2006). Epicardial cells undergo epithelial to mesenchymal transition (EMT) as early as 12 hours post injury (González-Rosa et al., 2012; Kim et al., 2010).

The epicardium and endocardium regenerate earlier than the myocardium (González-Rosa et al., 2011; Lepilina et al., 2006). This suggests that they could create a scaffold to guide and stimulate CM proliferation and migration. The peak of CM proliferation occurs at 7 days post injury (dpi) (Sallin et al., 2015) in comparison to the complete regeneration process takes from 30 to 130 days, depending on the injury model.

III Plasticity during regeneration

The general axiom during regeneration is that each cell type is derived from the same cell type, as it occurs for example in the axolotl limb (Kragl et al., 2009), where muscle can give rise to muscle, but not cartilage or epidermis; dermis potential is restricted to cartilage and tendons; and Schwann cells only make the same type of cells. Similar results were obtained in the adult zebrafish fin (Tu and Johnson, 2011). In this structure, osteoblast, dermal fibroblasts, endothelial cells, melanocytes/xanthophores, iridophores, intraray glia and lateral line constitute restricted cell lineages.

That said, there are some reported cases of change of cell fate during regeneration. For example, He et al. showed that upon hepatocyte loss in zebrafish embryos, biliary cells transdifferentiate to hepatocytes (He et al., 2014). Interestingly, this process does not occur in the adult mouse, in which most of the new hepatocytes are derived from fully differentiated hepatocytes (Wang et al., 2017).

Another example of transdifferentiation is the zebrafish notochord, which is composed of two cell types: vacuolated and sheath cells. Vacuolated cells provide hydrostatic pressure that contributes to the rigid support to the embryo, while sheath cells are a single cell epithelial layer that

surrounds the vacuolated cells and secretes components of the extracellular matrix (ECM) to provide turgor pressure to the vacuolated cells (Apschner et al., 2014; Ellis et al., 2013). Upon mechanical stress, vacuolated cells are damaged and can be restored by transdifferentiation of sheath cells (Garcia et al., 2017).

Finally, the conversion from atrial to ventricular CMs upon ablation of the latter in the embryonic zebrafish heart has also been reported (Zhang et al., 2013).

All of these examples were reported in the zebrafish embryo, and so it remains unknown whether cell fate plasticity is also possible in the adult.

IV Fibrosis during heart repair and regeneration

IV.1 Fibrosis and myocardial infarction

Myocardial infarction and the ensuing cessation of blood flow cause acute necrosis of CMs. As part of an accompanying pathological remodelling response, a fibrotic scar is formed shortly after the injury that, in the short term, prevents ventricular wall rupture. However, in the long term, fibrosis accumulates in the heart, leading to stiffening of the ventricle and the progressive worsening of cardiac function (Gourdie et al., 2016).

IV.2 Fibroblast markers

The study of cardiac fibroblasts has been hindered by the lack of good fibroblast markers. Among the traditional markers, DDR2 is also expressed in the epicardium (Morales et al., 2005), FSP1 expression can be found in endothelial, smooth muscle and immune cells (Kong et al., 2013) and Thy1 (CD90) is expressed in endothelial and immune cells (Hudon-David et al., 2007).

Two markers that have been shown to be more specific for resident fibroblasts are *Col1a1* (Moore-Morris et al., 2014) and *Tcf21* (Kanisicak et al. 2016).

After injury, the best performing markers for activated fibroblasts are Col1a1 (Moore-Morris et al., 2014) and Postn (Kanisicak et al., 2016). An advantage of these markers is that they define the fibroblast identity by expression of an ECM protein that has a clear functional relationship with fibrosis. As mentioned above, CD90 can be used as a fibroblast-specific antigen, and can be made more specific by utilizing fluorescent-activated cell sorting (FACS) to exclude hematopoietic cells ($CD45^-Ter119^-$), macrophages ($CD11b^-$) and endothelial cells ($CD31^-$). However, by using this strategy it would be possible to detect any contribution from endothelial

or circulatory cells to fibroblasts only if there is a complete transdifferentiation from these cell types to fibroblasts.

IV.3 Origin of resident fibroblasts in mammalian models

Initial studies reported that in an uninjured mouse heart, fibroblasts constitute 27-50% of the total number of cells based on histology and FACS analysis (Banerjee et al., 2007; Nag, 1980; Zak, 1974). However, later studies, using *Pdgfra*:GFP and *Col1a1*:GFP transgenic lines to mark resident fibroblast, showed that they represent a much lower proportion of the total cell number. The overall percentage of different cell types in the heart has been calculated as: fibroblasts (≈ 12%), CMs (≈ 32%), endothelial and endocardial cells (≈ 55%), leukocytes (≈ 8%) and pericytes (≈ 6%), (Pinto et al., 2015).

The origin of resident fibroblasts was analysed by using *Col1a1*:GFP as a marker for them (Moore-Morris et al., 2014). In this study they showed that 85% of *Col1a1*:GFP-positive cells in the heart were shown to arise from the epicardium, while the other 15% are derived from the embryonic endocardium (Moore-Morris et al., 2014). This was validated in a second study using FACS analysis of the surface markers $CD90^{+}CD45^{-}Ter119^{-}CD11b^{-}CD31^{-}$: 75% of resident fibroblasts were derived from the epicardium, 15% from the endocardium and 5% from the neural crest (Ali et al., 2014). A more recent study using *Tcf21* as a marker concluded that the overwhelming majority of resident fibroblasts were derived from the epicardium (Kanisicak et al., 2016).

IV.4 Origin of activated fibroblasts in mammalian models

As mentioned earlier, after a cardiac injury such as MI, fibroblasts accumulate at the site of injury. These cells are occasionally also termed “activated fibroblasts”, because they activate ECM protein expression or “myofibroblasts”, because they acquire contractile capabilities and express the smooth muscle marker α-SMA. However, in a recent work using a pressure-overload model of heart disease, which leads to cardiac hypertrophy and fibrosis, α-SMA was found to be restricted to a subset of activated fibroblasts (Moore-Morris et al., 2014). Because of this incongruity, the term “myofibroblast” will be avoided in this thesis, and I will instead use “activated fibroblast” to refer to population of the mesenchymal cells that accumulate upon injury and produce large amounts of ECM proteins.

Different cell types have been proposed to contribute to activated cardiac fibroblasts. For instance, endothelial cells were identified to contribute *via* endocardial to mesenchymal transition in

models of diabetes (Widyantoro et al., 2010) and pressure overload (Zeisberg et al., 2007). One caveat to these studies, however, is that they were based on the use of FSP-1 as a fibroblast marker, which was later proved to be not specific for fibroblasts (Kong et al., 2013).

Bone marrow-derived cells have also been reported to give rise to fibroblasts in response to cardiac injury (Haudek et al. 2006; Möllmann et al. 2006; van Amerongen et al. 2008), but their precise contribution remains controversial and the results cannot be supported by others (Ali et al., 2014; Kanisicak et al., 2016; Moore-Morris et al., 2014; Ruiz-Villalba et al., 2015).

Using *Postn* as a marker, Kanisicak *et al*. showed that *Tcf21*$^{+}$ resident fibroblasts made up the overwhelming source of activated fibroblasts after MI injury, pressure overload, or infusion of a fibrosis-promoting neuroendocrine agonist cocktail (Kanisicak et al., 2016). This result is in good agreement with the detection of fibroblast proliferation in a pressure overload model (Ali et al., 2014), and with the finding that resident fibroblast with an endocardial and epicardial origin are the main contributors to activated fibroblasts in the same injury model (Moore-Morris et al., 2014).

IV.5 Fibroblast fate and function in mammals

An important question is the fate of activated fibroblasts long time after injury. In a pressure overload model, rather than being eliminated by apoptosis, *Postn*$^{+}$ activated fibroblasts were found to become partially inactive after cessation of angiotensin II and phenylephrine administration (Ali et al., 2014; Kanisicak et al., 2016). Importantly, these findings were obtained in models of mammalian heart repair, and do not imply that the same process occurs in heart regeneration, where fibrotic tissue is substituted by regenerated myocardium.

To study the importance of fibroblasts to heart repair after myocardial injury, Kanisicak *et al*. ablated *Postn*$^{+}$ cells, which strongly decreased survival after MI (Kanisicak et al., 2016), supporting the hypothesis that fibroblast are essential to prevent ventricular wall rupture after MI.

IV.6 Fibrosis during zebrafish heart regeneration

There are several pieces of evidence to suggest that there are resident fibroblasts in the zebrafish heart.

Using electron microscopy, Lafontant *et al*. detected a sheet of mesenchymal cells separating the trabeculae from the cortical layer, which were surrounded by collagen fibres (Lafontant et al., 2013). In different studies, a population of cells labelled with a *wt1a* regulatory sequence was

identified in a similar location (Peralta et al., 2014) and lineage tracing of *tcf21*$^{+}$ epicardial cells also marked cells in the region (Kikuchi et al., 2011b). However, it is not clear whether these findings refer to the same cells, and if they express other fibroblast markers apart from collagen XII (Marro et al., 2016).

Upon cryoinjury in the zebrafish there is an extensive fibrotic response (González-Rosa et al., 2011); surprisingly, however, this does not impede regeneration.

Some of this fibrosis originates from the epicardium, as *postnb* and *col1a2* expression is upregulated in *wt1b*:GFP positive cells upon cryoinjury (González-Rosa et al., 2012). In a different study, col1a1 was also detected adjacent to endocardial cells (Münch et al., 2017), suggesting that these cells can also contribute to fibrotic tissue deposition, but it is not clear whether they become fibroblasts. Whether another cell type can contribute to fibrosis remains unexplored.

As zebrafish heart regeneration progresses, the fibrotic tissue regresses; although it is unknown whether this is mediated by inactivation of ECM-producing cells or by their elimination. Lineage tracing using *tcf21* revealed the long term persistence of *tcf21*-derived cells in the regenerated myocardium (Kikuchi et al., 2011b). However, it has not been demonstrated whether these cells were the same as those expressing collagen and *postnb* in the short term after injury.

A previous study has shown that heart regeneration is impaired by *tgf-β* receptor inhibition (Chablais and Jazwinska, 2012), pointing to the possibility that fibrosis is concomitant with and necessary for heart regeneration. However, this effect could be mediated by a reduction of fibrosis or by direct inhibition of CM proliferation by Tgf-β, since phosphorylated Smad3, an intracellular signalling component of the Tgf-β superfamily, has also been detected in CMs close to the injury area.

In this thesis, different ablation and lineage tracing strategies are developed to identify the origin, fate and role of fibroblasts, as well as the plasticity of CMs during zebrafish heart regeneration.

OBJECTIVES

OBJECTIVES

1. To analyse the plasticity of CMs during zebrafish development.

2. To study the plasticity of CMs during zebrafish heart regeneration.

3. To characterise the origin, fate and role of fibroblasts during zebrafish heart regeneration.

METHODS

METHODS

I Animal handling and generation of transgenic lines

All experiments were approved by the Community of Madrid "Dirección General de Medio Ambiente" in Spain. Animals were housed and experiments performed in accordance with Spanish and Swiss bioethical regulations for the use of laboratory animals. Fish were maintained at a water temperature of 28 ºC.

The construct to generate Tg(*tbx5a*:*tdTomato*) transgenic zebrafish lines were made by recombining the and the tdTomato cassette (Supplementary File 1), into the bacterial artificial chromosome (BAC) *CH73-99A14*. The construct for *Tg(tbx5a:mCherry-p2A-CreER^{T2})*^{cn4} was generated recombining the *iTol2Amp* cassette (Suster et al., 2011) (Table 1, primers 1,2) and *mCherry-p2A-CreER^{T2}* (Supplementary File 2; Table 1, primers 3,4) into the same BAC. The construct to generate Tg(*tbx5a*:*CreER^{T2}*)^{cn3} was made by recombining *iTol2Amp-γ-crystallin:RFP* (Supplementary File 3; Table 1, primers 2,5) and CreER^{T2} (Supplementary File 3; Table 1, primers 4,6) cassettes into the same BAC. *Tg(vmhcl:loxP-myctagBFP-STOP-loxP-NTR-mCherry)*^{cn5} was generated using a construct obtained from recombining *iTol2Amp* (Table 1, primers 1,2) and *loxP-myctagBFP-STOP-loxP-mCherry-NTR* (Supplementary File 4; Table 1, primers 7,8) cassettes into the BAC *CH73-204E19*.

The construct to generate Tg(*postnb:citrine*)^{cn6} was made by recombining the *iTol2Amp* cassette (Suster et al., 2011) followed by the citrine-Kan cassette (Table 1, primers 11, 12) into the BAC CH211-38D6. The construct to generate Tg(*postnb:CreER^{T2}*)^{cn7} was made by recombining the *iTol2Amp-Cryst:GFP* cassette (Supplementary File 5; Table 1, primers 1, 2) followed by *CreER^{T2}-frt-Kan-frt* (Supplementary File 2; Table 1, primers 13, 14) into the BAC CH73-370H18. The plasmid used to generate the Tg(*col1a2:loxP-tagBFP-loxP-mCherry-NTR*)^{cn8} line was constructed by recombining the *iTol2-CrystCFP* (Donà et al., 2013) (Table 1, primers 15, 16) and *loxP-tagBFP-loxP-mCherry-NTR* (Supplementary File 4; Table 1, primers 9, 10) cassettes into the BAC CH211-122K13. Once the transgenic line was established, *Cre* mRNA was injected at 50 ng µl−1 to recombine the loxP sites to generate Tg(*col1a2:loxP-mCherry-NTR*)^{cn11}.

Plasmid templates for recombineering and the plasmid to generate Tg(*wt1a:CreER^{T2}*)^{cn10} (Supplementary File 6) using the promoter reported previously (Bollig et al., 2009) were cloned using Gibson Assembly (NEB). Recombineering was performed combining the pRed/ET system (GeneBridges, Germany) and EL250 bacteria (Lee et al., 2001).

Table 1. Primers used for BAC recombineering. Red, homology arms. Green, minimal kozak sequence. Capital letters, overlapping with template sequence.

Primer number	Primer name	Sequence
1	pTarBAC_HA1_iTol2_F	gcgtaagcggggcacatttcattacctctttctccgcacccgacatagatC CCTGCTCGAGCCGGGCCCAAGTG
2	pTarBAC_HA2_iTol2_R	gcggggcatgactattggcgcgccggatcgatccttaattaagtctactaA TTATGATCCTCTAGATCAGATC
3	tbx5_HA1_mCherry_F	ctttttgtttctgtatttaggcctcacggtagacatcgtacaggcctctccAC CATGGTGAGCAAGGGC
4	tbx5a_HA2_kanFRT_R	ttcgctgtcactgggagagttttggagccgaaaggtgtcttcactgtccgc GGAGGCTACCATGGAGAAG
5	pTarBAC_HA1_Cryst_F	gcgtaagcggggcacatttcattacctctttctccgcacccgacatagatT ACCGGGCCCCCCCTCGAGTCC
6	tbx5_HA1_CreERT2_F	ctttttgtttctgtatttaggcctcacggtagacatcgtacaggcctctccacc atgTCCAACCTGCTGACTGTGCACC
7	vmhcl_HA1_loxP_F	atgtcctgtactgcttctaacaagttcttcttttccataatttaaggttgACC GGTGGATCCACTATAAC
8	vmhcl_HA2_kanFRT_R	ttccgcaggtaaggcgctgcggccccaaaaacagacatttcagcatcgcc GGAGGCTACCATGGAGAAG
9	col1a2_HA1_loxP_F	aagtagttaaaccagggcactgcggcacaaggagtctgcatgtcggtttA CCGGTGGATCCACTATAAC
10	col1a2_HA2_kanFRT_R	tacgaagtcactgcaagcagcaacagaatccgggtatccacaaagctga gGGAGGCTACCATGGAGAAG
11	postnB_HA1_citrine_F	cctcagctcaagcccatttcttgctctgaagtctcacagaggagaaagca ACCATGGTGAGCAAGGGCGAGGAG
12	postnB_HA2_kan_R	tcaaaggcagacagcacaaagagtgcaaaagtagctgcaaagaggagc ttTCAGAAGAACTCGTCAAGAAGGCG
13	postnb_HA1_CreERT2_F	cctcagctcaagcccatttcttgctctgaagtctcacagaggagaaagcaa ccatgTCCAACCTGCTGACTGTGCACC
14	postnb_HA2_kanFRT_R	tcaaaggcagacagcacaaagagtgcaaaagtagctgcaaagaggagc ttGGAGGCTACCATGGAGAAG
15	pTarBAC_HA2_iTol2_AmpCryeCFP	cgcggggcatgactattggcgcgccggatcgatccttaattaagtctacta GAAACAGCTATGACCATGTAA
16	pTarBAC_HA1_iTol2_AmpCryeCFP	gcgtaagcggggcacatttcattacctctttctccgcacccgacatagatC CCTGCTCGAGCCGGGCCCAAGTG

The plasmid to generate the Tg*(fli1a:CreER^{T2})^{cn9}* line was obtained using Gateway (Kwan et al., 2007) to recombine the plasmids *p5E-fli1ep* (Kwan et al., 2007), *pME-CreER^{T2}* (Villefranc et al., 2007) and p5E-pA (Mosimann et al., 2011) into the *pDestTol2pA2* (Kwan et al., 2007) backbone.

Tg*(-3.5ubb:loxP-lacZ-loxP-eGFP)^{cn2}* (Di Donato et al., 2016) was outcrossed for 6 generations to isolate the best insertion. BAC DNA was injected at 25 ng µl^{-1} into one-cell stage zebrafish embryos along with 1 nl of 50 ng µl^{-1} synthetic *Tol2* mRNA in Danieau buffer. Transient *ltbp3:TagRFP-2A-Cre* embryos in the stable *tbx5a:GFP* background were generated by injecting a Tol2 plasmid containing the vector *ltbp3:TagRFP-p2A-Cre* (Zhou et al., 2011) into one-cell stage Tg*(tbx5a:GFP)* embryos. Around 150 embryos survived the microinjection and were screened for mCherry expression. The transgenic line *drl:mCherry* (in full Tg*(-6.3drl:mCherry)*) based on transgene vector *pCM330* was generated using Multisite Gateway assembly of *pCM293* (*pENTR5'* backbone containing 6.35kb of the zebrafish *drl* locus (*ZDB-GENE-991213-3*) amplified with primers *5'-GTCAGCACCAGATGCCTGTGC-3'* (forward) and *5'-CCAAGTGTGAATTGGGATCG-3'* (reverse) as described (Mosimann et al., 2015)), Tol2kit (Kwan et al., 2007) *#386* (*pME-mCherry*), *#302* (*p3E_SV40polyA*), and *#394* (*pDestTol2A2*) (in full *pDestTol2pA2_drl:mCherry*, referred to as *drl:mCherry*). Plasmid DNA was injected at 25 ng µl^{-1} into one-cell stage zebrafish embryos that were then raised and screened for germline transmission of the transgenic reporter with subsequent outcrossing to isolate a single transgene insertion. The *drl:mCherry* transgenics used in the study are at least seventh-generation transgenics.

Table 2. Summary of the transgenic lines used in this thesis.

Transgenic line	Phenotype	Reference
col1a2:loxP-tagBFP-loxP-mCherry-NTR	Expression pattern specific to *col1a2* expressing cells. It allows ablation of cell subpopulations upon activation by Cre and Mtz administration.	Generated during this thesis.
col1a2:loxP-mCherry-NTR	Expression pattern specific to *col1a2* expressing cells. It allows ablation of *col1a2*$^{+}$ cells upon Mtz administration.	Generated during this thesis.
drl:mCherry	Within the heart, labels the FHF-derived CMs when analysed before 72 hpf. Circulatory and endocardial cells are also labelled.	Generated by Anastasia Felker and Christian Mosimann (unpublished).
fli1a:GFP	GFP expression in endothelial and endocardial cells.	(Lawson and Weinstein, 2002)
fli1a:CreER^{T2}	CreER^{T2} expression in endothelial and endocardial cells.	Generated by Juan Manuel González-Rosa (unpublished).
kdrl:mCherry	mCherry expression in endothelial and endocardial cells.	Generated by E. Ober.
ltbp3:tagRFP-CreER^{T2}	Within the heart, labels the SHF-derived CMs. Other structures in the fish are also labelled, including the notochord.	(Zhou et al., 2011) This line was not generated; instead, the plasmid was transiently injected.

myl7:mb-mCherry	Expression of mCherry in CM membrane.	(Rohr et al., 2008)
myl7:nuc-mCherry	Expression of mCherry in CM nuclei.	(Mably et al., 2003)
postnb:citrine	Citrine expression in activated cardiac fibroblasts in the injured adult heart. Expression is also detected in some CMs near the atrio-ventricular canal, and in valves and skin fibroblasts.	Generated during this thesis.
postnb:CreER^{T2}	Citrine expression in activated cardiac fibroblasts in the injured adult heart. Expression is also detected in some CM near the atrio-ventricular canal, and in valves and skin fibroblasts.	Generated during this thesis.
tbx5a:CreER^{T2}	CreER^{T2} expression in FHF-derived ventricular CMs, atria, pectoral fin and dorsal retina.	Generated during this thesis.
tbx5a:GFP	GFP expression in FHF-derived ventricular CMs, atria, pectoral fin and dorsal retina.	Generated by Carolina Minguillon (Ocaña et al., 2017).
tbx5a:mCherry-p2a-CreER^{T2}	mCherry and CreER^{T2} expression in FHF-derived ventricular CMs, atria, pectoral fin and dorsal retina.	Generated during this thesis.
tbx5a:tdTomato	tdTomato expression in FHF-derived ventricular CMs, atria, pectoral fin and dorsal retina.	Generated by Carolina Minguillon (unpublished).
tcf21:CreER^{T2}	Within the heart, expression in epicardial and epicardial-derived cells.	(Kikuchi et al., 2011b)
ubb:loxP-GFP-loxP-mCherry (ubi:switch)	LacZ ubiquitous expression. Cells that express and activate the Cre recombinase, change expression from LacZ to GFP.	(Mosimann et al., 2011)
ubb:loxP-lacZ-loxP-GFP	LacZ ubiquitous expression. Cells that express and activate the Cre recombinase change expression from LacZ to GFP.	Generated during this thesis.
vmhcl:loxP-tagBFP-loxP-mCherry-NTR	Expression pattern specific to the cardiac ventricle. It allows ablation of cell subpopulations upon activation by Cre and Mtz administration.	Generated during this thesis.
wt1a:GFP	In the embryonic heart, GFP expression in epicardium and its precursors. In the adult heart, expression is limited to resident cardiac fibroblasts. Expression is also detected in other structures, including kidney and some neurons.	(Bollig et al., 2009)
wt1a:CreER^{T2}	In the embryonic heart, CreER^{T2} expression in epicardium and its precursors. In the adult heart, expression is limited to resident cardiac fibroblasts. Expression is also detected in other structures, including kidney and some neurons.	Generated during this thesis.

In adults, 10 µM 4-OHT (Sigma, H7904) was administered at the indicated times and treatments were performed overnight. Prior to administration, the 10 mM stock (dissolved in ethanol) was heated for 10 minutes at 65 °C (Felker et al., 2016). For genetic labelling in

tbx5a:*mCherry-p2A-CreER^{T2};3.5ubb:loxP-lacZ-loxP-eGFP* embryos, 4-OHT was administered at 10 µM from 24 to 48 hours post-fertilisation (hpf), and at 5 µM from 48 to 84 hpf. Cryoinjury was performed as previously described (González-Rosa and Mercader, 2012). For genetic ablation experiments and their controls, 4-OHT was administered at 5 µM from 24 to 48 hpf and then Mtz (SIGMA) was added at 10 mM from 96 to 168 hpf.

For all the experiments involving Cre recombination or cell ablation, hemizygous fish were used, except for Tg(*postnb*:*CreER^{T2}*;*ubi:switch*) lines, which were hemizygous for *postnb*:CreER^{T2} and homozygous for *ubb:switch* allele.

5-bromodeoxyuridine (BrdU) was added to E3 water at 5 mg/mL with 0.5% DMSO from 4 to 7 dpf to label embryos. For adults, 20 µL of BrdU 20 mg/mL in PBS was injected per fish.

II Histology

Samples for Fig. 6, Fig. 7, Fig. 8, Fig. 15, Fig. 22, Fig. 24 C–F, Fig. 28 A–D, Fig. 33 C–F and Fig. 38 were fixed in 4% paraformaldehyde (PFA) in phosphate-buffered saline (PBS) overnight at 4°C. Samples were then washed in 0.1% Tween20 (Merck) in PBS, dehydrated through an ethanol series and embedded in paraffin wax. Samples were sectioned at 7 µm using a microtome (Leica). Sections mounted on Superfrost slides (Fisher Scientific) and dried overnight at 37 °C.

Sections were deparaffinised in xylol, rehydrated and washed in distilled water. Connective tissue was stained using Acid Fuchsine Orange G (AFOG).

Samples for Fig. 20 and Fig. 21 were treated as described in the RNAScope manufacturer protocol.

The remaining sections were prepared by fixing in 4% PFA washing in PBS + 0.1% Tween20, and then incubating in 15% saccharose overnight at 4 °C. Then sections were embedded 30% gelatin 15% saccharose and snap frozen at -80 °C in isopentane. Tissue was cut at 8 µm on a cryostat (Leica).

III Whole mount immunofluorescence in adults

For immunofluorescence, whole mount hearts were fixed in 4% PFA overnight, washed in 0.1% Tween20 in PBS and permeabilised with 0.5% Triton-X100 (Sigma) in PBS for 20 minutes. Several washing steps were followed by at least 2 hours of blocking with 5% goat serum, 5% BSA and 20 mM $MgCl_2$ in PBS, followed by incubation with antibodies overnight.

IV Quantitative real-time (qRT) polymerase chain reaction

RNA from cardiac ventricles was extracted using 0.5 mL Trizol Reagent (Ambion, Life Technologies). One ventricle was used per biological replicate. RNA was transcribed to cDNA using the High-Capacity cDNA Reverse Transcription Kit (Applied Biosystems). qRT-PCR was performed using Power SYBR Green PCR Master Mix (Applied Biosystems, Life Technologies) and normalizing *col1a2* and *postnb* expression with the geometric mean of the expression level of two constitutive genes: *EF1-alpha* and *rps11*. Primers used are shown in Table 3.

Table 3. Primers used for qRT-PCR

Gene	*Forward Primer*	*Reverse Primer*
col1a2	AGTGGAGCTTCTGGTCCAAG	CTCCCTTCACTCCAACAGGT
postnb	ATGAGACCCCAGGCTGAGT	TCCATGGACATCACCTCATC
EF1-alpha	CAGCTGATCGTTGGAGTCAA	TGTATGCGCTGACTTCCTTG
rps11	GATGGCGGACACTCAGAAC	CCAATCCAACGTTTCTGTGA

V *in situ* mRNA hybridisation, RNAScope, immunofluorescence, TUNEL, imaging and image analysis

in situ hybridisation

In situ hybridization (ISH) on paraffin sections and on whole mount larvae was performed as described (González-Rosa et al., 2012; Mercader et al., 2006) using *tbx5a* (cDNA kindly provided by C. Neumann), *GFP* (cDNA kindly provided by J.L. Gómez-Skarmeta), *nppa* (González-Rosa et al., 2014), *col1a2* (González-Rosa et al., 2012) and *postnb* (González-Rosa et al., 2012) riboprobes.

RNAScope

RNAScope (Advanced Cell Diagnostics, Hayward, CA) was performed following the manufacturer's instructions for formalin-fixed paraffin-embedded samples with standard tissue pretreatment and the 2.5 HD RED detection kit.

Immunuohistochemistry and TUNEL in sections

Paraffin sections were deparaffinised, rehydrated and washed in distilled water. Epitopes were retrieved by heating in 10 mM citrate buffer (pH 6.0) for 15 minutes in a microwave at full power. Gelatine sections were incubated instead 30 min in 0.1% Tween20 in PBS at 37 ºC to dissolve the gelatin. Non-specific binding sites were saturated by incubation for at least 1 hour in blocking solution (5 % BSA, 5 % goat serum, 20mM MgCl2 in PBS). Endogenous biotin was blocked with the avidin-biotin blocking kit (Vector, Burlingame, CA, USA).

Whole mount immunofluorescence

Embryos were fixed in 4 % PFA overnight, washed in 0.1% Tween20 in PBS and permeabilised with 0.5 % Triton-X100 in PBS (Sigma) for 20 minutes. Several washing steps were followed by 2 hours of blocking with 5 % goat serum, 5% BSA and 20 mM MgCl2 in PBS, followed by incubation with antibodies overnight. BrdU immunofluorescence was performed as described (Jahangiri et al., 2016).

Antibodies

Primary antibodies used were as follows: anti-MHC (MF20, DSHB, 1:20 and F59, DSHB, 1:20), anti-GFP (AVES, GFP-1010, 1:500; 632592, Clontech, Mountain View, CA, USA, 1:100), anti-RFP (ab34771, Abcam, 1:200), anti-Xirp2a (Otten et al., 2012) -a kind gift from C. Otten and S. Seyfried (1:500) anti-Laminin (L9393, Sigma, 1:200), anti-mKate (Cai et al., 2013) to detect tagBFP (1:500), anti-col1a1 (SP1.D8, DSHB, 1:20), anti-RFP (ab34771, AbCam, 1:200), anti-Mef-2 (Santa Cruz Biotechnology, C21, sc-313, 1:200), anti-BrdU (BD Biosciences, B44, 1:100). Biotin- or Alexa (488, 568, 633) -conjugated secondary antibodies and streptavidin-Cy3 (Jackson Immuno Research Laboratories) were used at 1:300. Nuclei were stained with 4’,6-diamidino-2-phenylindole (DAPI) and slides were mounted in Fluorsave (Calbiochem).

TUNEL

Apoptosis was detected by TUNEL staining using the *in situ* cell death detection kit from Roche (Mannheim, Germany).

Imaging

Embryos were imaged with a Zeiss 780 confocal microscope fitted using a 20x objective with a dipping lens. Z-stacks were taken every 1 µm. Three-dimensional images were reconstructed with ImageJ software. A Leica TCS SP-5 or Nikon A1R confocal microscope was used for imaging of histological sections. The percentage of tagBFP cells was quantified using ImageJ considering the area of tagBFP and comparing it with the area of MHC staining.

A Leica TCS SP-5 confocal microscope was used for imaging of immunofluorescence on sections and whole mount heart and a Nikon 90i microscope was used to image non-fluorescent sections.

Image analysis

Percentage of *tbx5a*-derived cells in Fig. 11 was quantified applying a median filter of radius 1 using ImageJ. The GFP^+ and MHC^+ areas were measured. The same set of images were used to quantify the percentage of GFP^+ CMs in the trabeculae and in the regenerated compact layer, applying the same threshold for both regions.

For analysis of the extent of (injury area)/(injury area + myocardium) for Fig. 38, the total ventricular tissue area and IA on all sections on a slide of each heart (collected on 5 slides) were measured.

VI Echocardiographies

Measurements and analysis were performed as described (González-Rosa et al., 2014).

VII Heart dissociation, sorting and RNA-Seq library production

Zebrafish hearts were dissected and the atrio-ventricular canal was carefully removed in order to obtain a pool of exclusively ventricular cells. The ventricles were dissociated according to previous protocols (Tessadori et al., 2012) with minor modifications. The enzyme concentration was doubled, and time of digestion increased to 1 hour and 40 minutes with gentle agitation while pipetting with a cut 1000 µL tip every 20-30 minutes. Then, one volume of PBS + 10% fetal bovine serum (FBS) was added and the mixture was centrifuged for 8 minutes at 250 g and re-suspended in PBS + 1% FBS. Specifically, the following enzyme concentrations were used: liberase TH (Sigma, 200 mg/L), Elastase (Serva, 1:250), Pronase E (Serva, 1:100 dilution of the 26.3 mg/mL stock), DNase (Qiagen, 1:20000) and 2,3-butanedione monoxime (BDM; 10 mM).

All reagents were dissolved in Tyrode's low calcium (in mM): NaCl 140, KCl 5.4, $CaCl_2$ 0.01, $MgCl_2$ 1.0, glucose 5.5, and HEPES 5.0; pH was set to 7.4 with NaOH.

For *myl7:nuc-mCherry*$^+$ cell isolation, whole ventricles were used after carefully removing the atrio-ventricular canal to avoid the presence of strong *tbx5:GFP*$^+$ cells in that area. For *kdrl:mCherry*$^+$; *postnb:citrine*$^+$ and *postn:CreER*^{T2} lineage traced cells, only the apex was used. For *wt1a:GFP*$^+$ and *wt1a:GFP*$^-$ cell isolation, the whole ventricle was used.

Cells were sorted using SONY Synergy sy3200 sorter and RNA was extracted using the Arcturus Pico Pure RNA isolation kit (Thermofisher) following the manufacturer's instructions.

mRNA (0.25-1 ng) was used to generate barcoded RNA-Seq libraries using the Ovation Single Cell RNA-Seq System (NuGEN) with two rounds of library amplification. The size of the libraries was calculated using the Agilent 2100 Bioanalyzer. Library concentration was determined using the Qubit® fluorometer (ThermoFisher Scientific). Libraries were sequenced on a HiSeq2500 (Illumina) platform to generate 60-base single reads. FastQ files for each sample were obtained using CASAVA v1.8 software (Illumina). Four biological replicates consisting of 5 pooled hearts were used per sample.

VIII RNA-Seq analysis

Sequencing adaptor contaminations were removed from reads using cutadapt 1.9.1 software (Martin, 2011) and the resulting reads were mapped and quantified on the transcriptome (Ensembl gene-build 10, release 82) using RSEM v1.2.25 (Li and Dewey, 2011). Only genes with at least 1 count per million in at least 2 samples were considered for statistical analysis. Data were then normalised and differential expression tested using the bioconductor package EdgeR(Robinson et al., 2010). We considered as differentially expressed those genes with a Benjamini-Hochberg adjusted p-value ≤ 0.05 and LFC ≥ 1. For the Tg(*wt1a:GFP*) and Tg(*tbx5a:GFP*) samples paired analysis was used. Heatmap was made using ggplot library and heatmap.2 function.

IX Data availability

The RNA-Seq Dataset has been uploaded to GEO with accession number GSE87596, GSE101204, GSE101200 and GSE101199.

RESULTS

RESULTS

I *tbx5a* labels the derivatives of the zebrafish first heart field

While the presence of a FHF and a SHF in the zebrafish has recently been described (de Pater et al., 2009; Mosimann et al., 2015; Zhou et al., 2011), their contribution to the adult zebrafish heart remains unknown.

Mammalian *Tbx5* labels the derivatives of the FHF in the adult ventricle (Bruneau et al., 1999; Takeuchi et al., 2003). To test if this also holds true in zebrafish, we generated a *tbx5a:GFP* BAC transgenic reporter line. We chose *tbx5a* rather than the *tbx5b* because it is more strongly expressed in the heart and because *tbx5a* mutants reproduce key phenotypes of mammalian *Tbx5* perturbations (Albalat et al., 2010; Garrity et al., 2002; Pi-Roig et al., 2014). The *tbx5a:GFP* line recapitulated the endogenous gene expression pattern at 72 hpf, with expression detected in the embryonic heart, retina and limb (Fig. 3). This pattern is analogous to that detected in mouse and chick embryos (Chapman et al., 1996; Gibson-Brown et al., 1998).

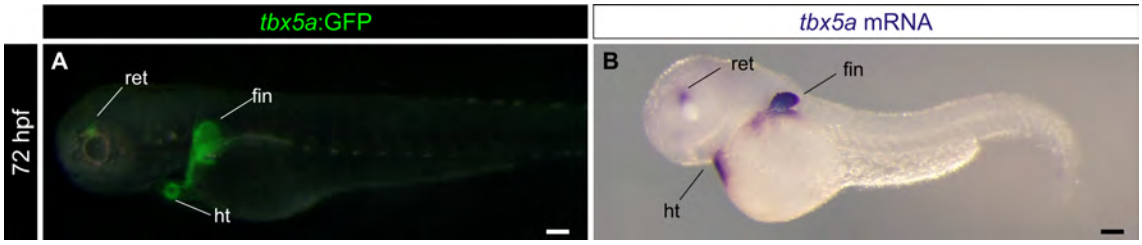

Figure 3. Characterisation of the *tbx5a*:GFP reporter line. A, Lateral view of a *tbx5a*:*GFP* larvae at 3 dpf. A merged fluorescent and brightfield image is shown. **B**, mRNA ISH with a *tbx5a* antisense riboprobe on the same staged larva as that shown in A (n = 7/7). ht, heart tube; ret, retina. Scale bars, 100 μm.

When we analysed the expression pattern in the early heart tube at 32 hpf, homogeneous GFP expression was detected within the entire cardiac tube (Fig. 4 A–C). However, at 56, 72 hpf and 5 dpf, stages at which the SHF progenitors have already been added to the heart tube, the most anterior part of the ventricle (arterial pole) was *tbx5a:*GFP^{-} (Fig. 4 D–L; Supplementary Video 1). The atrium was *tbx5a:*GFP^{+} at all stages analysed.

This result shows that *tbx5a*:GFP labels the derivatives of the FHF in the ventricle, while at least part of the derivatives of the anterior SHF are *tbx5a*:GFP^{-}. Instead, the posterior SHF derivatives that contribute to the venous pole of the heart are *tbx5a*:GFP^{+}.

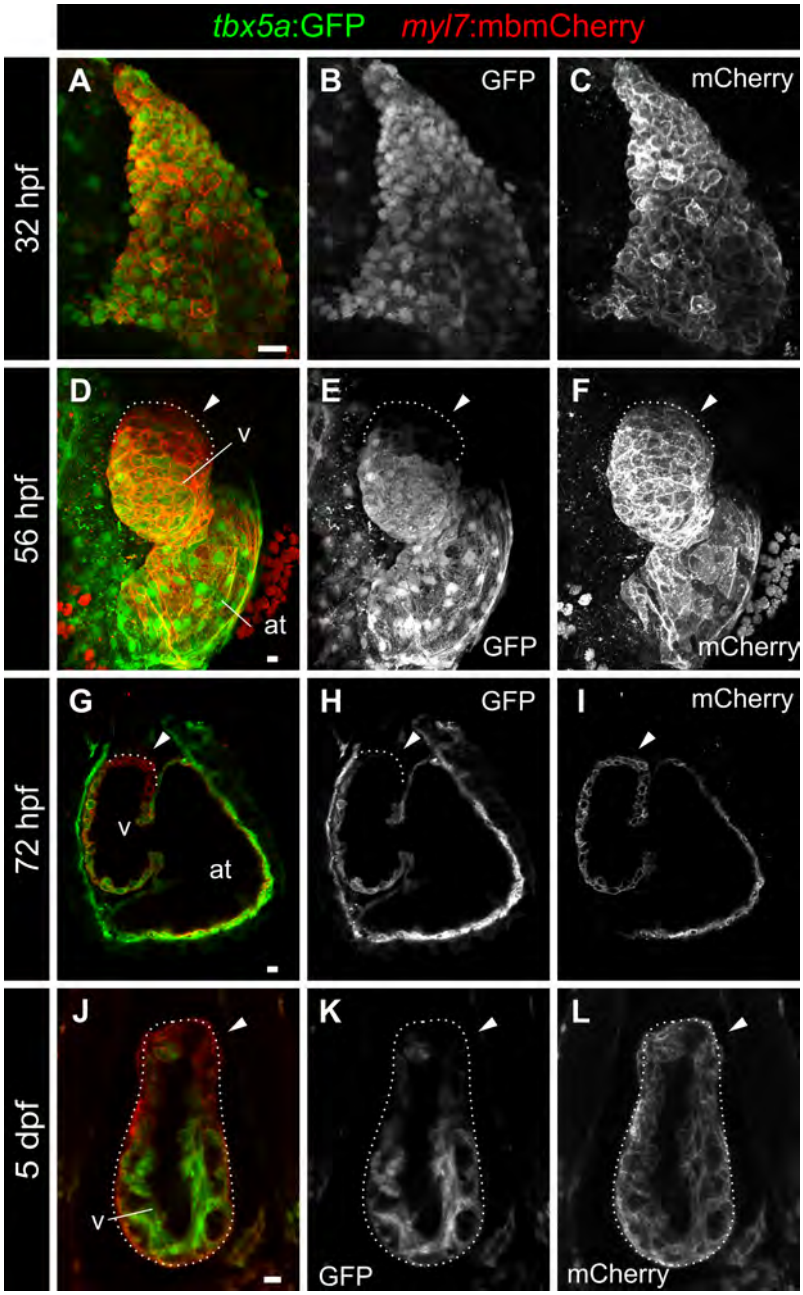

Figure 4. Expression profile of *tbx5a* positive CMs in embryonic zebrafish hearts. **A–F**, Whole mount immunofluorescence of *tbx5a:GFP*;*myl7*:*mbmCherry* double transgenic zebrafish hearts at 32 (**A–C**, n = 5/5) and 56 hpf (**D–F**, n = 3/3). **G–L**, Confocal optical sections of *tbx5a:GFP*;*myl7*:*mbmCherry* hearts at 72 hpf (**G–I**, n = 5/5) and 5 dpf (**J–L**, n = 6/6). GFP (green) labels *tbx5a*$^{+}$ cells and mCherry (red) marks cells expressing the pan-myocardial marker *myosin light chain 7* (*myl7*). Shown are ventral views, cranial is to the top. At 32 hpf all CMs are *tbx5a*:GFP^{+} but at 56, 72 hpf, 4 and 5 dpf *tbx5a*:GFP^{-} CMs can be observed in the distal ventricle (arrowheads). Arrowheads indicate the *tbx5a*$^{-}$ distal domain. The atrio-ventricular canal and large portions of the atrium are also GFP^{+}. at, atrium; v, ventricle; Scale bars, 10 µm.

We next compared the *tbx5a*:GFP expression pattern with that of two previously established markers for FHF and SHF in zebrafish, *drl* and *ltbp3*, respectively. In *tbx5a*:GFP; *drl*:mCherry hearts, the outflow tract region was negative for both marker genes both at 56 and 72 hpf. However, while *tbx5a*:GFP expression was stable in CMs from 56 to 72 hpf, *drl*:mCherry was

highly expressed in circulatory and endocardial cells, and at 72 hpf was undetectable in most of the CMs (Fig. 5 A–H; Supplementary Video 2,3). This establishes that *tbx5a* is a better marker to study FHF-derived CMs. To compare the expression pattern of *tbx5a*:GFP with *ltbp3*, we injected *ltbp3:TagRFP-2a-Cre* BAC DNA into the *tbx5a*:GFP transgenic background, and we found that the *tbx5a*:GFP^{-} region was positive for *ltbp3*:tagRFP (Fig. 5 I–L; Supplementary Video 4). Overall, these results support the hypothesis that *tbx5a* labels FHF-derived CMs.

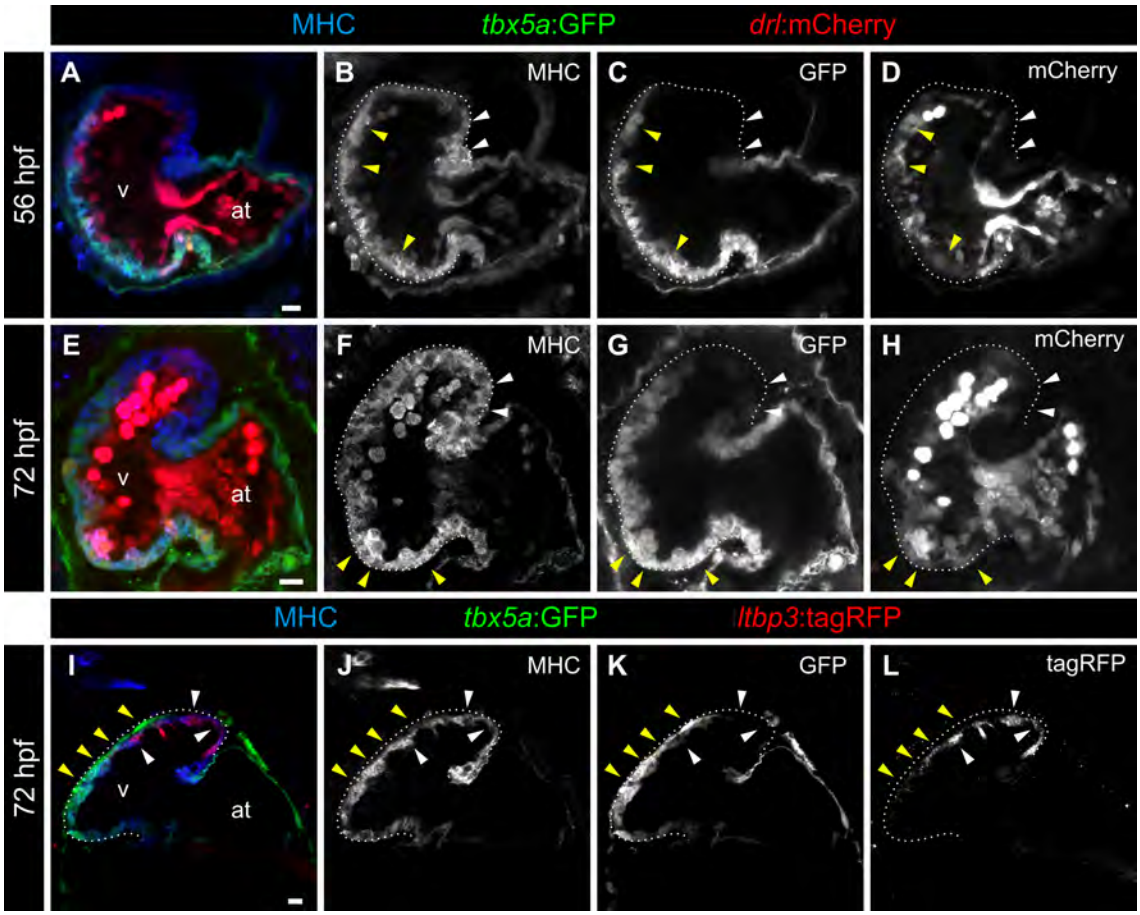

Figure 5. The pattern of *tbx5a:*GFP expression is similar to that of *drl*:mCherry and complementary to *ltbp3*:mCherry. A–H, Confocal optical sections of 56 (n = 5/5) and 72 hpf (n = 7/7) *tbx5a*:*GFP*;*drl*:*mCherry* double transgenic zebrafish larvae. GFP (green) labels *tbx5a*$^{+}$ cells, mCherry (red) *drl*$^{+}$ cells and anti-MHC immunofluorescence labels all CMs. The ventricle is outlined with dotted lines. The *tbx5a:*GFP^{-} and *drl:*mCherry^{-} distal ventricle is marked with white arrowheads, while the yellow arrowheads point to the domains positive for both markers. Note that *drl:*mCherry is also expressed in endocardial cells and red blood cells in the lumen of the heart. **I–L**, Confocal optical sections of 72 hpf hearts from *tbx5a*:*GFP* embryos transiently injected with *ltbp3:TagRFP-2A-Cre*. Shown is a representative heart out of 8 larvae. GFP labels *tbx5a*$^{+}$ cells, mCherry *ltbp3*$^{+}$ cells, and MHC labels all CMs. The yellow arrowheads point to *tbx5a:*GFP^{+} cells that are *ltbp3:*mCherry^{-} while the white arrowheads denote *ltbp3*:mCherry^{+} cells within the *tbx5a:*GFP^{-} domain. at, atrium; v, ventricle. Scale bars, 10 µm.

II *tbx5a* is expressed in FHF-derived trabecular CMs

In the adult zebrafish, the *tbx5a*:GFP expression pattern becomes restricted to the trabeculae, not being expressed in the cortical layer CMs, consistent with the recently reported pattern obtained using an enhancer fragment located 16 kb upstream of the *tbx5a* transcription start site (Goldman et al., 2017). Interestingly, we also found a small ventricular domain near the bulbus arteriosus (BA) and the atrium, where the trabeculae are also *tbx5a*:GFP^{-} (Fig. 6; Fig. 7). This pattern was confirmed by *tbx5a* ISH (Fig. 8).

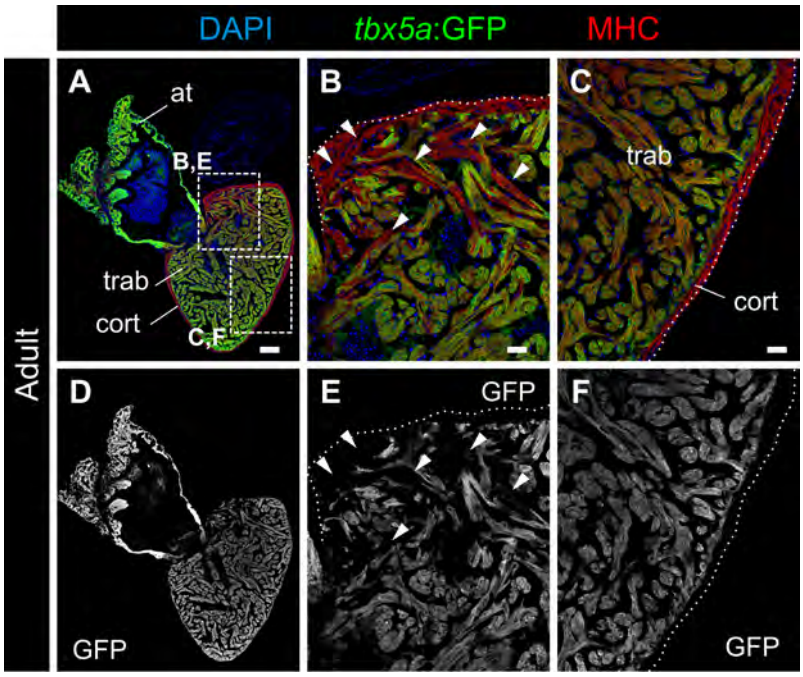

Figure 6. Expression profile of *tbx5a*-positive CMs in adult zebrafish hearts. **A–C**, Sagittal sections through a *tbx5a:GFP* adult uninjured heart immunostained with GFP (green) and MHC(red). Nuclei are counterstained with DAPI (blue). **D–F,** Single channels for GFP shown in A–C. The trabecular myocardium is *tbx5a*:GFP^{+} whereas the cortical layer is *tbx5a*:GFP^{-}. Note *tbx5a*:GFP^{-} CMs (arrowhead) in the basal part of the ventricle close to the atrio-ventricular canal (n = 13/13). at, atrium; cort, cortical layer; trab, trabecular layer. Scale bars, 100 µm (**A**), 25 µm (**B**,**C**).

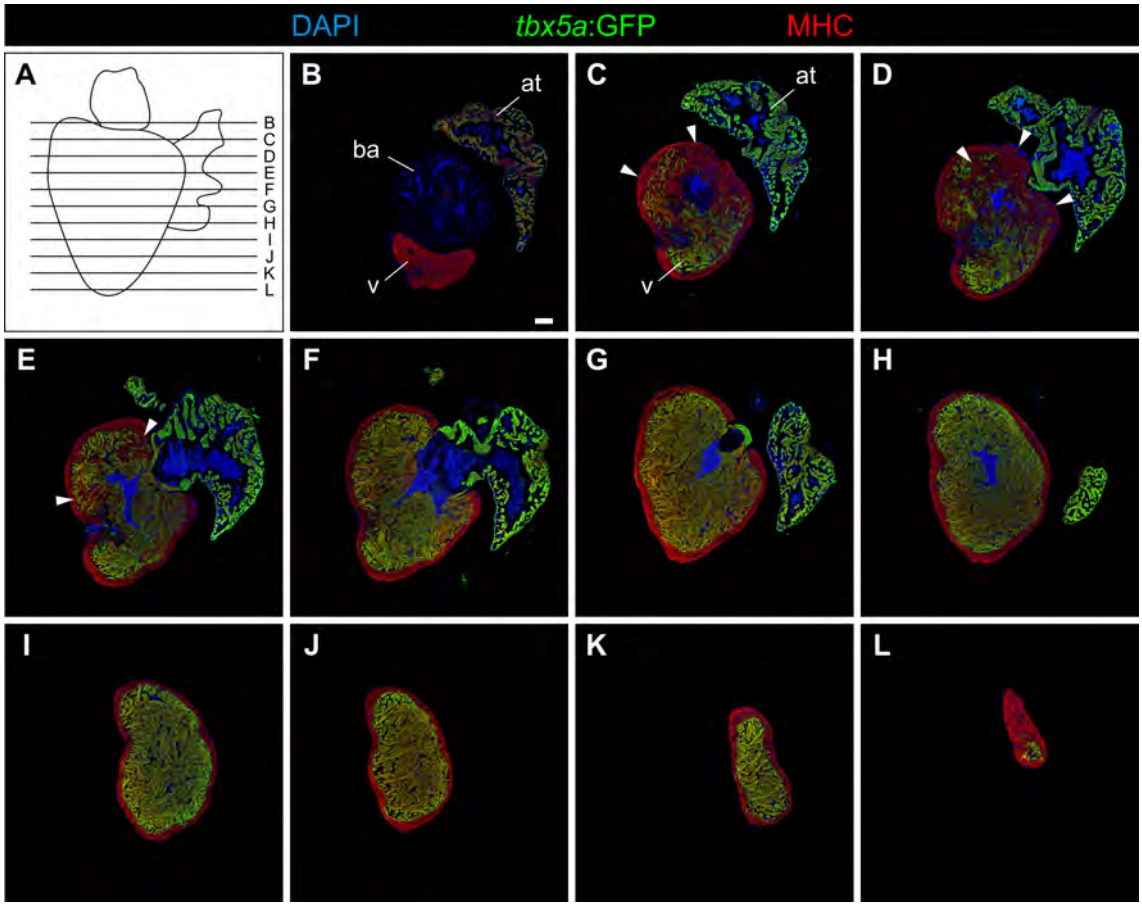

Figure 7. Serial sections of a *tbx5a*:*GFP* transgenic adult heart. A, Scheme showing the direction used for sectioning the heart and domain represented in images B–L. **B**–**L**, Serial sections of a *tbx5a*:*GFP* transgenic adult heart immunostained for GFP (*tbx5a*$^{+}$ cells; green) and MHC (CMs; red). Nuclei are counterstained with DAPI. Arrowhead marks the *tbx5a*:GFP negative region in the basal ventricle (n = 13/13). at, atrium; ba, bulbus arteriosus; v, ventricle. Scale bar, 100 µm.

tbx5a^{-} CMs in the adult heart could derive from embryonic *tbx5a*$^{+}$ cells that have switched-off their expression, or from progenitor cells that never expressed *tbx5a*. To understand how the adult pattern arises during development, we designed a system that allowed us to simultaneously label the *tbx5a* pattern and its lineage. In the *tbx5a:mCherry-p2a-CreER*^{T2}*;ubb:loxP-lacZ-loxP-GFP* double transgenic line, mCherry reproduces the *tbx5a* pattern, while GFP labels the cells that expressed *tbx5a* at the time of 4-OHT administration (Fig. 9 A).

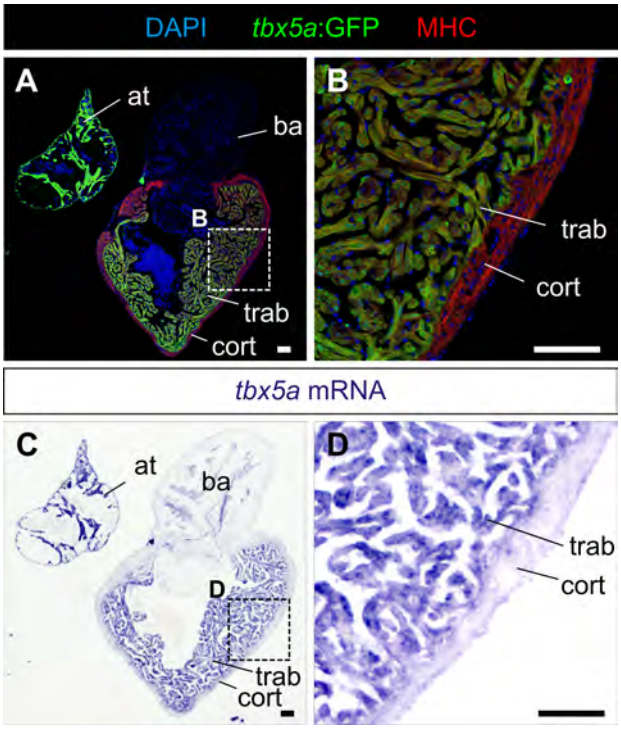

Figure 8. The transgenic *tbx5a:GFP* reporter line recapitulates the expression of endogenous *tbx5a*. **A,B**, Sagittal section through an adult *tbx5a*:*GFP* zebrafish heart immunostained for GFP and MHC, n=8. **C,D**, mRNA ISH with a *tbx5a* antisense riboprobe on the adjacent section shown in A and B. Note expression of GFP and *tbx5a* mRNA in the trabecular myocardium and their absence of expression in the cortical myocardium. B and D are zoomed views of boxed areas in A and C (n = 8/8). at, atrium; ba, bulbus arteriosus; cort, cortical layer; trab, trabecular layer. Scale bars, 100 μm.

This transgenic combination was not leaky, and GFP-expressing cells were visible only upon 4-OHT administration (Fig. 9 B). After treatment with 4-OHT from 24 hpf to 84 hpf, most of the atrial CMs and posterior ventricular CMs were labelled, as were some epicardial cells (Fig. 9 C–F).

When analysed in adult hearts, the cortical layer was mCherry^{-}, in agreement with our observations using the reporter *tbx5a:GFP*. However, it was GFP^{+} (Fig. 9 G–R) and thus derived from an embryonic *tbx5a*$^{+}$ population. By contrast, the basal domain was both mCherry^{-} and GFP^{-}. Thus, these cells had never expressed *tbx5a* indicating that the lack of *tbx5a* expression reflects the SHF developmental origin of these CMs.

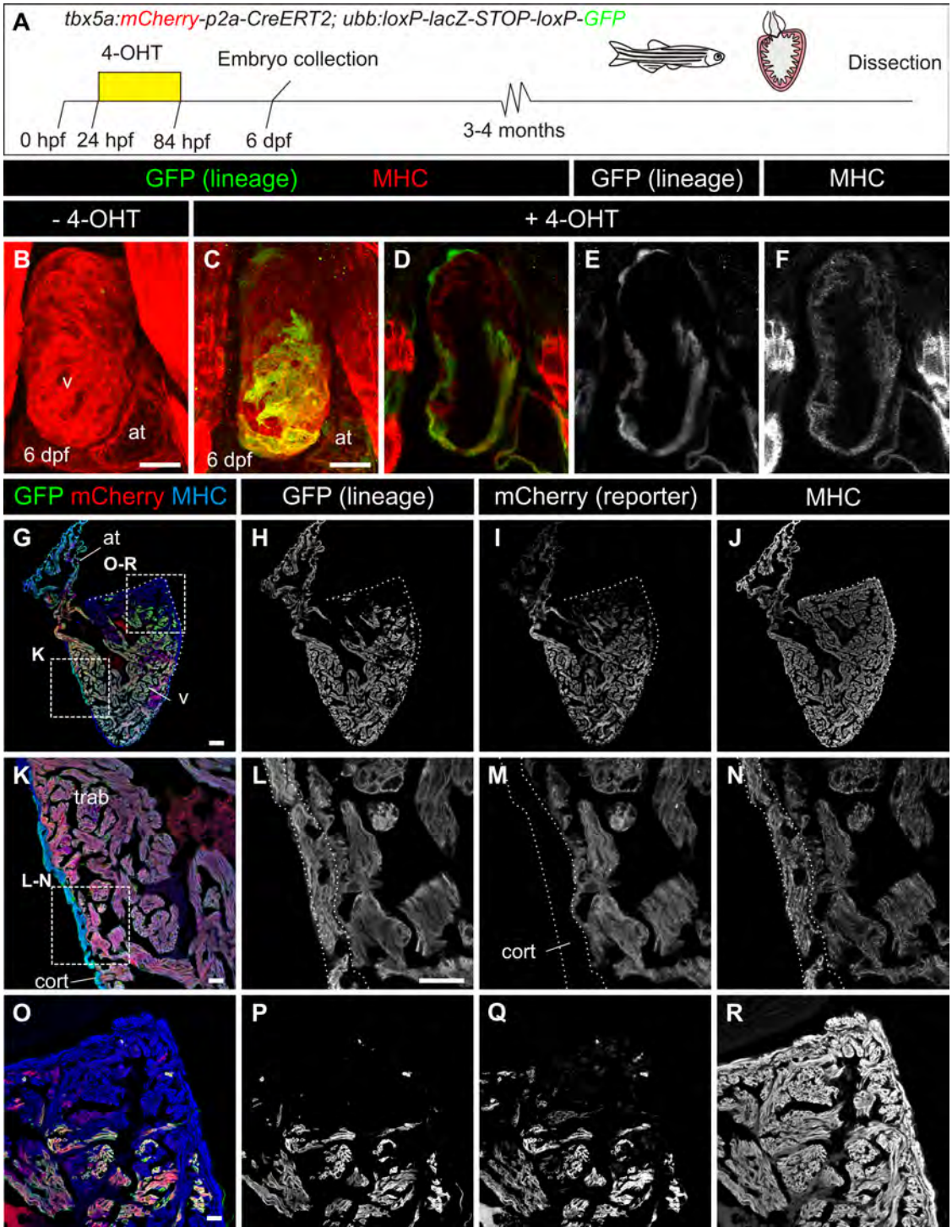

Figure 9. Fate mapping of *tbx5a*-derived cells during cardiac development. A, Hearts from *tbx5a*:*mCherry-p2A-CreER*^{T2};*ubb*:*loxP-LacZ-STOP-loxP-GFP* zebrafish fixed at different stages postfertilisation. *tbx5a* expression was revealed by mCherry expression; 4-OHT was administered to trace the fate of *tbx5a*-derived cells by GFP expression. **B–F**, Whole mount ventral view of hearts at 6 dpf stained for GFP (green) and MHC (red). **B**, In the absence of 4-OHT administration no GFP^{+} cells are visible (n = 5/5). **C–F**, 4-OHT was added from 24 to 84 hpf. GFP expression is observed in the proximal part of the ventricle (n = 8/8). In some cases, GFP expression was also found in epicardial cells located in the distal part of the ventricle. **G–R**, Immunofluorescence staining of adult heart sections recombined as in C (n = 5/5). Shown are merged and single channels for GFP (green), mCherry (red) and anti-MHC staining (blue). at, atrium; cort, cortical layer; trab, trabecular layer; v, ventricle. Scale bars 100 µm (**G**), 25 µm (**B**, **C**, **K**, **L**, **O**).

III CMs plasticity during development

We evaluated the potential plasticity of FHF- and SHF-derived CMs by designing a very specific ablation system that would allow the ablation of FHF-derived ventricular CMs.

We generated a *tbx5a:CreER*^{T2} line and crossed it into a ventricular-specific *vmhcl:loxP-tagBFP-loxP-mCherry-NTR* line (Fig. 10 A–F) (Singh et al., 2016; Wu et al., 2015). In this system, 4-OHT administration allows the labelling of *tbx5a*-derived ventricular CMs with mCherry-NTR. These cells can be ablated in a second step by administering Mtz.

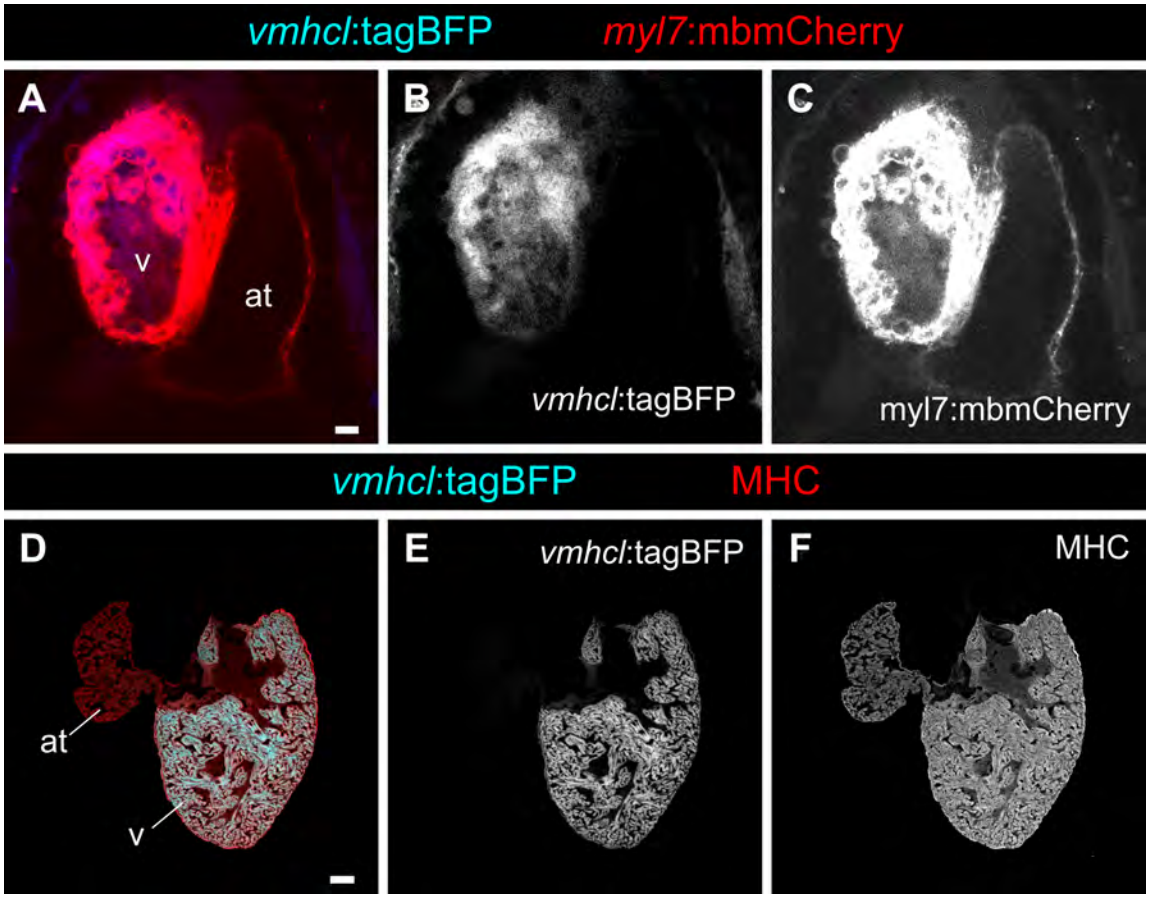

Figure 10. Controls of FHF ablation. A–C, Hearts from larvae at 4 dpf showing that the *vmhcl:loxP-tagBFP-loxP-mCherry-NTR* line is specific for ventricular CMs (n = 10/10). **D–F**, Specificity and expression is maintained in the adult (n = 10/10). **G–J**, *tbx5a*:*CreER*^{T2};*ubb*:*loxP-GFP-loxP-mCherry* at 4 dpf treated as shown in G revealing that all atrial CMs are *tbx5a*$^{+}$-derived (mCherry, red) (n = 9/9). at, atrium; v, ventricle. Scale bars, 10 µm (A, H), 100 µm (D).

In addition to being tissue specific, this strategy provides precise temporal control, allowing the possibility to independently control cell labelling and ablation. Moreover, as cells are genetically labelled by the Cre recombinase, our system allows the lineage tracing of cells after ablation.

We labelled the FHF-derived ventricular CMs with mCherry by administering 4-OHT from 24 to 48 hpf, while the SHF-derived ventricular CMs remained tagBFP^{+} (Fig. 11 A–C). When these

fish reached adulthood, the majority of the ventricle was mCherry^{+}, whereas only a few CMs next to the atria and the BA were tagBFP^{+} (Fig. 11 D,E). This supports our previous results on the contribution of FHF and SHF to the adult heart. Surprisingly, in those hearts that had been treated with Mtz to ablate the FHF-derived cells, we found that the whole ventricle was derived from the few SHF-derived ventricular CMs that had not been ablated (Fig. 11 F–H; Fig. 12).

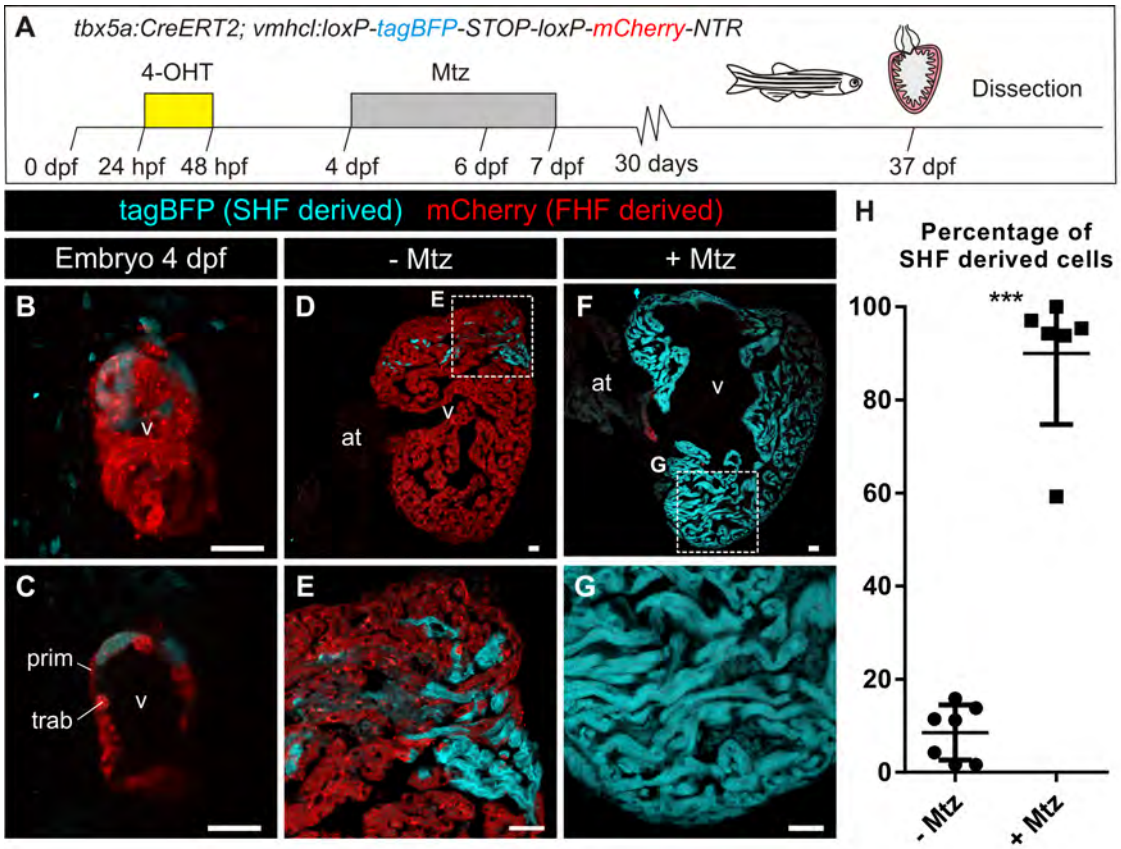

Figure 11. Genetic ablation of *tbx5a*-derived ventricular CMs. A, *tbx5a*$^{+}$ ventricular CMs were genetically ablated in *tbx5a*:*CreER*^{T2};*vmhcl*:*loxP-tagBFP-loxP-mCherry-NTR* double transgenic zebrafish. Recombination was induced by administration of 4-OHT. Cell ablation was induced by administration of Mtz from 4 to 7 dpf. Hearts were dissected 30 days later and at 6 dpf to evaluate cell death. **B**,**C**, Ventral views of larval hearts at 4 dpf. Anterior is to the top. Note that the proximal ventricle, including primordial layer and trabeculae, is completely mCherry^{+}, and that the distal ventricle is blue (tagBFP^{+}) (n = 7/7). **D,E**, Sagittal section of the ventricle of an adult recombined heart. Most cells are mCherry^{+}. Only the *tbx5a*$^{-}$ region is tagBFP^{+} (n = 7/7). E is a zoomed view of boxed area in D. **F**,**G**, Sagittal section of an Mtz-treated fish. Most of the CMs are tagBFP^{+} (n = 6/6). G is a zoomed view of boxed area in F. **H**, Quantification of the percentage of myocardium that is tagBFP^{+} (SHF-derived), mean±s.d; *** P<0.0001 by two-tailed unpaired t-test. at, atrium; prim, primordial layer; v, ventricle. Scale bars, 25 µm.

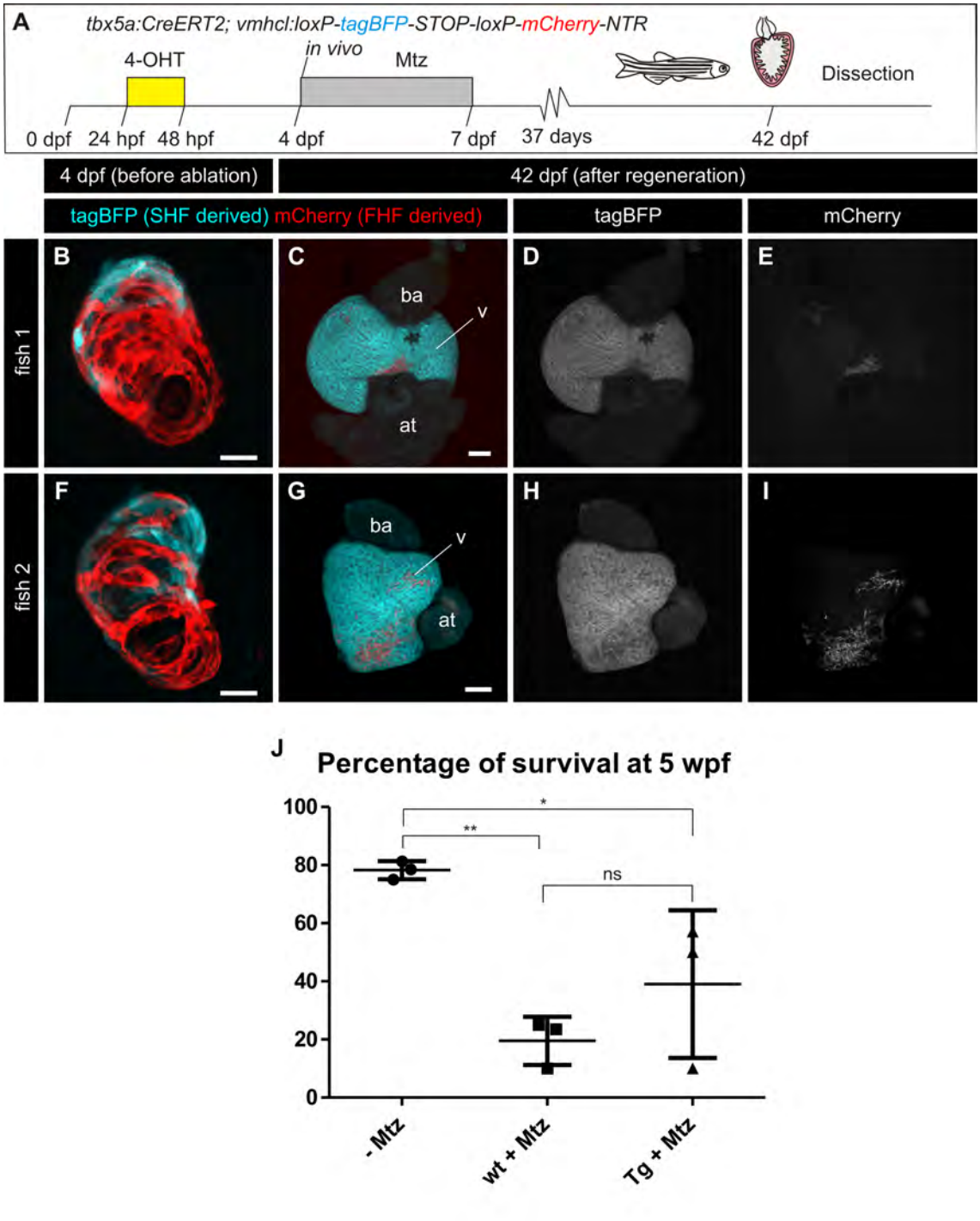

Figure 12. Longitudinal assessment of *tbx5a*-derived ventricular CMs genetic ablation. A, *tbx5a*$^{+}$ ventricular CMs were genetically ablated in individual *tbx5a*:*CreER*^{T2};*vmhcl*:*loxP-tagBFP-loxP-mCherry-NTR* double transgenic zebrafish. Recombination was induced by administration of 4-OHT. Fish were individualised, imaged at 4 dpf and cell ablation was induced by administration of Mtz from 4 to 7 dpf. **B**,**F**, Maximum projection of confocal z-stacks of 4 dpf embryos. **C**–**E**, **G**–**I**, 42 dpf zebrafish hearts that had regenerated after ablation. at, atrium; ba, bulbus arteriosus; v, ventricle. Scale bars, 25 µm (B,F), 100 µm (C,G). **J**, Percentage of survival at 5 wpf; mean±s.d **P<0.01; *P<0.05; ns, non-significant by one-way ANOVA followed by Tukey's multiple comparisons test. Each point represents the survival percentage of a group comprising 14-22 fish each. –Mtz: same stages control fish; sib + Mtz= *tbx5a*:*CreER*^{T2} and *vmhcl*:*loxP-tagBFP-loxP-mCherry-NTR* single transgenic siblings; Tg + Mtz= *tbx5a*:*CreER*^{T2};*vmhcl*:*loxP-tagBFP-loxP-mCherry-NTR* double transgenic fish.

Structural regeneration was almost perfect, with the only difference being that the regenerated heart was more rounded than those hearts in which we had not ablated CMs. The recovery was also functional. While there was a decrease in ventricular contractility at larval stages immediately after ablation (Fig. 13 A–E; Supplementary Video 5), cardiac function was recovered in the adult heart (Fig. 13 F).

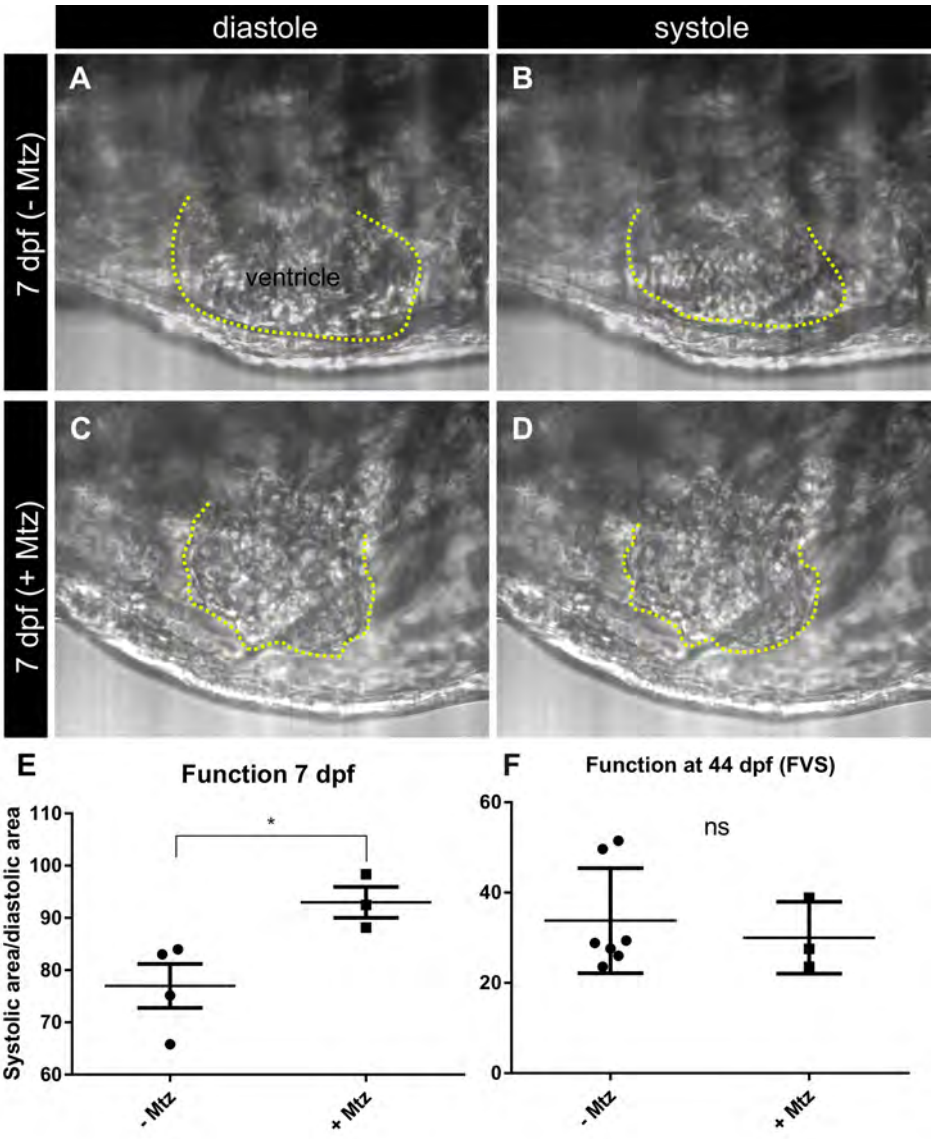

Figure 13. Cardiac performance after ablation of *tbx5a*-derived cells. *tbx5a*$^{+}$ ventricular CMs were genetically ablated in *tbx5a:CreER*^{T2}*;vmhcl:loxP-tagBFP-loxP-mCherry-NTR* double transgenic zebrafish. Recombination was induced by administration of 4-OHT at 1 and 2 dpf. Animals were divided into two groups. Cell ablation was induced in one group by administration of Mtz from 4 to 7 dpf. Videos were acquired at 7 dpf, immediately after the last Mtz treatment. **A**–**D,** Still images from the videos from two Mtz-treated (from a total of 4) and two non-treated (from a total of 3) animals. Shown are lateral views of the heart, the head is to the left. The ventricle is outlines in yellow. Note the irregular shape and overall smaller area in Mtz-treated hearts. **E**, The maximum (diastolic) and minimum (systolic) ventricular area was measured to determine ventricular function. P=0.0348 by a two-tailed t-test. Deficient contraction was detected upon Mtz treatment. **F**, Assessment of ventricular fractional volume shortening (FVS) by echocardiography at 44 dpf. Shown are individual measurements as well as mean±s.d; ns, P = 0.6262 by two-tailed unpaired t-test.

We further confirmed these results by TUNEL staining. Whereas a significant number of mCherry^{+}/TUNEL^{+} CMs was detected in the Mtz-treated fish, they were not detected in the untreated fish (Fig. 14 A–F). To gain more insight into the mechanisms driving this regeneration, we added BrdU to fish water simultaneously with Mtz treatment (Fig. 14 H–L) and fixed them at 6 dpf. A significant increase in the proliferation of tagBFP^{+} cells but not of mCherry^{+} cells was detected, supporting the idea that tagBFP^{+} cells contribute to the regeneration of the ventricle. Interestingly, the tagBFP^{+} domain had already expanded at that time (Fig. 14 I), indicating that regeneration is at least partially concurrent with cell death.

Overall, our results demonstrate that the loss of FHF-derived CMs is compensated by an expansion of SHF-derived CMs.

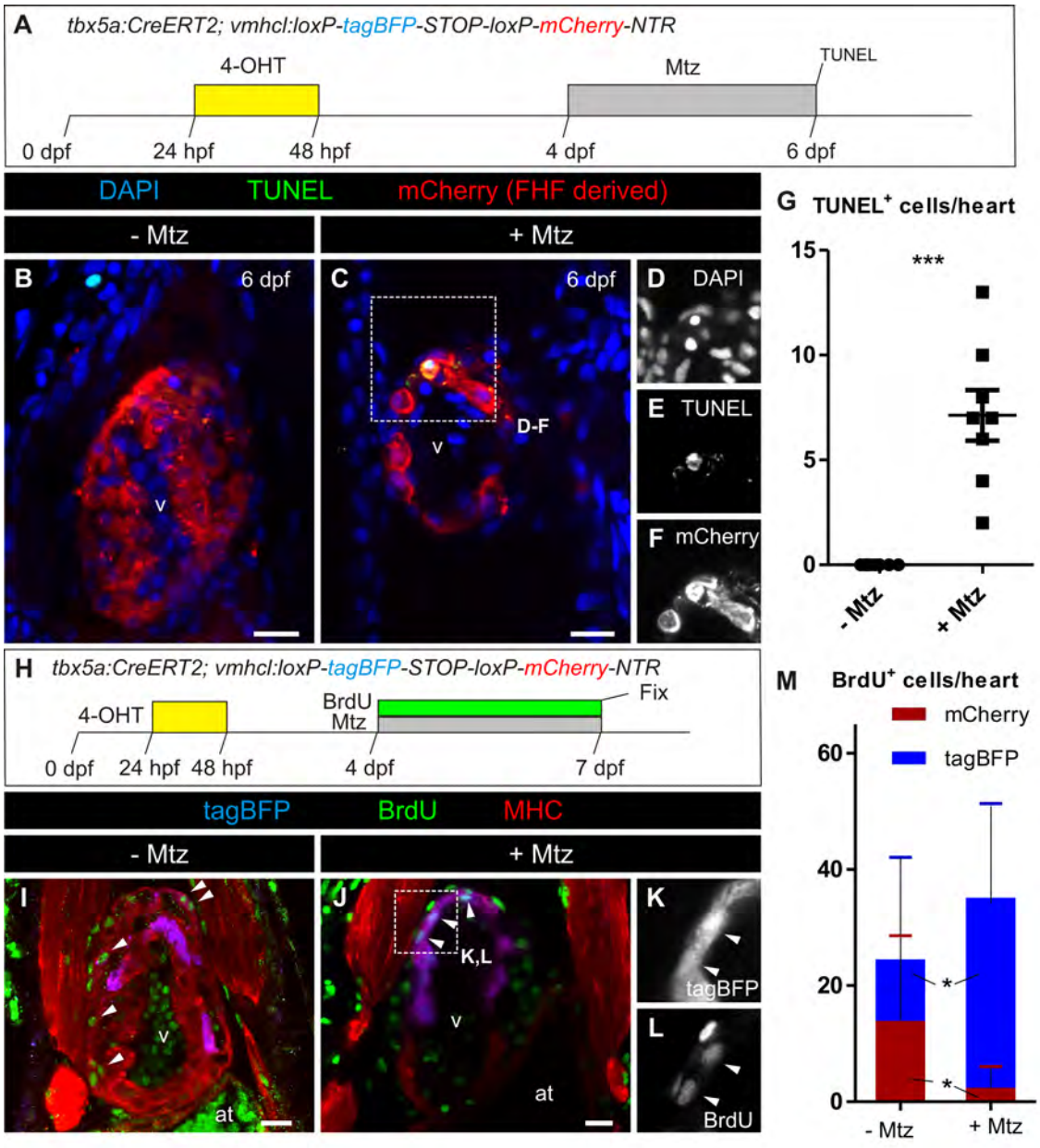

Figure 14. Genetic ablation of *tbx5a*-derived ventricular CMs. A, Schematic representation of 4-OHT and Mtz treatment. **B**,**C**, Optical sections of 6 dpf fish treated with 4-OHT and Mtz as indicated in A (B, n = 8) or only with 4-OHT (C, n = 8) immunostained for mCherry (red) and TUNEL (green). Note that some mCherry$^+$ cells are rounded and are TUNEL$^+$. **D**–**F**, Single channels of selected area in **C**. **G**, Quantification of the number of TUNEL$^+$ cells per heart, mean±s.d; ***P=0.0004 by Mann-Whitney non-parametric t-test. **H**, Schematic representation of the BrdU treatment to assess proliferation. **I**,**J**, Fish were treated with 4-OHT and BrdU (I, n = 8) or with 4-OHT, Mtz and BrdU (J, n = 11). **K**,**L**, Single channels of the boxed area in **J**. **M**, Quantification of BrdU$^+$/mCherry$^+$ and BrdU$^+$tagBFP$^+$ cells per heart. Shown are means±s.d (n = 8 for -Mtz hearts and n = 11 for + Mtz hearts, from two technical replicates) *P=0.0240 for tagBFP$^+$ cells and P=0.0371 for mCherry$^+$ cells by two-tailed t-test. at, atrium; prim, primordial layer; trab, trabeculae; v, ventricle. Scale bars, 25 µm.

IV Cardiomyocyte plasticity during adult heart regeneration

We next explored whether the observed CM plasticity remains in the adult. To study the contribution of trabecular CMs, we first analysed the expression pattern of the trabecule-specific marker *tbx5a* during regeneration using the *tbx5a*:GFP transgenic line. At 1 dpi (Fig. 15 A–F), no GFP expression could be found in the cortical layer. At 3, 7 and 21 dpi (Fig. 15 G–U), a few *tbx5a*:GFP$^+$ CMs could be observed in the cortical layer close to the injured area. Nonetheless, at 130 dpi, the regenerated cortical myocardium was *tbx5a*:GFP$^-$ (Fig. 15 V–Z). At this stage we could also detect that the newly regenerated cortical layer is thicker, in agreement with previous studies (González-Rosa et al., 2014).

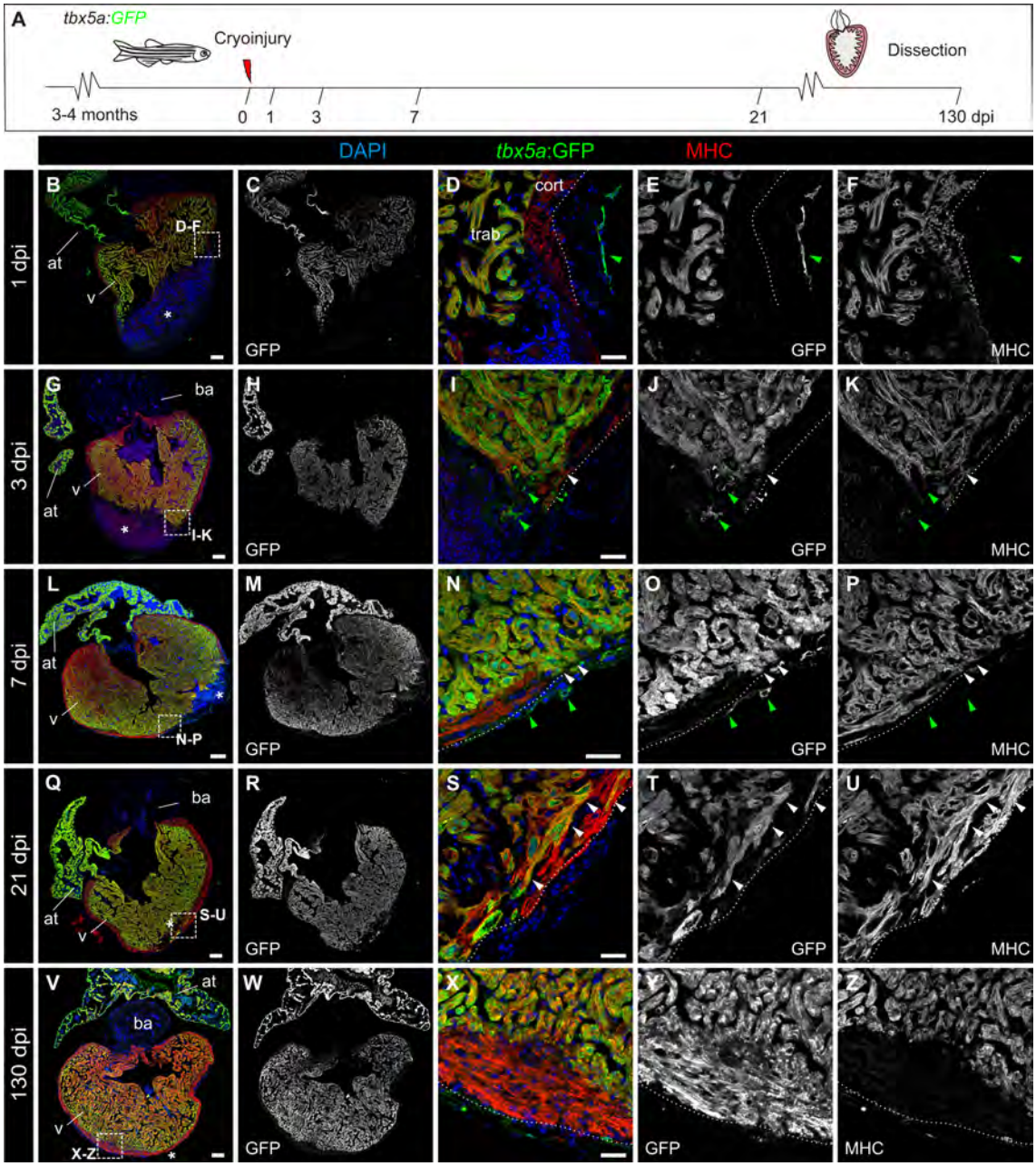

Figure 15. Expression of *tbx5a*:GFP during adult heart regeneration. A, Illustration of the experimental setup. **B**–**Z**, Sagittal sections through *tbx5a:GFP* hearts at 1 (**B**–**F**, n = 4/4), 3 (**G**–**K**, n = 4/5), 7 (**L**–**P**, n = 3/3), 21 (**Q**–**U**, n = 4/4) and 130 (**V**–**Z**, n = 4/4) days post injury (dpi). Sections were immunostained with anti-GFP (green) and anti-MHC (red). Nuclei are counterstained with DAPI (blue). Asterisks indicates the injury area. The expression of *tbx5a*:GFP is limited to the trabecular myocardium. *tbx5a*:GFP expression is also visible in a few myosin-negative cells within the epicardial layer (green arrowheads). At 130dpi, a *tbx5a*:GFP^{-} thickened cortical myocardium covers a *tbx5a*:GFP^{+} trabecular myocardium at the injury site (**V**–**Z**). White arrowheads point to *tbx5a*:GFP^{+} CMs; green arrowheads label *tbx5a*:GFP^{+} non-CMs. Scale bars, 100 µm (**B**,**G**,**L**,**Q**,**V**), 25 µm (**D**,**I**,**N**,**S**,**X**).

Two explanations can be offered for the transient expression of *tbx5a* in cortical CMs: (a) *tbx5a* is re-expressed transiently in the cortical layer during regeneration, or (b) trabecular CMs are contributing to the new cortical layer.

To address this, we used the *tbx5a:mCherry-p2a-CreER^{T2};ubb:loxP-lacZ-loxP-GFP* double transgenic line. Upon recombination in the adult stage, GFP expression was restricted to the trabeculae in uninjured hearts (Fig. 16 A–G), and only were detected GFP$^+$ cells observed in the cortical myocardium (2 cells in 1/6 completely sectioned hearts). All of the GFP-labelled CMs were also mCherry$^+$. At 21 and 90 dpi, when heart regeneration had progressed, the newly formed cortical layer was mCherry$^-$; as expected, but surprisingly, there were some GFP$^+$ CMs that had switched off mCherry expression (Fig. 16 N–X). Based on the percentage of trabecular CMs that are GFP$^+$, the recombination efficiency was estimated to be 10 ± 6 %. In the newly formed cortical layer, 7 ± 4 % of CMs were GFP$^+$ (n = 10). These results indicate that trabecular CMs contribute to 70 ± 40 % of the regenerated cortical layer.

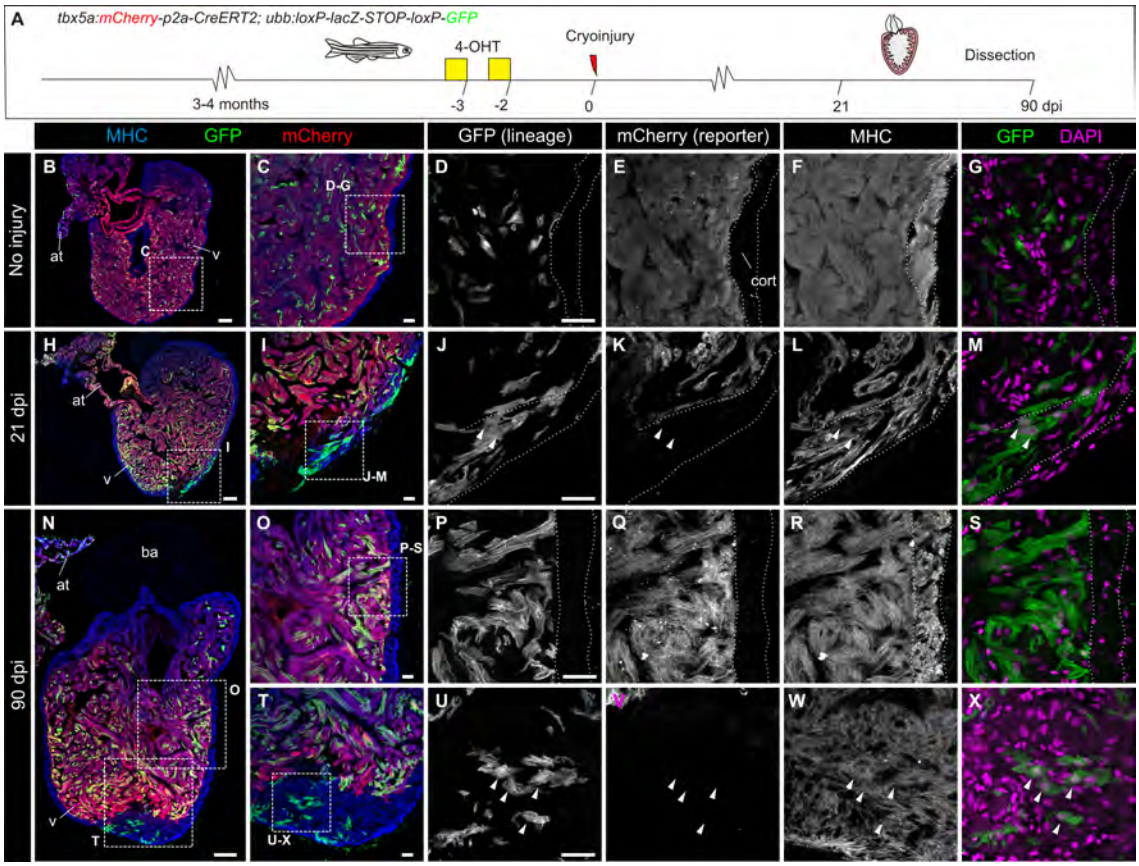

Figure 16. Contribution of *tbx5a*-derived cells during regeneration of the adult zebrafish heart. A, *tbx5a*:*Cherry-p2A-CreER^{T2}* was crossed into *ubb*:*loxP-lacZ-STOP-loxP-GFP*. 4-OHT was added 2 and 3 days before cryoinjury to induce recombination of *loxP* sites. Hearts were fixed at 21 and 90 dpi and sectioned for immunofluorescent detection of GFP$^+$ *tbx5a*-derived cells and mCherry$^+$ *tbx5a*-expressing cells. Nuclei were counterstained with DAPI. **B**, In the uninjured heart, mCherry expression was homogeneous in the trabecular myocardium and absent in the cortical layer (n = 7/7). GFP$^+$ cells were found in the trabecular layer. **C**, Zoomed view of boxed area in B**. D**–**G**, Single channels of boxed area shown in C. **H**,**N**, Section of a hearts at 21 (**H**, n = 6/7) and 90 dpi (**N**, n = 6/6). Upon cryoinjury to the ventricular apex, *tbx5a*$^+$ CMs in general were restricted to the trabecular myocardium. **O**–**S**, *tbx5a*-derived CMs were present also in the cortical layer, particularly at the site of injury (**I**–**M**,**T**–**X**). Nuclear counterstaining revealed GFP$^+$ cell bodies in the cortical layer (arrowheads). at, atrium, ba, bulbus arteriosus; v, ventricle. Scale bars, 100 µm (**B**,**H**,**N**), 25 µm (**C**,**D**,**I**,**J**,**O**,**P**,**T**,**U**).

Importantly, this result cannot be explained by leakiness of the genetic system, as no recombined cells could be observed in the absence of 4-OHT treatment (Fig. 17 A–K). The possibility that residual 4-OHT triggers recombination of the *tbx5a*$^{+}$ cells in the cortical layer was also excluded by doing the 4-OHT treatment long time before the cryoinjury (Fig. 17 L–Q).

Our results indicate that trabecular CMs contribute to the regeneration of the cortical layer and during this process they switch off the trabecular marker *tbx5a*.

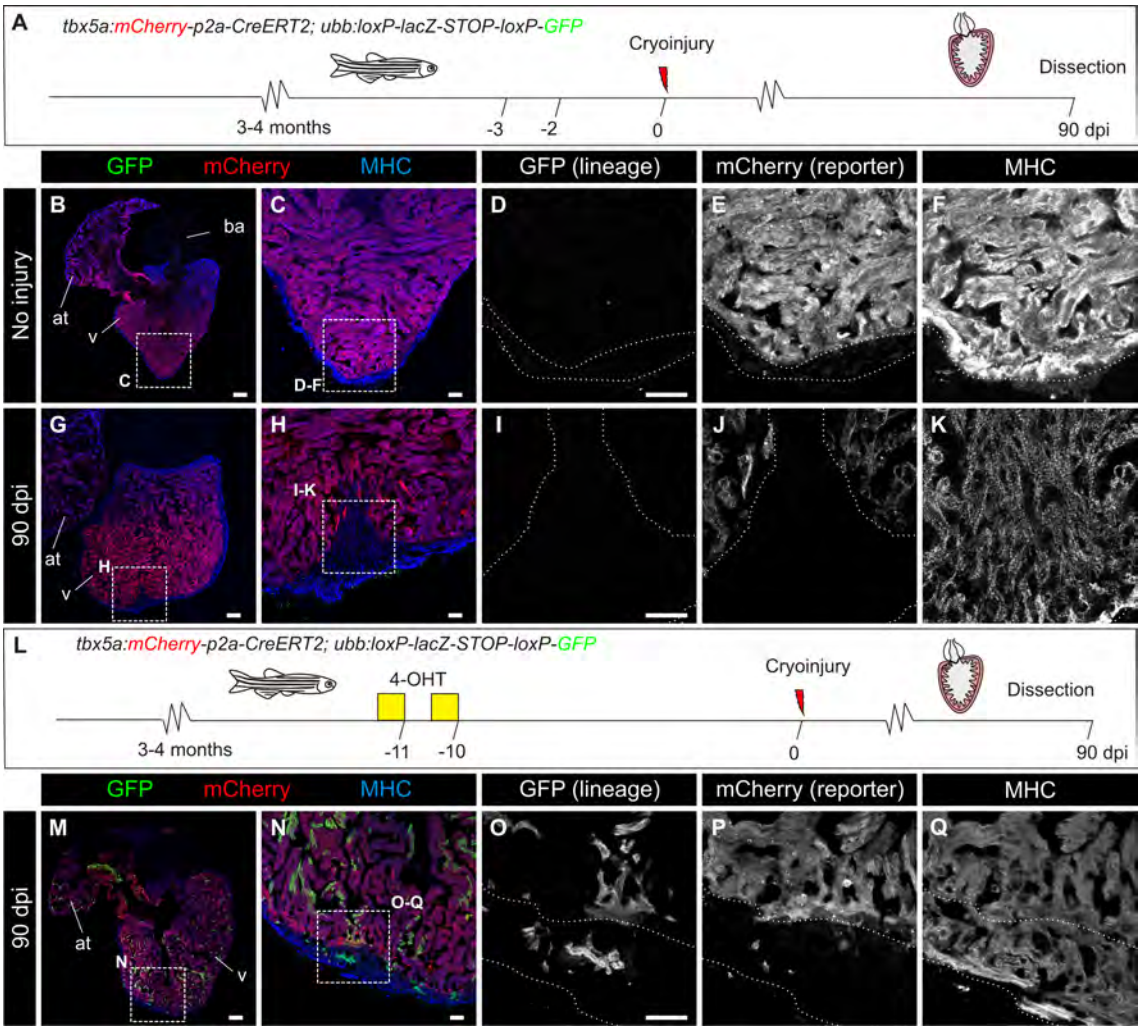

Figure 17. Trabecular CMs lineage tracing control experiments. A–K *loxP* sites in *tbx5a*:*Cherryp-2a-CreER*^{T2};*ubb*:*loxP-lacZ-STOP-loxP-GFP* do not recombine in the absence of 4-OHT **A**, *tbx5a:Cherry-p2A-CreER*^{T2} was crossed into *ubb*:*loxP-lacZ-STOP-loxP-GFP*. Fish were cryoinjured but not treated with 4-OHT. **B–L**, Heart before injury. No recombined cells were observed (n = 4/4). **G–K**, Hearts were injured and dissected at 90 dpi. Again, no GFP^{+} recombined cells were visible at the regenerated area (n = 3/3). **L–Q**, Recombination is not due to the persistence of 4-OHT in the adult fish beyond cryoinjury. **L**, *tbx5a*:*mCherry-p2a-CreER*^{T2} was crossed into *ubb*:*loxP-lacZ-STOP-loxP-GFP*. Fish were treated with 4-OHT during days 11 to 10 before the injury. **M–Q**, Contribution of GFP^{+} trabeculae to the new compact layer and *tbx5a*:mCherry switch off in these cells can be observed (n = 3/3). at, atrium; v, ventricle. Scale bars, 100 µm (**B**,**G**,**M**), 25 µm (**C**,**D**,**H**,**I**, **N**,**O**).

V New cortical layer markers and their expression pattern during regeneration

Aside from *nppa* (Jensen et al., 2012) and the here reported *tbx5a*, no other markers have been reported to differentiate the cortical from the trabecular myocardium in the zebrafish. To ascertain whether *tbx5a*-derived trabecular CMs not only relocate into the cortical region and switch off *tbx5a* but also adopt the expression of cortical marker genes, we performed RNA-Seq analysis to compare *tbx5a*$^{-}$ and *tbx5a*$^{+}$ CMs isolated from adult ventricles (Fig. 18 A,B). We found that the top gene differentially expressed between the two populations was *tbx5a*, further supporting the notion that our transgenic line recapitulates the endogenous pattern. Interestingly, we found that CM junction- (*xirp2a*), non-muscle actomyosin- (*acta2* and *myh10*), ECM- (*lama5*) and caveolin-related (*ehd2b* and *cav1*) genes were expressed specifically in the cortical layer (Fig. 18 C,D; Supplementary Table 1).

To validate some of these genes as cortical layer myocardium markers, we performed immunohistochemistry to detect the protein product of the actin-binding gene *xirp2a*. It was enriched in the cortical and primordial layer of an uninjured hearts, with a pattern mirroring that of *tbx5a*:GFP (Fig. 19 A–F). Interestingly, it was more strongly expressed in the primordial layer. Strikingly, upon injury and regeneration, the *tbx5a*-derived GFP^{+} cells that contributed to the cortical layer and switched off *tbx5a*:mCherry also expressed Xirp2a (Fig. 19 G–R).

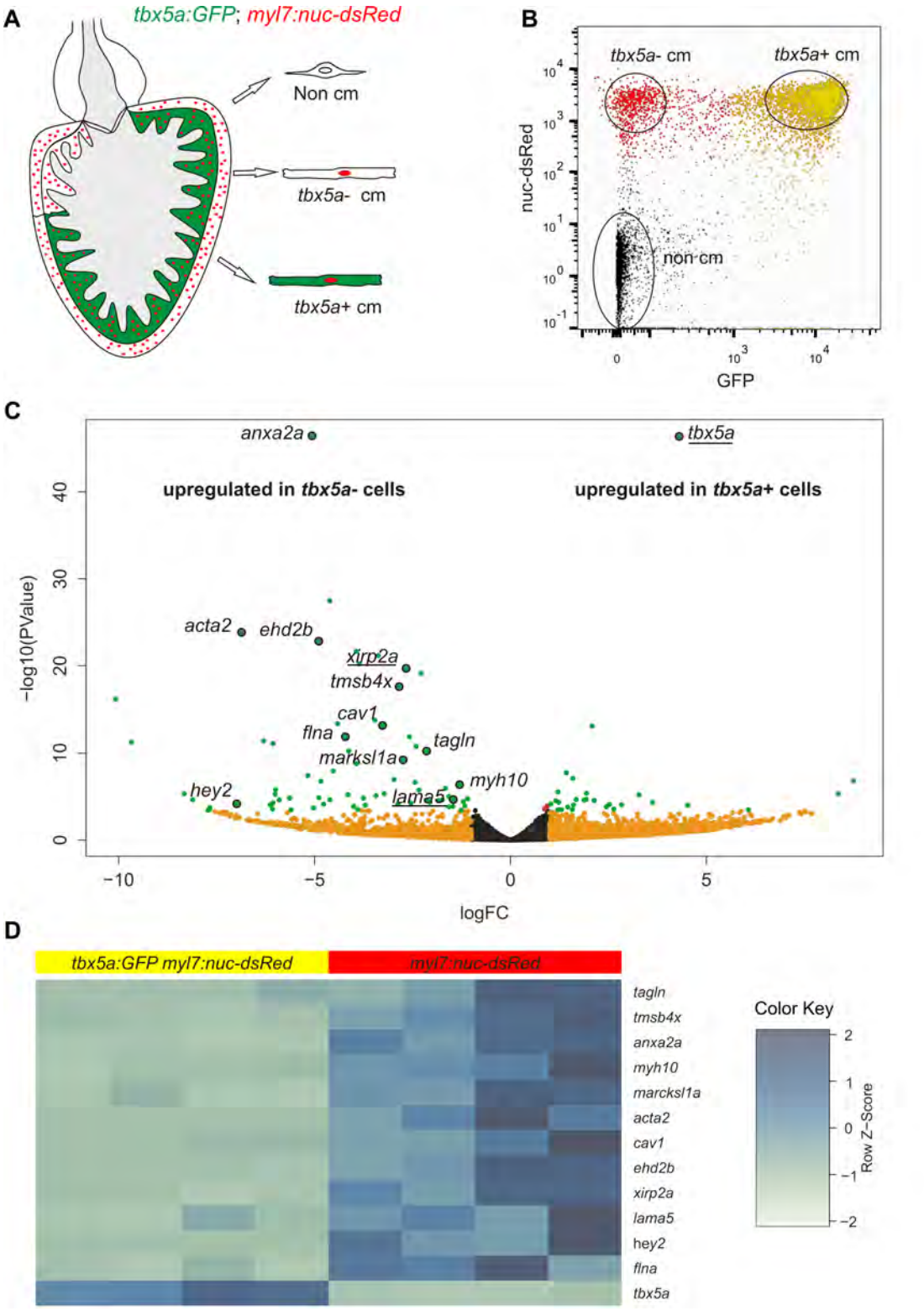

Figure 18. *tbx5a*$^{+}$ and *tbx5a*$^{-}$ CMs from adult ventricles exhibit distinct expression profiles. A,B, GFP^{+}/nuc-dsRed^{+} and GFP^{-}/nuc-dsRed^{+} CMs were FACS-sorted from adult *tbx5a*:*GFP;myl7*:*nuc-dsRed* ventricles. **C**, Volcano plot representing RNA-Seq results comparing both populations. Black, false discovery rate (FDR) > 0.05, log fold change (LFC) < 1; orange, FDR > 0.05, LFC > 1; red, FDR < 0.05, LFC < 1; green, FDR < 0.05, LFC > 1. **D**, Heatmap of genes differentially expressed in *tbx5a*$^{+}$ and *tbx5a*$^{-}$ cardiomyocytes from adult hearts. Dark blue, higher expression; light blue, lower expression.

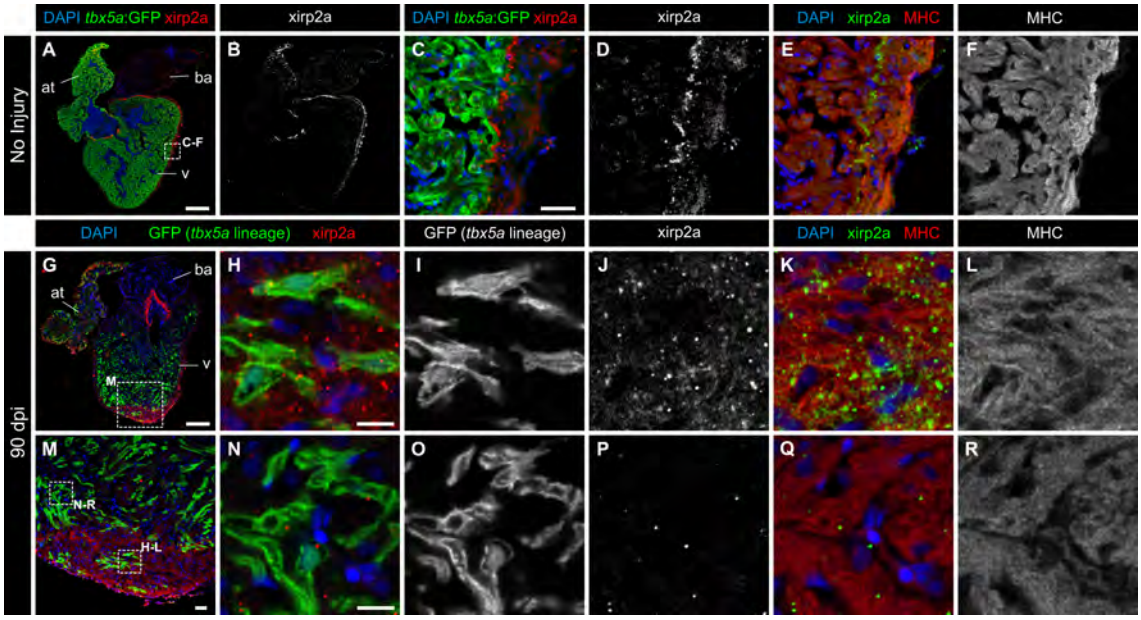

Figure 19. Trabecular *tbx5a*-derived CMs within the cortical myocardium express the cortical layer marker Xirp2a. A–R, Immunofluorescence with anti-Xirp2a and GFP on ventricle sections**. A–F**, uninjured adult *tbx5a*:*GFP* ventricle. Xirp2a expression was observed in the cortical layer but not in the trabecular layer showing a complementary pattern with *tbx5a:GFP* as predicted by RNA-Seq (n = 3/3). **G–R**, Double transgenic *tbx5a*:*mCherry-p2a-CreER*^{T2};*ubb*:*loxP-lacZ-loxP-GFP* were treated with 4-OHT from 84 to 72 and 60 to 48 hours before cryoinjury. Hearts were fixed at 90 dpi. GFP^{+} cells marking the *tbx5a* lineage within the cortical layer were positive for Xirp2a, while GFP^{+} cells within the trabecular layer did not express this marker (n = 6/6). at, atrium; ba, bulbus arteriosus; dpi, days postinjury; v, ventricle. Scale bars, 100 µm (**A**,**G**), 25 µm (**C**,**M**), 10 µm (**H**,**N**).

We further supported our results by RNAScope ISH against *lama5* (Fig. 20) and *hey2* (Fig. 21), a well stablished compact layer marker in mammalian models (Koibuchi and Chin, 2007). *nppa*, a direct target of *Tbx5* in mammals, and previously reported to be specifically expressed in trabecular zebrafish CMs, was used to test whether cortically located *tbx5a*-derived cells retained a trabecular phenotype. Results showed that whereas *hey2* and *lama5* were upregulated in the *tbx5a*-lineage traced CMs, *nppa* was downregulated (Fig. 22).

Taken together, our results indicate that trabecular *tbx5a*$^{+}$ CMs undergo a complete phenotypic switch to become cortical layer CMs. While the cortical myocardium has previously been reported to regenerate from CMs within the same layer (Gupta and Poss, 2012; Tekeli et al., 2017), our results reveal that other populations, including trabecular CMs, can also contribute to cortical layer repair in response to injury.

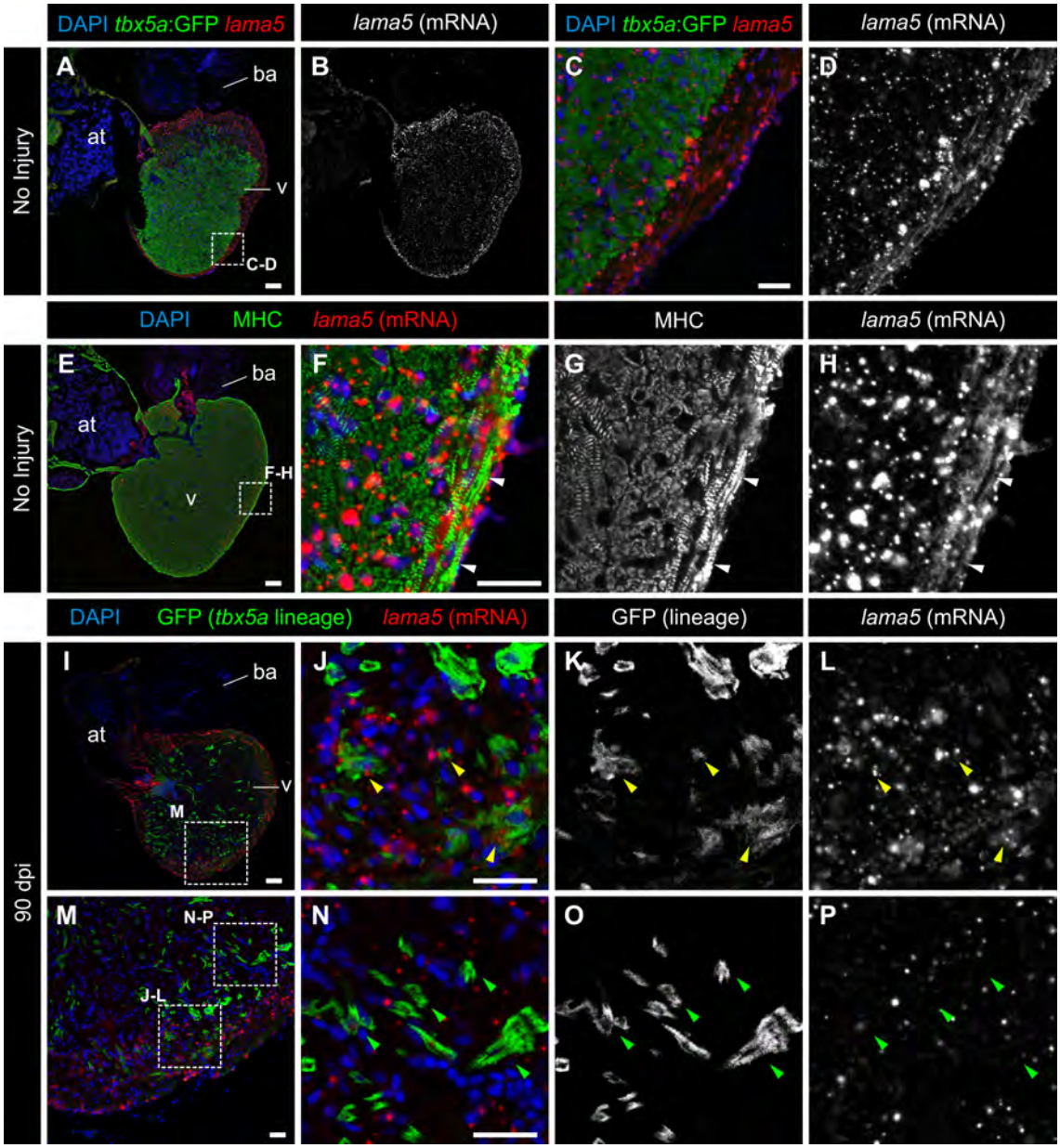

Figure 20. *tbx5a*-derived CMs within the cortical layer are *lama5* positive. GFP immunofluorescence and *lama5* RNAScope *in situ* detection on sagittal sections of *tbx5a*:*GFP* (A–H) or *tbx5a*:*mCherryp-2a-CreER*^{T2};*ubb*:*loxP-lacZ-loxP-GFP* double transgenic animals, recombined before injury and fixed at 90 dpi (I–P). Nuclei were counterstained with DAPI. **A–D,** Uninjured heart. *tbx5a*:GFP (green) does not co-localise with *lama5* (red). *lama5* is expressed at higher and more homogenous levels in the cortical layer (n = 4/4). **E–H,** Uninjured heart; anti-MHC (green) is used to mark CMs. In the cortical layer, regions of *lama5*/MHC co-localisation were detected (white arrowheads) (n = 4/4). **I–P,** 90 dpi regenerated hearts. *tbx5a*:*mCherryp-2a-CreER*^{T2};*ubb*:*loxP-lacZ-loxP-GFP* were treated with two 12 hours pulses of 4-OHT at 6 and 7 days before the injury. GFP^{+} cells marking the *tbx5a* lineage within the cortical layer were positive for *lama5* (yellow arrowheads). GFP^{+} cells within the trabecular layer were negative for that marker (green arrowheads) (n = 11/11). at, atrium; ba, bulbus arteriosus; v, ventricle. Scale bars, 100 µm (**A**,**E**,**I**), 25 µm (**C**,**F**,**J**,**N**).

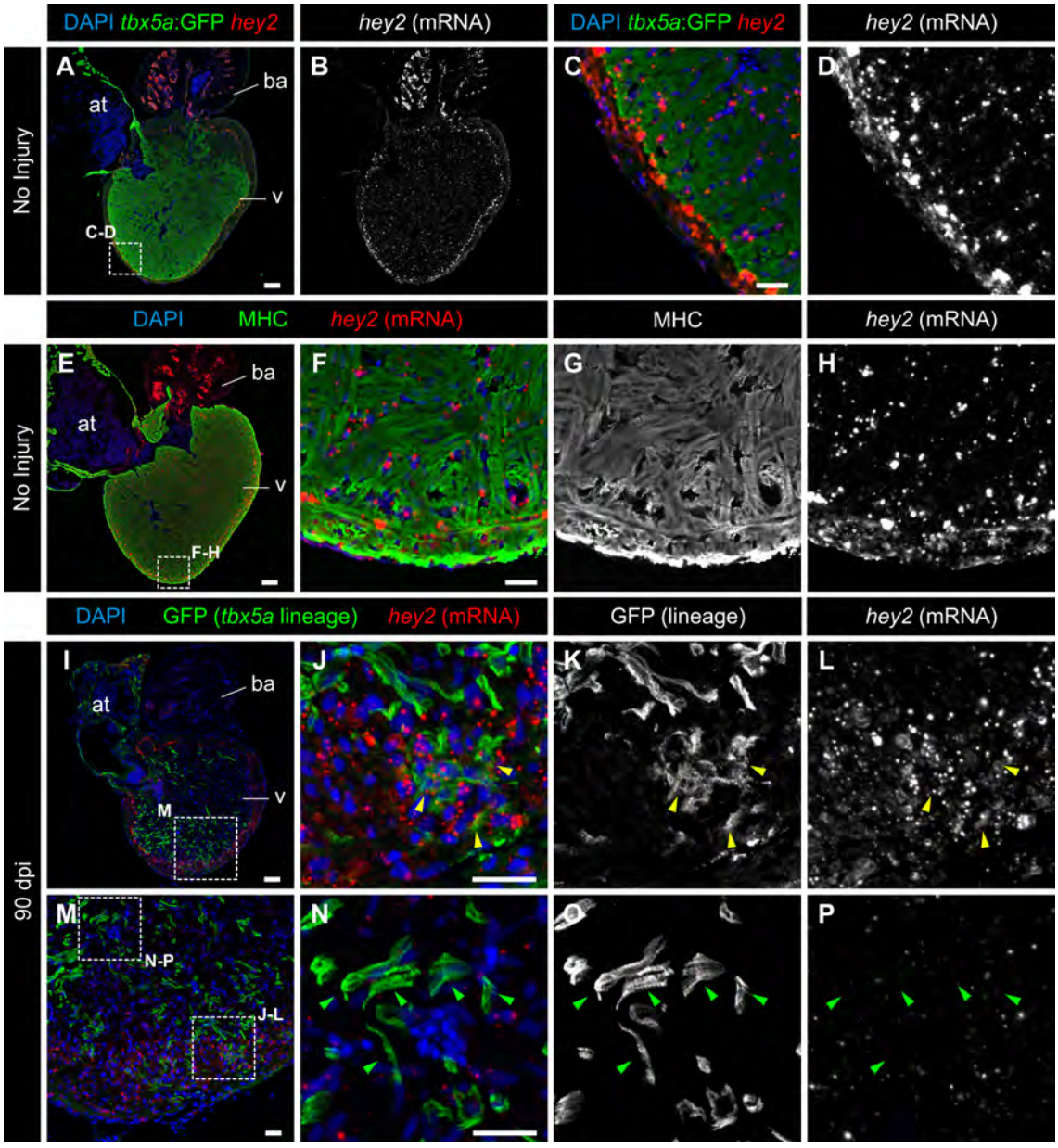

Figure 21. *tbx5a*-derived CMs within the cortical layer are *hey2* positive. GFP immunofluorescence and *hey2* RNAScope *in situ* detection on sagittal sections of *tbx5a*:*GFP* (**A**–**H**) or *tbx5a*:*mCherryp-2a-CreER*^{T2};*ubb*:*loxP-lacZ-loxP-GFP* double transgenic animals, recombined before injury and fixed at 90 dpi (I–P). Nuclei were counterstained with DAPI. **A–D,** Uninjured heart. *tbx5a*:GFP (green) does not co-localize with *hey2* (red). *Hey2* is expressed at higher and more homogenous levels in the cortical layer (n = 3/4). **E–H,** Uninjured heart**;** anti-MHC (green) is used to mark CMs. In the cortical layer, regions of *hey2*/MHC co-localisation were detected (white arrowheads) (n = 3/4). **I–P,** 90 dpi regenerated hearts. *tbx5a*:*mCherryp-2a-CreER*^{T2};*ubb*:*loxP-lacZ-loxP-GFP* were treated with two 12 hours pulses of 4-OHT at 6 and 7 days before the injury. GFP^{+} cells marking the *tbx5a* lineage within the cortical layer were positive for *hey2* (yellow arrowheads). GFP^{+} cells within the trabecular layer were negative for that marker (green arrowheads) (n = 5/6). at, atrium; ba, bulbus arteriosus; v, ventricle. Scale bars, 100 µm (**A**,**E**,**I**), 25 µm (**C**,**F**,**J**,**N**).

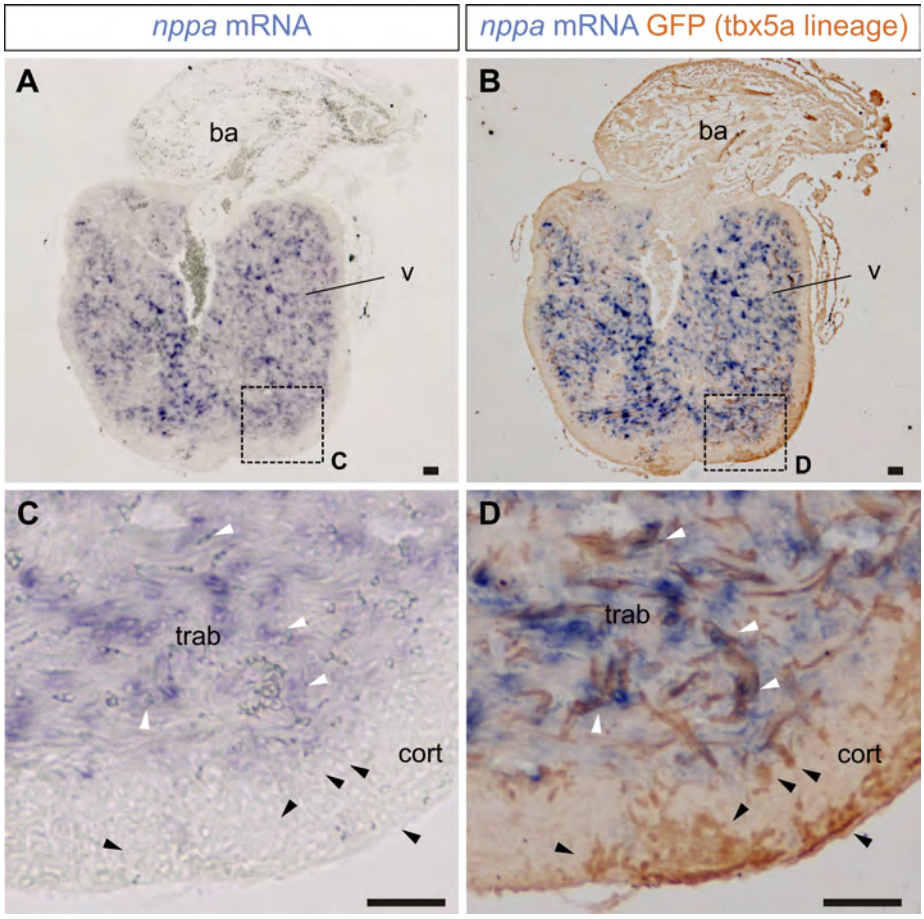

Figure 22. *tbx5a*-derived CMs within the cortical layer are *nppa* negative. A, *nppa* mRNA ISH on sagittal sections of *tbx5a*:*mCherryp-2a-CreER*^{T2};*ubb*:*loxP-lacZ-loxP-GFP* double transgenic animals, recombined before injury and fixed at 90 dpi followed by GFP immunofluorescence. **B**, *nppa* is expressed in the trabecular layer (white arrowheads). In the cortical region, tbx5a-derived GFP^{+} cells are visible, which are not positive for the trabecular marker *nppa* (black arrowheads) (n = 7/7). **C** and **D** are a zoomed with of boxed areas in **A** and **B.** ba, bulbus arteriosus; cort, cortical layer; trab, trabecular layer; v, ventricle. Scale bars, 50 µm.

VI Resident fibroblasts contribute to fibrotic tissue deposition during regeneration

Shortly after cryoinjury, a fibrosis scar is formed at the injured region, which regresses during the regeneration process (González-Rosa et al. 2011). We next sought to investigate the cell types that contribute to the production of fibrotic scarring and the fate of these fibroblasts.

While it is known that pre-existent fibroblasts are the main source of activated fibroblasts upon injury in the mammalian heart (Ali et al., 2014; Kanisicak et al., 2016; Moore-Morris et al., 2014), this has not been studied in the zebrafish. A population of cells located between the trabecular and compact layers has been described by electron microscopy. These cells have a mesenchymal morphology and are surrounded by collagen fibres (Lafontant et al., 2013).

Different strategies used to mark this population label both the epicardium and the resident fibroblast populations (Kikuchi et al. 2011; González-Rosa et al. 2012). These findings led to the conclusion that the group including epicardial and EPDCs contribute to fibroblasts (González-Rosa et al. 2012). We first confirmed this result using the *tcf21:CreER^{T2};col1a2-loxP-tagBFP-loxP-mCherry-NTR* double transgenic fish, in which mCherry the cells that express *tcf21* at the time of 4-OHT administration and *col1a2* at the time of fixation. We treated these fish with 4-OHT early in development (Fig. 23 A); we then subjected the fish to heart cryoinjury their heart at adulthood and fixed them at 7 dpi. The presence of red cells in these hearts confirmed the contribution of epicardial/EPDCs to ECM production after cryoinjury (Fig. 23).

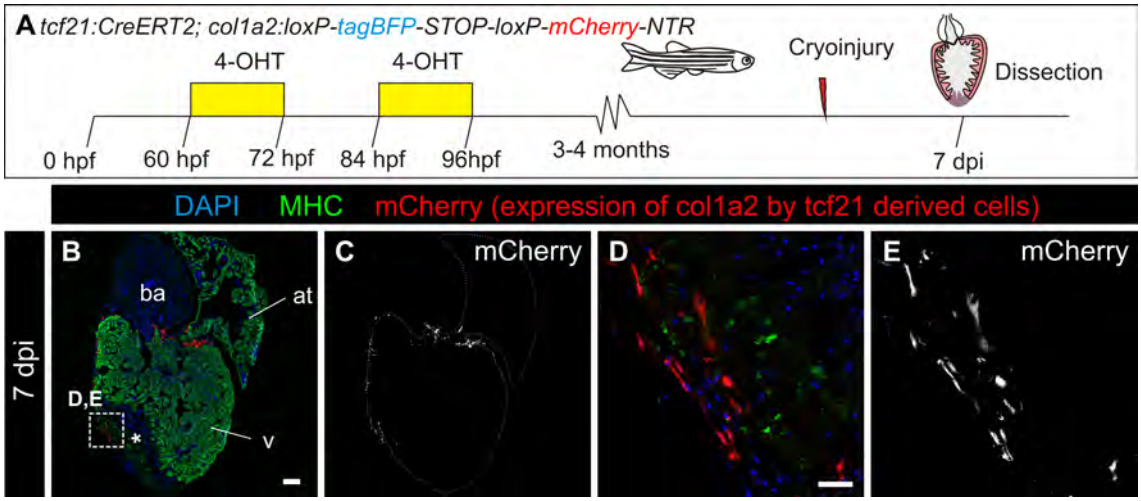

Figure 23. *tcf21*-derived cells express *col1a2* after cryoinjury. A, Experimental scheme for tracing the fate of *tcf21*-derived cells expressing *col1a2*. The *tcf21:CreER^{T2}* line was crossed into the *col1a2:loxP-tagBFP-STOP-loxP-mCherry-NTR* line, in which mCherry-NTR is not expressed. Upon 4-OHT administration, recombination of loxP sites leads to activation of mCherry expression under the control of the *col1a2* promoter. Hearts from animals at 7 dpi were dissected and sectioned. **B**–**E**, Immunofluorescence on the heart sections with anti-MHC (green), and mCherry (red). Nuclei were counterstained with DAPI. D–E are merged and individual channels of the boxed area in B. Arrowheads mark mCherry^{+} cells, which express *col1a2* (n = 5/5). at, atrium; ba, bulbus arteriosus; v, ventricle. Scale bars, 25 µm (**D**), 100 µm (**B**).

A good candidate line to exclusively label the resident fibroblast population is *wt1a:GFP* (Peralta et al., 2014). To determine if they could be considered cardiac fibroblasts, we performed an RNA-Seq experiment in which we compared these cells to the remainder of cells in the zebrafish ventricle. Results showed that *wt1a*:GFP^{+} cells were enriched in epicardial genes, but not endocardial or myocardial genes, suggesting an epicardial origin for this population. Moreover, they expressed several ECM genes, and also 8/9 genes described as the best fibroblast markers for mammalian resident fibroblasts (Fig. 24 A,B; Supplementary Table 2).

To evaluate the contribution of these cells to cardiac fibrosis after cryoinjury, we performed ISH against *postnb*. While in uninjured hearts expression was below detection limits (Fig. 24 C,D), at 7 dpf, *wt1a*:GFP^{+} cells robustly expressed *postnb* (Fig. 24 E,F).

We next evaluated *col1a2* expression by crossing the *wt1a:GFP* transgenic line to a newly generated *col1a2:mCherry-NTR* line. We calculated that 57 ± 8 % of *wt1a*:GFP^{+} cells expressed *col1a2*:mCherry-NTR (Fig. 24 G–K), supporting the idea that *wt1a*:GFP labels resident fibroblasts. At 7 dpi, 40 ± 20 % of *wt1a*:GFP^{+} cells also expressed *col1a2*:mCherry (Fig. 24 L-P), suggesting that upon injury, these cells contribute to fibrosis. As this experiment was not based on lineage tracing, there could be alternative explanations, such as the upregulation of *wt1a*:GFP in fibroblasts that had never expressed *wt1a*:GFP.

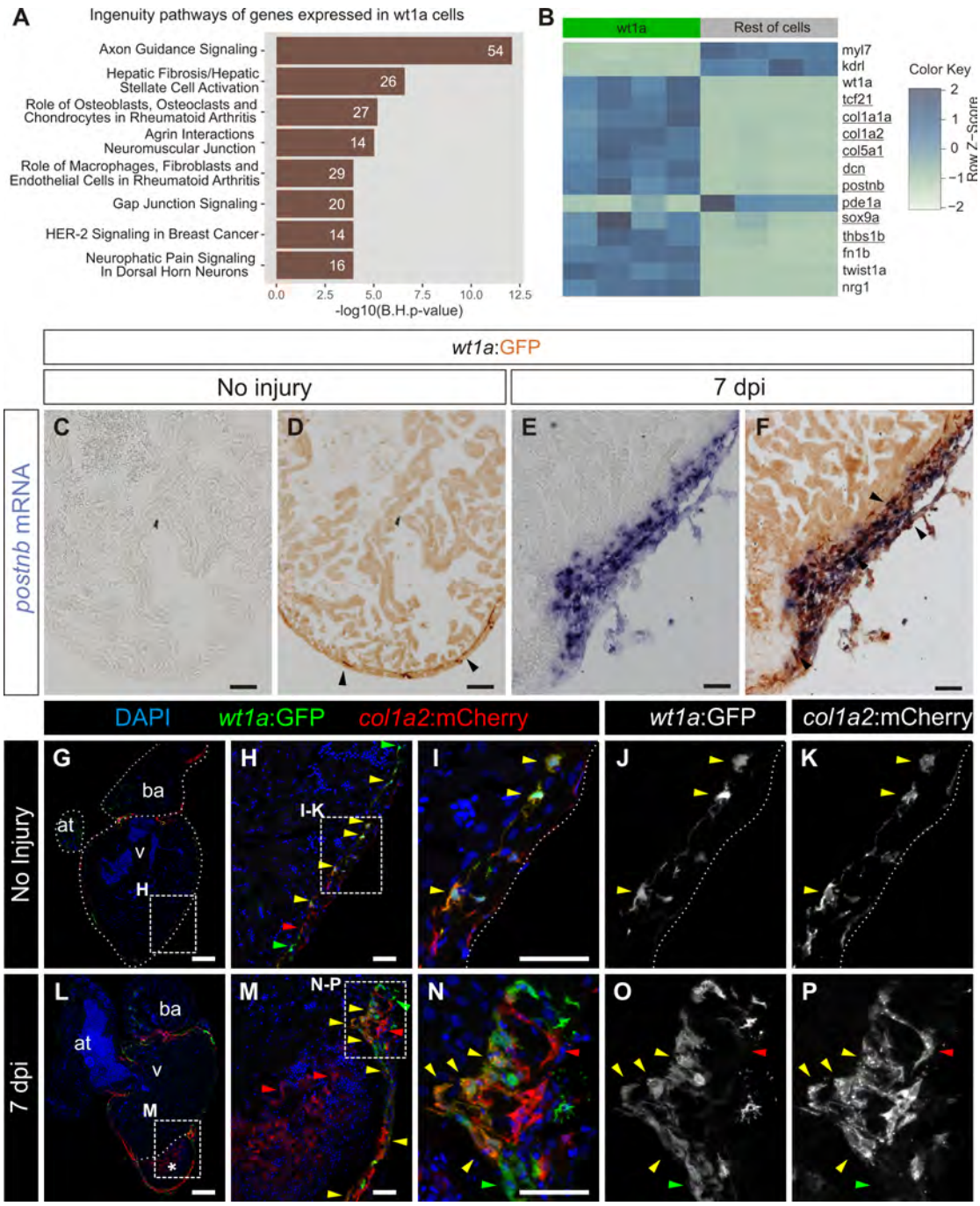

Figure 24. Intracardiac fibroblasts contribute to transient fibrosis during zebrafish heart regeneration. A,B, Transcriptome analysis of *wt1a*:GFP cells isolated from adult zebrafish hearts. A, Ingenuity pathways enriched in *wt1a*:GFP^{+} ventricular cells compared with all GFP^{-} cells. Number of genes differentially expressed in each pathway are indicated. B, Heat map indicating upregulation of fibrotic marker genes (*underlined*) in the *wt1a*:GFP^{+} cell fraction and myocardial (*myl7*) and endocardial genes (*kdrl*) in the GFP^{-} fraction. 4 pools of 3-5 ventricles each were used per condition. **C**–**F**, ISH against *postnb* mRNA (purple) followed by anti-GFP immunohistochemistry (brown) on ventricular sections of Tg(*wt1a*:GFP) hearts without injury (C,D, n = 3/3) and at 7 dpi (E,F, n = 4/4). Arrowheads mark *wt1a*:GFP^{+} cells. **G**–**P**, Immunofluorescence staining on sections of *wt1a:GFP; col1a2:mcherry-NTR* double transgenic zebrafish hearts without injury (G–K, n = 5/5) or at 7 dpi (L–P, n = 4/4). Red arrowheads mark *col1a2*:mCherry^{+} cells, green arrowheads *wt1a*:GFP^{+} cells, and yellow arrowheads double positive cells in the subepicardial layer of the ventricle (H–K) or injury area (M–P). at,atrium; ba, bulbus arteriosus; v, ventricle. Scale bars, 25 µm (**H**,**I**,**M**,**N**), 50 µm (**C**–**F**), 100 µm (**G**,**L**).

To rule out this possibility, we generated a *wt1a:CreER*^{T2} line and labelled these cells before injury. In the uninjured heart, we could detect faint Col1a1 expression next to *wt1a*-lineage labelled cells. However, at 7 dpi, there was an increase in Col1a1 expression adjacent to these cells (Fig. 25).

Overall, our results indicate that *wt1a*:GFP labels the cardiac resident fibroblasts, and these cells contribute to fibrosis in the zebrafish heart upon cryoinjury.

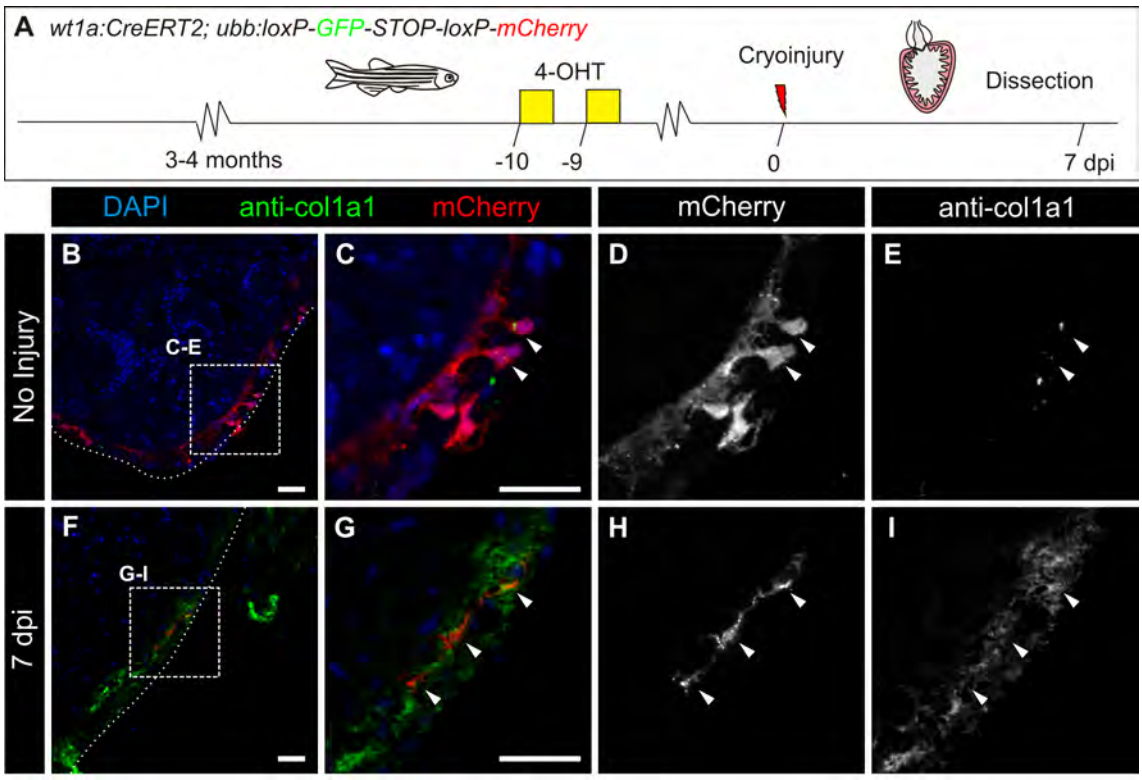

Figure 25. A–I, Lineage tracing of *wt1a*$^{+}$ cells. A, *wt1a*:*CreER*^{T2} was crossed into the *ubb:Switch* line and 4-OHT was added to adult uninjured fish 10 and 9 days before dissection. **B–I**, Immunofluorescence staining with anti-Col1a1 (green) and mCherry (red) on heart sections of uninjured hearts (B–E, n = 4/4) or hearts at 7 dpi (F–I, n = 4/4). Nuclei are counterstained with DAPI. Arrowheads mark *wt1a*-derived cells. Scale bars, 25 µm.

VII Endocardial cells produce collagen but do not become fibroblasts

Upon injury, endocardial cells can be detected in close proximity to collagen (Münch et al. 2017). To study their contribution to zebrafish heart fibrosis, and to investigate whether they transdifferentiate into fibroblasts upon injury, we used RNA-Seq to compare the expression profiles of endocardial *kdrl*:mCherry^{+} cells located at the apex before injury and at 7 dpi (Fig. 26 A; Supplementary Table 3). We detected an upregulation of fibrosis-related pathways (Fig. 26 B), as well as genes encoding different ECM proteins, including *fn1a*, *col12a1a*, *col1a2* and *loxl2b* (Fig. 26 C). Importantly, these cells do not downregulate the endocardial markers *fli1a* and *kdrl* (Fig. 26 C) and do not upregulate EMT markers (Fig. 27).

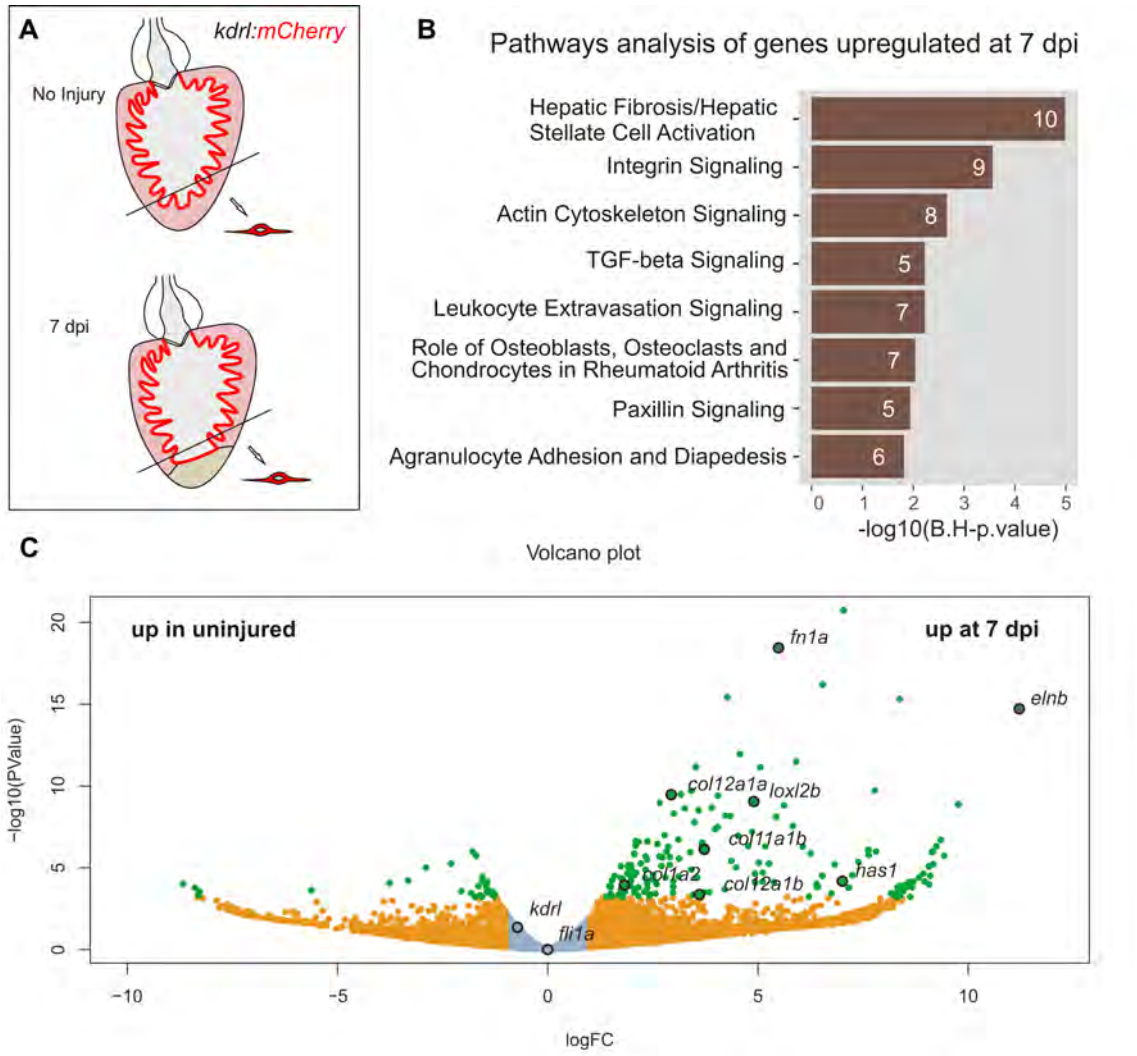

Figure 26. Endocardium-derived cells contribute to transient fibrosis during zebrafish heart regeneration. A, *kdlr*:mCherry^{+} cells were FACS-sorted from the ventricular apex of hearts with no injury or at 7 dpi. Transcriptome analysis was performed to compare the expression profile of both groups. **B**, Ingenuity pathway analysis. Number of genes differentially expressed in each pathway are indicated. **C**, Volcano plot; selected differentially expressed genes are highlighted. Light blue, false discovery rate (FDR) > 0.05, abs(log fold change [LFC]) < 1; orange, FDR > 0.05, abs(LFC) > 1; red, FDR < 0.05, abs(LFC) < 1; green, FDR < 0.05, abs(LFC) > 1. Three pools of 3–5 hearts were used for the uninjured condition and 5 pools of 3–5 hearts for the 7 dpi condition.

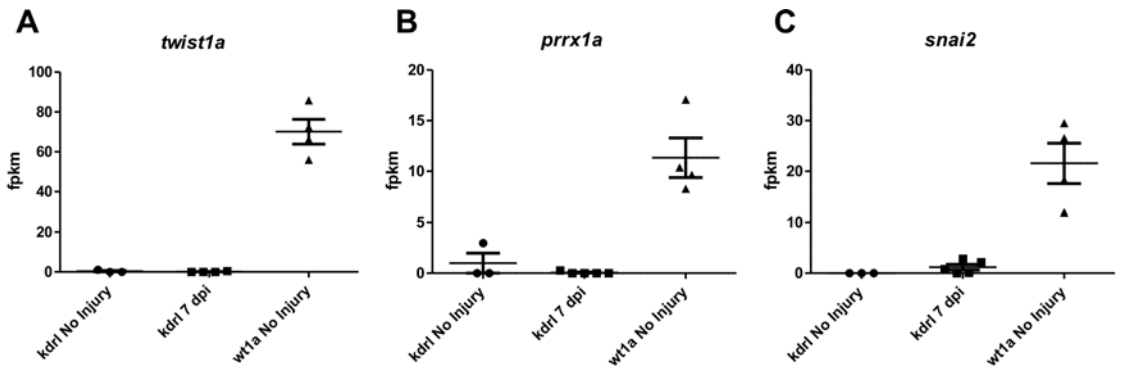

Figure 27. Epithelial to mesenchymal transition (EMT) markers are expressed by *wt1a*:GFP^{+} cells but not by *kdrl*:mCherry^{+} cells. A–C, Graphs show the fragments per kilobase of exon per million fragments mapped (fpkm) values for the same genes and samples. EMT genes were more abundant in *wt1a*$^{+}$ cells than in *kdrl*$^{+}$ cells both before and after injury.

These results were corroborated by anti-Col1a1 immunohistochemistry in a *fli1a:GFP* background, where we observed co-localisation (Fig 28 A–D). Next, *fli1a* cells were lineage traced using a newly generated *fli1a:CreER*^{T2} line crossed into the *ubb*:Switch line. In the adult heart, the entire endocardium was mCherry^{+}. At 7 dpi, *fli1a*-derived cells were in close contact with Col1a1 staining, supporting the idea that these cells contribute to collagen production (Fig 28 E–M). As collagen is extracellular, we confirmed this by crossing *fli1a:GFP* to *col1a2:mCherry* and we detected collagen expression in *fli1a*:GFP^{+} cells, more specifically in those cells close to the injury (Fig. 29 A–D). Finally, collagen-producing endocardial cells were lineage traced using the *fli1a:CreER*^{T2}*;col1a2:loxP-tagBFP-loxP-mCherry-NTR* line. Detection of the mCherry signal at 7 dpi (Fig. 29 E–I) confirmed that endocardial cells contribute to collagen deposition upon injury.

Altogether, our analysis shows that while endocardial cells contribute to fibrosis by collagen production, they do not convert to fibroblasts, as they do not undergo EMT.

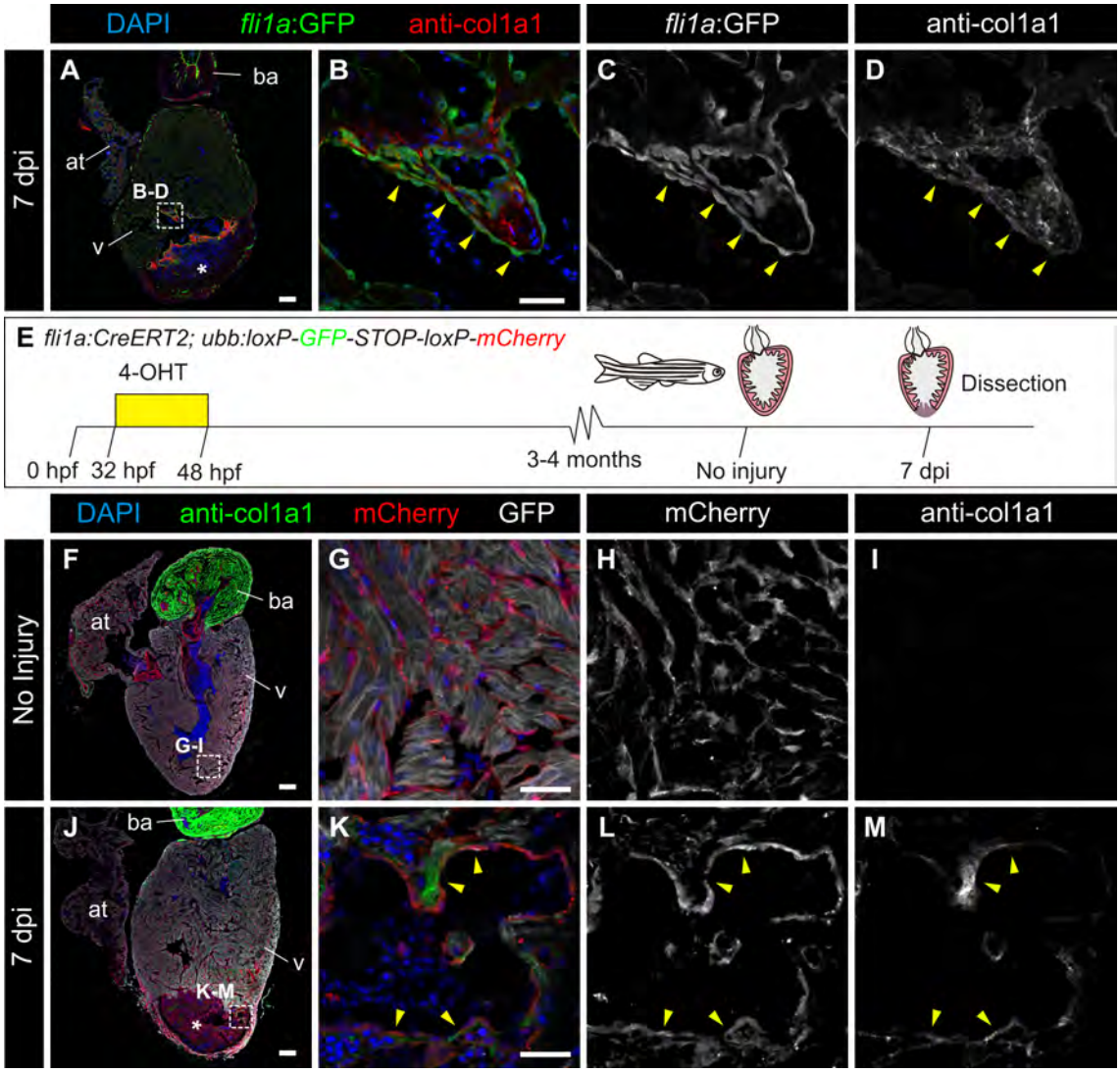

Figure 28. Endocardial cells at the injury area express collagen 1a1. A–D, Immunostaining with anti-GFP (green) and anti-col1a1 (red) antibodies in *fli1a*:GFP hearts at 7 dpi; nuclei are DAPI counterstained (blue). Panels show a whole heart sagittal section and merged and single channels of a zoomed view of the endocardial border close to the injury area (asterisk). Double positive cells for *col1a1* and *fli1a*:GFP can be detected (arrowheads) (n = 2/2). **E–M**, Lineage tracing of endocardial cells in the uninjured and injured heart. E, Experimental scheme for tracing the contribution of endocardial cells to fibrosis using the *ubb:Switch* reporter line. Panels F and J show immunofluorescence staining of whole-heart sagittal sections (F, uninjured, n = 5/5; J, 7 dpi, n = 5/5) with anti-mCherry (red), anti-col1a1 (green), and anti-MHC (grey); nuclei were DAPI counterstained (blue). Panels G–I and K–M are merged and single channels of a zoomed view of the endocardial border in the apex or close to the injury area (asterisk). *fli1a*-derived cells are $mCherry^{+}$ (red). Note that at 7 dpi, $mCherry^{+}$ cells (red) are closely associated with Col1a1 (green) deposits (arrowheads). at, atrium; ba, bulbus arteriosus; IA, injury area; v, ventricle. Scale bars, 25 µm (**B**,**G**,**K**), 100 µm (**A**,**F**,**J**).

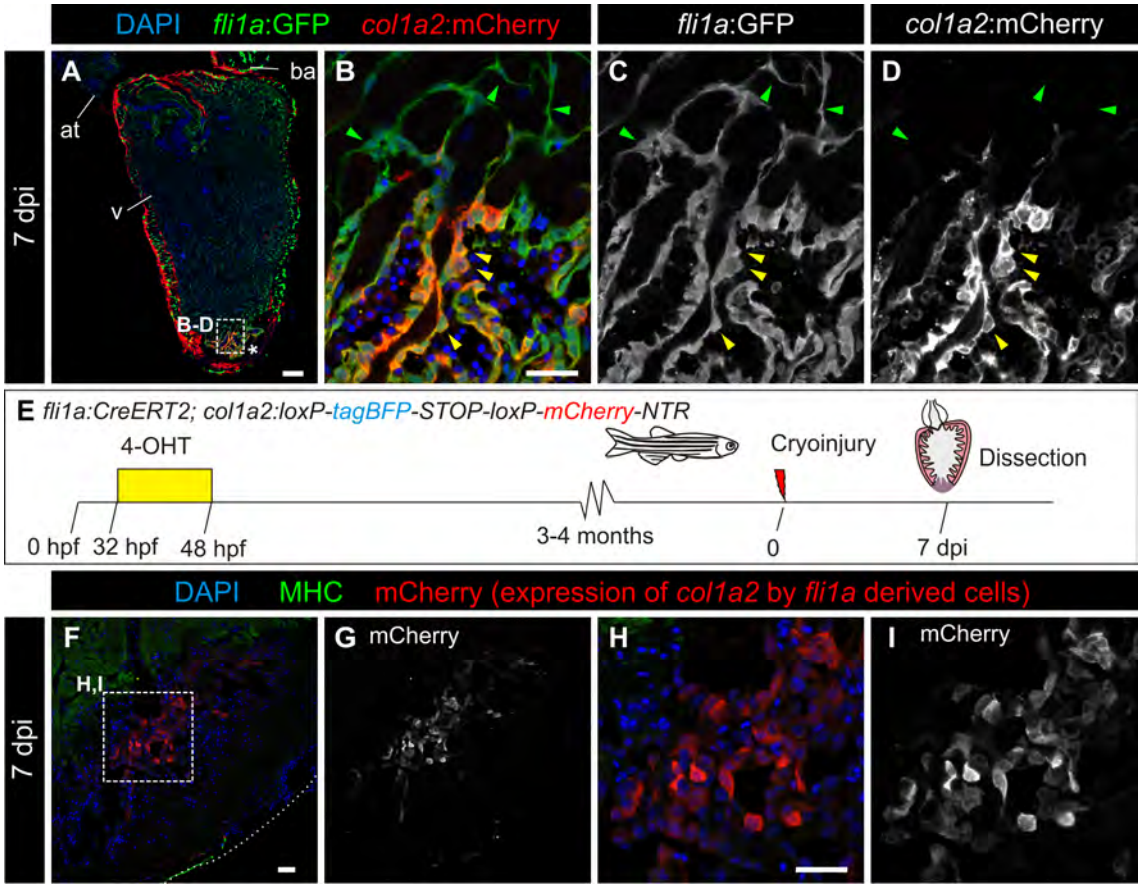

Figure 29. Endocardial cells at the injury area express col1a2. A–D, Immunofluorescence with anti-GFP (green) and anti-mCherry (red) on a heart section from an adult *fli1a:GFP;col1a2:mCherry-NTR* double transgenic fish. Note the presence of double-positive (yellow arrowheads) at the injury area, but not in the remaining the endocardium (green arrowheads) (n = 2/4). **E–I**, Lineage tracing of endocardial cells in an injured heart with exclusive labeling of cells expressing *col1a2* at the time of fixing. E, Experimental scheme for visualizing collagen-producing endocardial cells. F–I, Immunostaining on a heart section close to the injury area (asterisk). G shows the single channel for mCherry and H,I zoomed views of F. mCherry (red) marks *fli1a*-derived cells expressing *col1a2*, MHC marks the myocardium (green), and nuclei are counterstained with DAPI (blue) (n = 2/5). at, atrium; ba, bulbus arteriosus; v, ventricle. Scale bars, 25 µm (**B**,**H**), 100 µm (**A**,**F**).

VIII *Postnb* labels activated cardiac fibroblasts in the zebrafish heart

One of the best markers to label activated cardiac fibroblasts in the mammalian heart is Postn. To study these cells in the zebrafish heart, we generated a BAC *postnb:citrine* transgenic line. In uninjured hearts, the expression pattern was restricted to valves and pericytes covering large coronary arteries (Fig. 30 A–C). However, at 7 dpi, it was robustly detected at the injury site (Fig. 30 D,E). This makes *postnb:citrine* a good marker for activated cardiac fibroblasts. These cells proliferate mainly in the short-term after cryoinjury (Fig. 30 H). Interestingly, *postnb*:citrine^{+} cells did not co-localised with endocardial *kdrl*:mCherry^{+} cells (Fig. 30 F,G; see also Fig. 31 A), further supporting the idea that endocardial cells do not convert to *bona fide* fibroblasts.

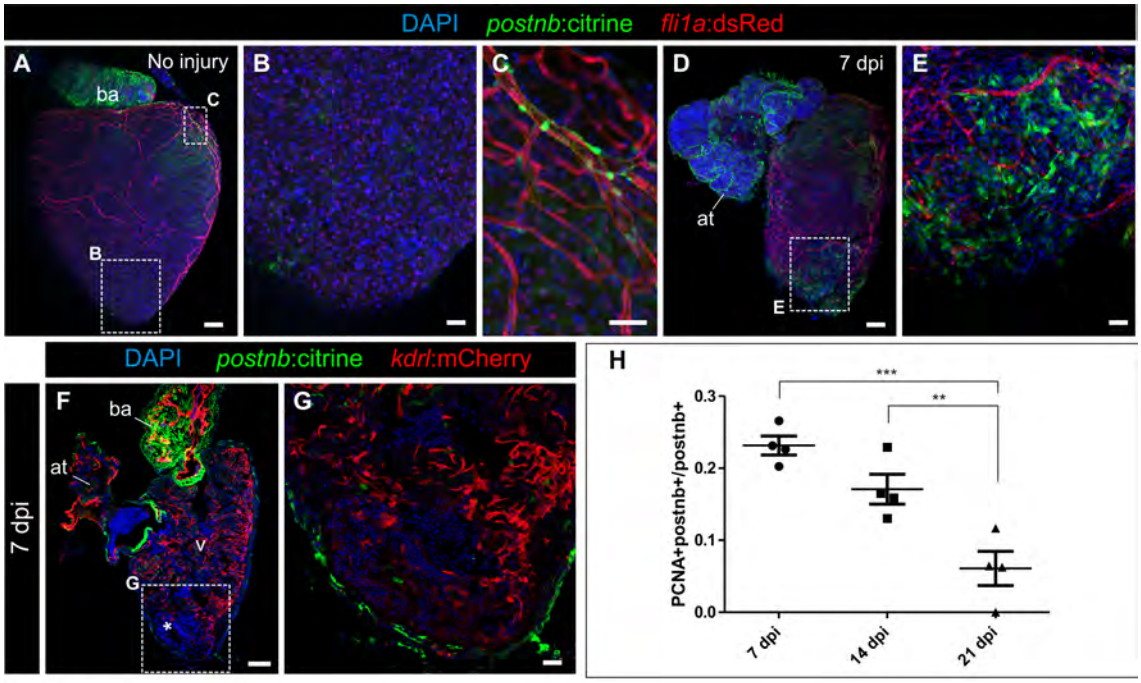

Figure 30. *periostin b* expression marks an activated cardiac fibroblast population upon ventricular cryoinjury. A–E, Whole-heart immunofluorescence in the *postnb*:*citrine*; *fli1a*:*dsRedEx* double transgenic line. Panels show a whole-heart view (A) and zoomed views (B,C) of the ventricular apex of an uninjured heart (n = 3/3) and a heart at 7 dpi (D,E) (n = 3/3). Perivascular cells can be observed in C. *postnb*:citrine is shown in green, *fli1a*:dsRedEx in red, and nuclei are counterstained with DAPI (blue). **F**,**G,** Immunofluorescence staining on a sagittal heart section of a *postnb*:citrine; *kdrl*:mCherry double transgenic zebrafish; G is a zoomed view of the injured ventricular apex (asterisk) in the heart in F. *postnb*:citrine is shown in green, *kdlr*:mCherry in red, and nuclei are counterstained with DAPI. *postnb*:citrine does not colocalise with either *fli1a*$^{+}$ nor *kdlr*$^{+}$ cells (n = 7/7). **H**, Quantification of proliferating *postnb*$^{+}$ cells postinjury (mean±s.d; ***P<0.001; **P<0.01 by one-way ANOVA followed by Tukey's multiple comparisons test). at, atrium; ba, bulbus arteriosus; v, ventricle. Scale bars, 25 µm (**B**,**C**,**E**,**G**), 100 µm (**A**,**D**,**F**).

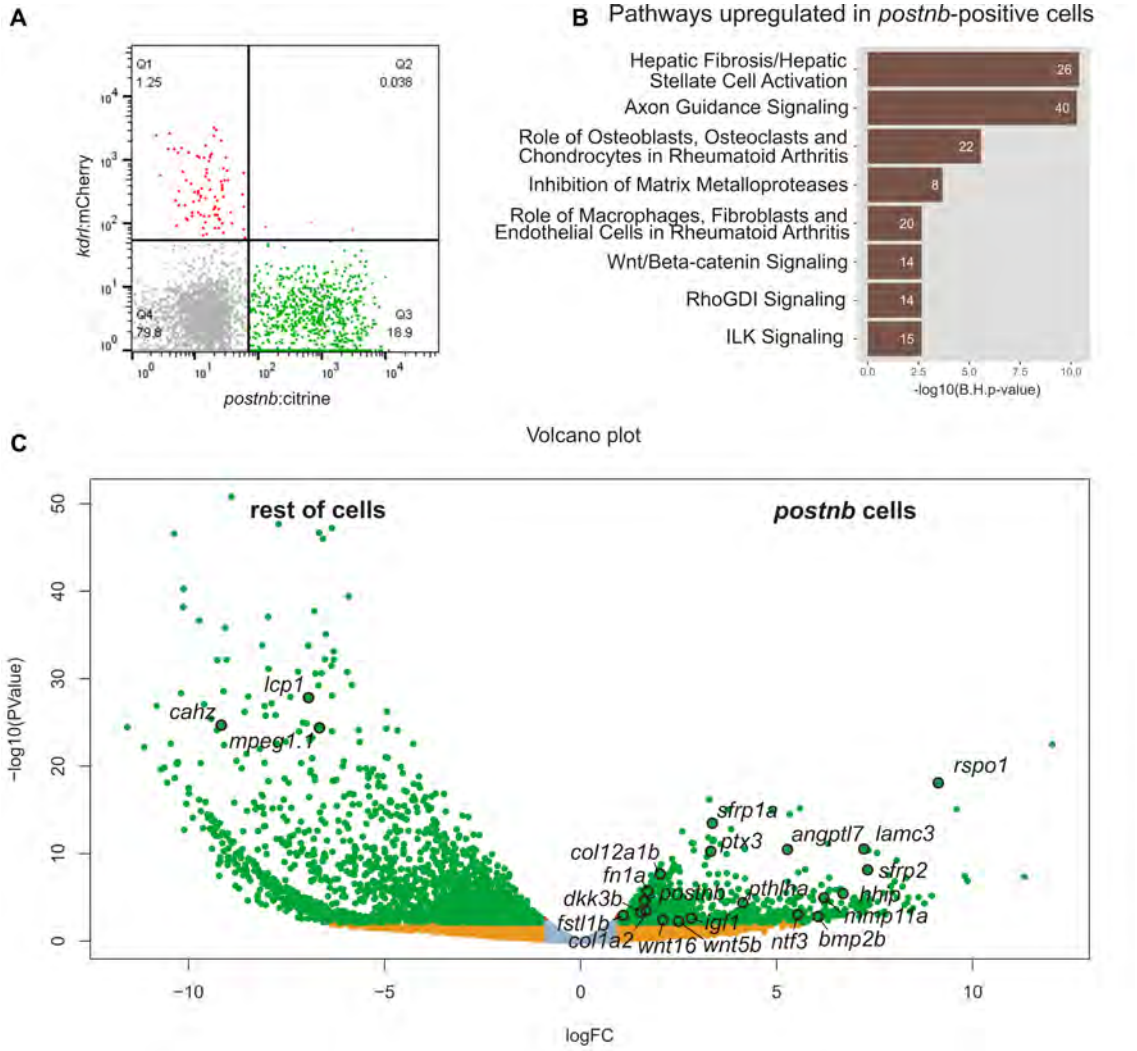

Figure 31. Expression profiling reveals expression of extracellular matrix proteins and secreted molecules in postnb$^+$ cells. A, FACS-sorted cells of hearts from *kdrl*:mCherry;*postnb*:citrine double transgenic zebrafish. No double-positive cells were detected. **B**,**C** Transcriptome analysis of *postnb*:citrine$^+$ cells isolated from the ventricular apex. B, Ingenuity pathway analysis. C, Volcano plot. Selected differentially expressed genes are highlighted. Light blue, false discovery rate (FDR) > 0.05, abs(log fold change [LFC]) < 1; orange, FDR > 0.05, abs(LFC) > 1; red, FDR < 0.05, abs(LFC) < 1; green, FDR < 0.05, abs(LFC) > 1. Three pools of 3-5 ventricular apices were used for *postnb*:citrine cells per condition, and 6 pools of 3-5 ventricular apices were used for the other cells.

A comparison of *postnb*:citrine and *col1a2*:mCherry-NTR populations in the injured heart revealed the presence of a double positive population as well as single-positive populations (Fig. 32 A,B). Immunofluorescence analysis identified *col1a2*:mCherry-NTR single-positive cells at the endocardial border (Fig. 32 C–G), which fits well with our results of endocardial cells producing *col1a2* (Fig. 28, Fig. 29). A high degree of heterogeneity was found at the epicardial side of the ventricle, with some *col1a2*:mCherry-NTR$^+$ cells, others only *postnb*:citrine$^+$ and some double-positive cells. This suggests a certain extent of heterogeneity within the fibroblast population.

To characterise *postnb*:citrine^{+} cells, we analysed the transcriptome of cells sorted from the injured ventricle. We identified pathways related to fibrosis and axon guidance (Fig. 31 A,B). When we compared with other cells at the injyry area, *postnb*:citrine^{+} cells were highly enriched for genes encoding secreted proteins. In total, 128/917 differentially expressed genes upregulated in the *postnb*:GFP^{+} population encoded secreted molecules, while only 12/2206 belonged to this category in the negative population ($P < 0.00001$ by chi-square test). *postnb*:GFP^{+} cells expressed ECM genes such as *postnb*, *col1a2*, *col12a1b* and *fn1a* as well as 12 matrix metalloproteases including *mmp2*, *mmp11a* and *mmp14a*. *postnb*:citrine^{+} cells also expressed several signaling molecules (Fig. 31 C; Supplementary Table 4), some of which influence heart development or regeneration, including *igf1* and *bmp2b* (Huang et al., 2013a; Wu et al., 2016), *Fstl1* (Wei et al., 2015) and *sfrp1a* (Barandon et al., 2004; Gibb et al., 2013). Others, among them *wnt5a*, *wnt16*, *rspo1* and *hhip* have not yet been studied in the context of heart regeneration (Fig. 31 C).

These results reveal that *postnb:*citrine marks activated fibroblasts, which not only express ECM genes but also genes responsible for ECM degradation. Furthermore, they express several secreted signalling molecules that could influence the process of heart regeneration.

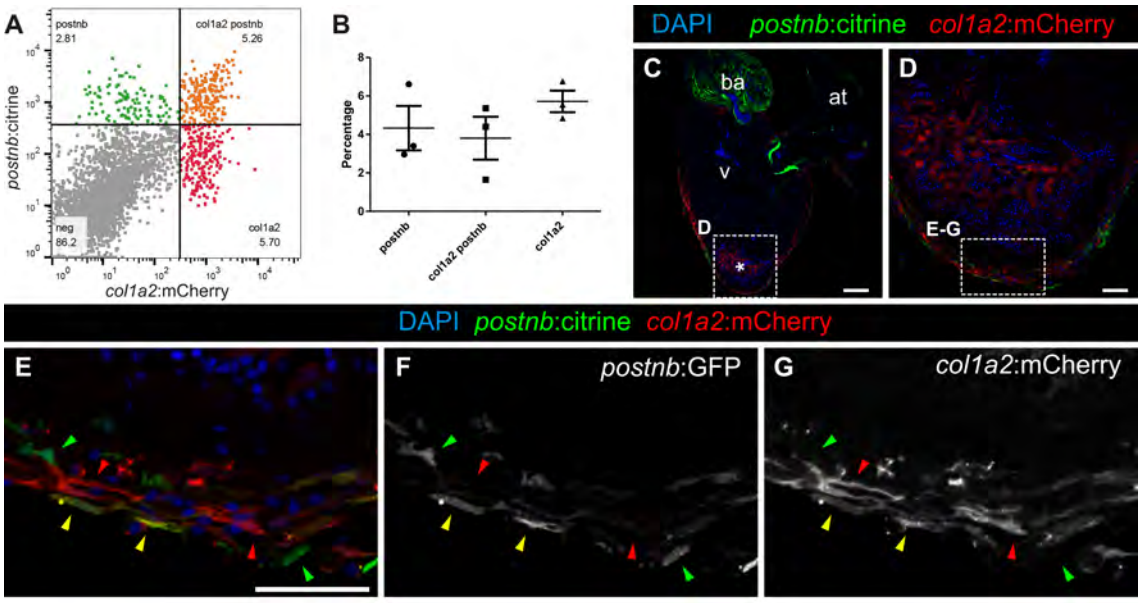

Figure 32. Colocalisation of *postnb*:citrine^{+} and *col1a2:*mCherry^{+} cells. A–B, FACS-sorted cells of hearts from *co1a2:mCherry;postnb:citrine* double transgenic fish. Based on these markers, three populations could be detected: double-positive, *postnb*$^{+}$, and *col1a2*$^{+}$ (n = 3/3). **C–G**, Immunofluorescence with anti GFP (green) and anti-mCherry (red) on a heart section from an adult *postnb:citrine;col1a2:mCherry-NTR* fish. Note the presence of double-positive (yellow arrowheads), *col1a2*$^{+}$ (red arrowheads), and *postnb*$^{+}$ cells (green arrowheads) (n = 7/7). at, atrium; ba, bulbus arteriosus; v, ventricle. Scale bars, 25 µm (**C**), 100 µm (**D,G**).

IX Mechanisms of fibrosis regression

When we analysed the dynamics of *col1a2* and *postnb* expression, we found that there is an early upregulation at 3 and 7 dpi, followed by a progressive decrease to the initial levels at 90 dpi (Fig. 33 A,B).

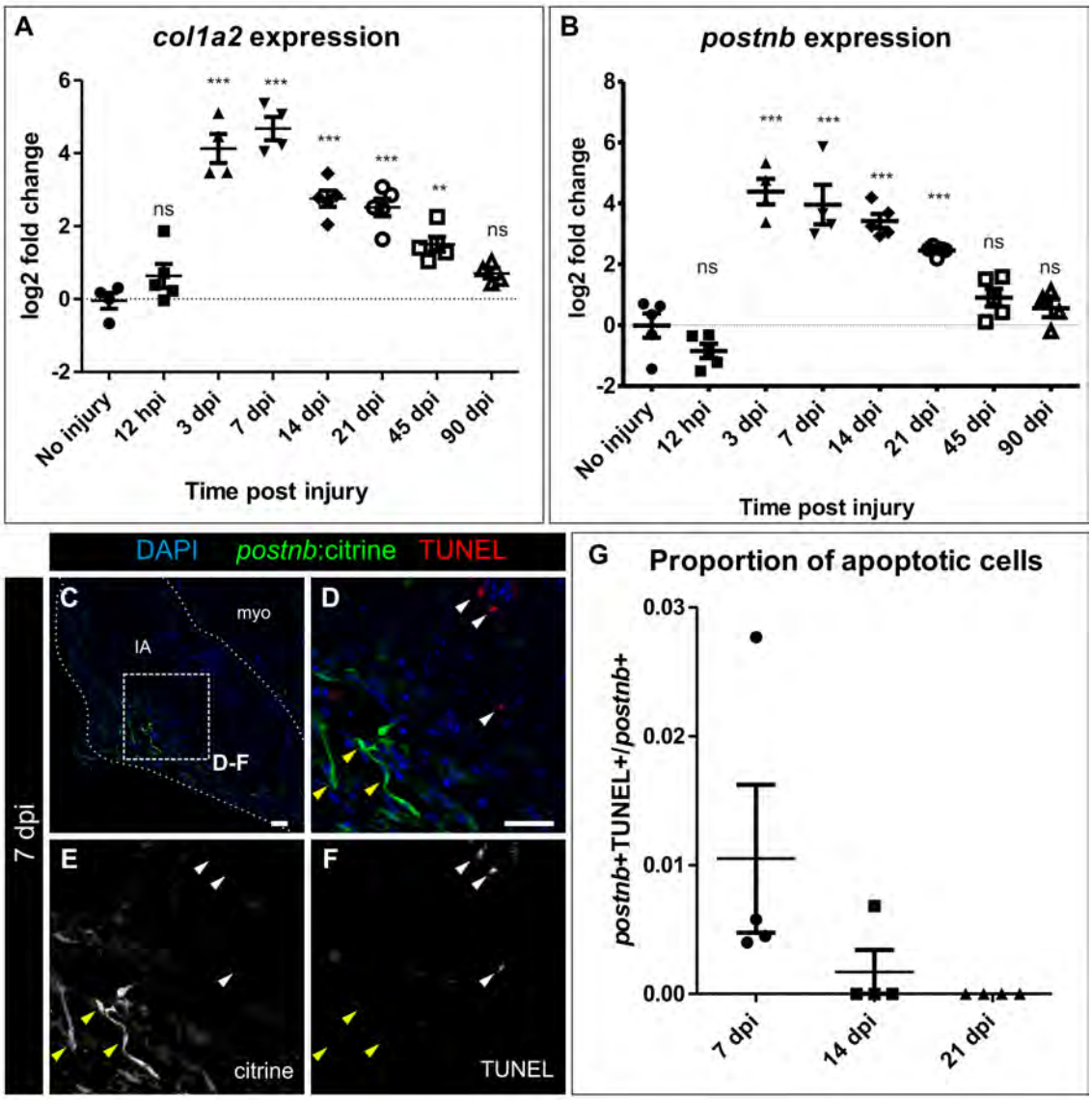

Figure 33. Apoptotic and senescent fibroblasts during heart regeneration. A–B, qPCR of *col1a2* and *postnb* in ventricles at different days postinjury. Symbols show data for individual samples, bars and whiskers show mean±s.d.; ***P<0.001; **P<0.01 by one-way ANOVA followed by Tukey's multiple comparisons test. *postnb* expression peaks at 3 and 7 dpi. **C–F,** TUNEL staining on *postnb*:citrine heart sections. Apoptotic cells are shown in red, *postnb*:citrine^{+} cells in green (anti-GFP immunofluorescence), and nuclei are DAPI counterstained (blue). **G,** Quantification of *postnb*$^{+}$ apoptotic (TUNEL^{+}) cells. Data are the percentage of TUNEL^{+}/*postnb*$^{+}$ cells at different stages postinjury. Note that only a very small proportion is TUNEL^{+}. IA, injury area; myo, myocardium. Scale bars, 25 µm.

We hypothesised that the decrease in the expression of these genes could be mediated by one of two mechanisms: (1) death of the cells expressing the ECM genes or (2) inactivation of the genes in these cells.

Accordingly, we first evaluated cell death by TUNEL staining, and in most cases ≤ 1% of the *postnb*:citrine^{+} cells were TUNEL^{+} (Fig. 33 C–G). To test the alternative hypothesis, *postnb*$^{+}$ cells were lineage traced using a *postnb:CreER*^{T2} transgenic line. By crossing it into the *ubb:Switch* line, and administering 4-OHT at 3 and 4 dpi, we labelled some cells at the injury area (Fig. 34 A–E) and very few CMs next to the atrio-ventricular valves (Fig. 35). Observation of the apex of these hearts after full regeneration showed that some fibroblasts remained in the regenerated myocardium (Fig. 34 F–I).

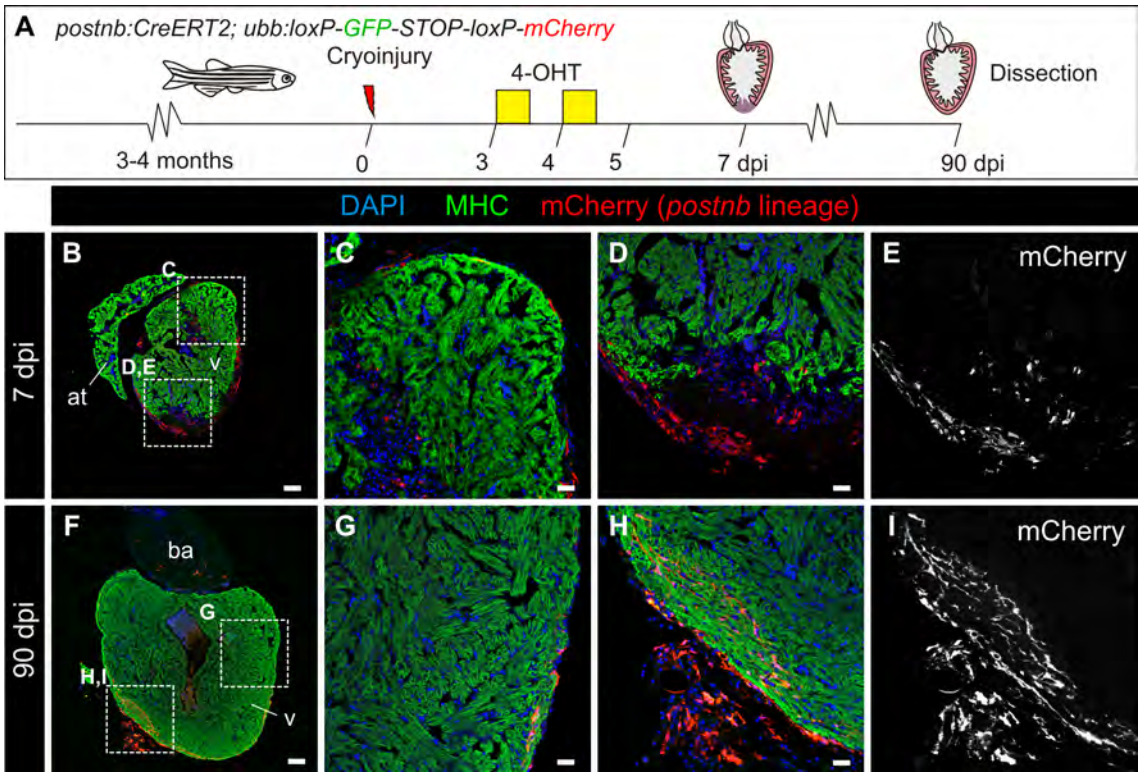

Figure 34. Persistence of *postnb*-derived cells in the regenerated myocardium. A, Experimental scheme. *postnb*:CreER^{T2} fish were crossed into the *ubb*:Switch reporter line. 4-OHT was added to fish water at 3 and 4 dpi, and hearts were dissected at different dpi. **B–I**, Immunofluorescence staining on heart sections at 7 dpi (B–E, n = 4/4) or 90 dpi (F–I, n = 5/5) with anti-MHC (green) and anti-mCherry (red, *postnb*-lineage); nuclei were counterstained with DAPI. Panels C–E and G–I show magnifications of boxed areas in B and F, respectively. Panels E and I show the single mCherry channel. at, atrium; ba, bulbus arteriosus; v, ventricle. Scale bars, 25 µm (**C**,**D**,**G**,**H**), 100 µm (**B**,**F**).

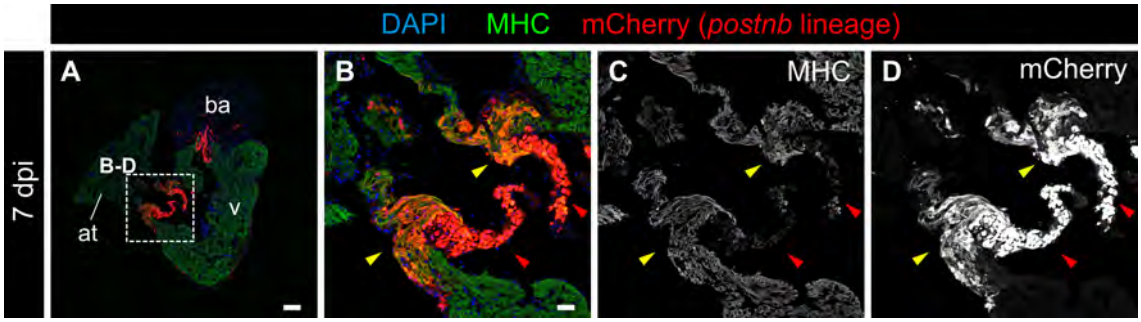

Figure 35. Characterization of *postnb*-derived cells in the atrio-ventricular canal. Immunofluorescence with anti-MHC (green) and anti-mCherry (red) on a heart section from an adult *postnb:CreER*^{T2} ; *ubb:Switch* double transgenic fish. Note the presence of *postnb*-derived CMs (yellow arrowheads) and cells within the valve leaflets (red arrowheads) (n = 4/4). at, atrium; ba, bulbus arteriosus; v, ventricle. Scale bars, 25 µm (**B**), 100 µm (**A**).

Next, *postnb* lineage-traced cells were sorted at 7 and 60 dpi to examine their expression profile (Fig. 36 A; Supplementary Table 5). Through this analysis, we could confirm that although the percentage of *postnb*-derived cells diminished at the injury area, the majority of *postnb*-derived cells remain there (Fig. 36 B). At 7 dpi, we detected an enrichment of ECM genes as well as genes related to the immune system (Fig. 36 C). Although the level of ECM genes decreased overall in these cells from 7 to 60 dpi, *col7a1l* and *col8a2* were found upregulated at 60 dpi (Fig. 36 D; Fig. 37 A,B). However, these genes were expressed at lower levels than *postnb* and *col1a2* at 7 dpi (Fig. 37 C–J). Moreover, genes were not expressed by *wt1a*$^{+}$ resident fibroblasts in the uninjured heart, indicating that the inactivation of fibroblasts does not fully revert the expression profile to a homeostatic baseline. Moreover, the gene signature of *postnb*-derived cells at 60 dpi resembles more the signature of *wt1a*:GFP cells than that of *postnb*-derived cells at 7 dpi (Fig. 37 K, L).

Overall, the data indicate that during fibrosis regression, activated fibroblasts partially return to a quiescent stage without fully resembling endogenous cardiac fibroblasts from an uninjured heart.

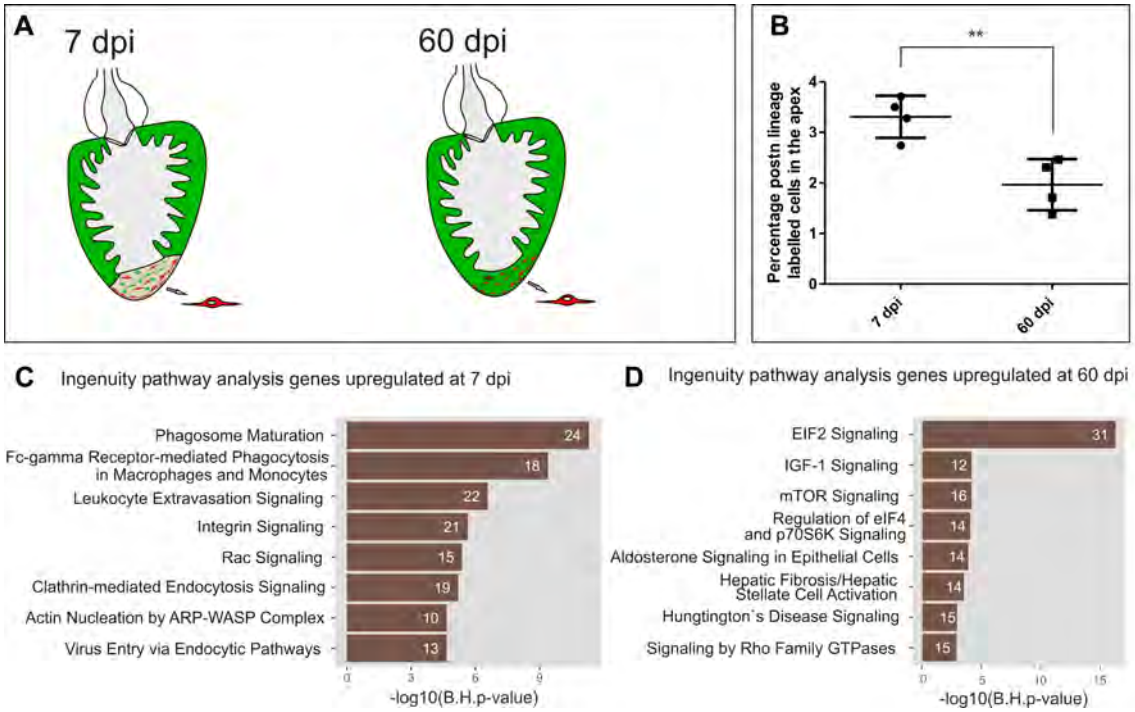

Figure 36. **Expression profiling of *postnb*-derived cells. A**, Representation of *postnb*-derived cell-sorting experiment. *postnb*-derived mCherry^{+} cells were sorted from the ventricular apex at 7dpi (injury response stage) and 60 dpi (late regeneration stage); transcriptome analysis was performed on isolated mCherry^{+} cells. **B**, Quantification of the percentage of *postnb*-derived cells at the injury area. Symbols show individual measurements and boxes and whiskers show mean±s.d; ** P=0.0064 by two-tailed unpaired t-test. **C,D** Ingenuity pathway analysis of *postnb*-derived cells at 7 and 60 dpi. The bars represent pathways enriched in *postnb*-derived cells compared with all other cells in the injury area. Number of genes differentially expressed in each pathway are indicated.

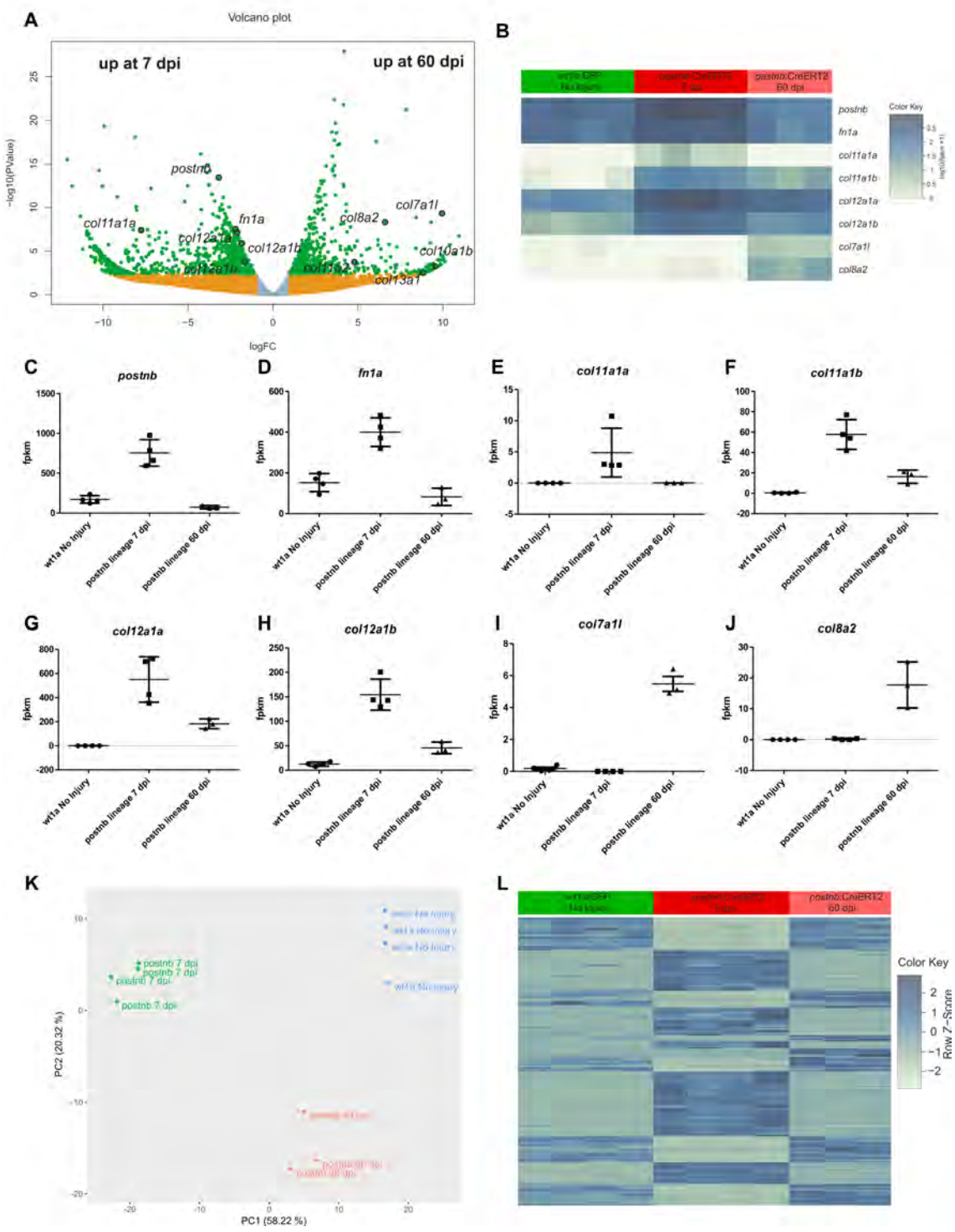

Figure 37. Comparison of the gene expression profile of resident intracardiac fibroblasts, activated fibroblasts, and inactivated fibroblasts. A, Volcano plot showing selected representative genes. Light blue, false discovery rate (FDR) > 0.05, abs(log fold change [LFC]) < 1; orange, FDR > 0.05, abs(LFC) > 1; red, FDR < 0.05, abs(LFC) < 1; green, FDR < 0.05, abs(LFC) > 1. **B**, Heatmap showing a subset of genes encoding ECM proteins as log(fpkm+1) expression level from the RNA-Seq analysis. **C**–**J**, Graphs show the fpkm values for the same genes and samples. ECM genes were more abundant in *postnb*-derived cells at 7 dpi. In some cases, the expression profile of *wt1a*:GFP and *postnb*-derived cells at 60 dpi did not coincide, suggesting that fibroblasts do not fully revert to a quiescent state during heart regeneration. The genes upregulated in *postnb*-derived cells at 60 dpi are expressed at low levels. **K**, Principal Component Analysis of RNA-Seq samples from uninjured *wt1a*:GFP^{+} cells and *postnb*-derived cells from hearts at 7

dpi and 60 dpi. **L**, Heat map of the top 200 genes differentially expressed between 7 and 60 dpi in *postnb*-traced cells. Expression levels of these genes are compared with the levels in *wt1a*:GFP^{+} cells from an uninjured heart. Note that *wt1a*:GFP^{+} cells are similar, but not equal, to 60 dpi *postnb*-traced cells with regards to gene expression. Colors indicate z-score calculated by row. Four pools of 3–5 hearts were used for 7 dpi, and three pools for 60 dpi.

X Fibroblast role during zebrafish heart regeneration

To test whether cardiac fibrosis could influence regeneration, we used the *col1a2:mCherry-NTR* line to ablate ECM producing cells after administering Mtz. At 35 dpi, no differences were observed in the injury area (Fig. 38), suggesting that *col1a2*$^{+}$ cell ablation does not enhance the regenerative capacity. Nonetheless, we analysed CMs proliferation at a shorter time point, during the window in which maximal CMs proliferation has been reported (Sallin et al., 2015) (Fig 39 A). In Mtz-treated animals, we observed fragmented cells and nuclei, indicating genetic ablation of *col1a2:mCherry-NTR*$^{+}$ cells (Fig. 39 B,C). By contrast, this was not detected in the untreated control group (Fig. 39 D,E). We next compared CM proliferation in cryoinjured hearts from Mtz-treated *col1a2:mCherry-NTR* fish and controls. Ablation of *col1a2*:mCherry-NTR^{+} cells led to a four-fold reduction in CM proliferation (Fig. 39 F–L).

In sum, our results not only suggest that fibrosis is compatible with regeneration, but also indicate that a transient fibrosis upon cryoinjury is necessary for subsequent CMs proliferation.

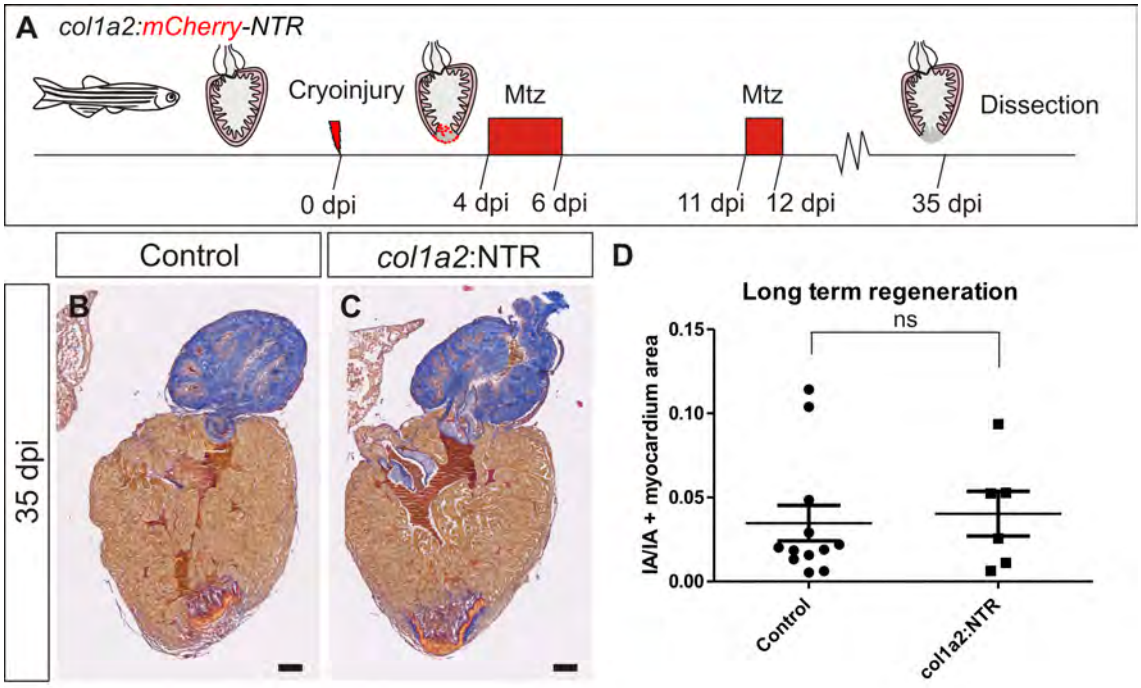

Figure 38. Genetic ablation of col1a2 expressing cells does not improve regeneration. A, Experimental scheme. *col1a2:mCherry-NTR* transgenic zebrafish were cryoinjured and treated with 10 mM Mtz between 4 to 6 and 11 to 12 dpi. Hearts were dissected at 35 dpi, sectioned and stained with AFOG to determine degree of regeneration. **B**–**C** AFOG stained sagittal sections through ventricles of a Mtz-treated *col1a2:loxP-tagBFP-loxP-mCherry-NTR* heart (control) and a Mtz-treated *col1a2:mCherry-NTR* heart. **D**, Quantification of the injury area versus total ventricular area from 12 control hearts and 6 *col1a2:NTR* hearts. No significant difference was observed between both groups, unpaired Student's t-test (P=0.75). Scale bars, 100 µm.

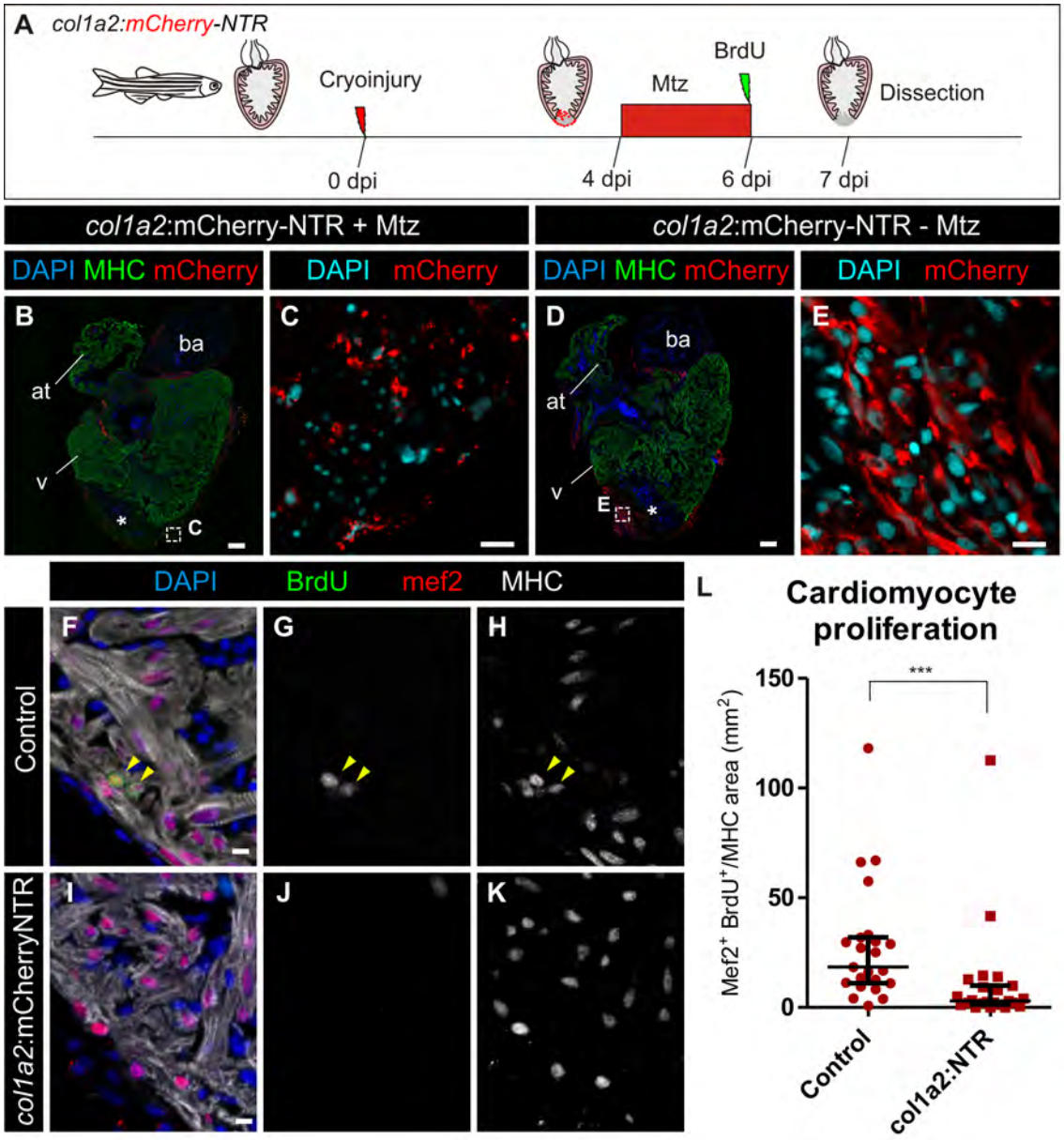

Figure 39. Genetic ablation of *collagen 1a2* expressing cells impairs CM proliferation in the cryoinjured heart. A, Schematic illustration of experimental set up. col1a2:mCherry-NTR fish were cryoinjured and treated with Mtz from 4 to 6 dpi. Mtz administration leads to cell death of NTR expressing cells. BrdU injection was performed one day prior to fixation to assess CM proliferation. **B**–**E**, Immunofluorescence on heart sections of *col1a2*:*mCherry-NTR* treated with Mtz (B,C, n = 8/8) or untreated controls (D,E, n = 3/3). C and E are zoomed views of panels B and D, respectively. mCherry is shown in red, MHC in green and nuclei (DAPI) in blue for B and D, and in cyan for C and E. Note that in Mtz-treated fish, *col1a2*:mCherry-NTR labels cells with fragmented nuclei and the homogeneous expression as shown in the control heart is lost. **F**-**K**, Immunofluorescence using anti-mef2 (red) and anti-MHC (white) to mark CMs and anti-BrdU (green) in *col1a2:loxP-tagBFP-loxP-mCherry-NTR* (control) and *col1a2:mCherry-NTR* treated with Mtz and BrdU as described in A. Nuclei are counterstained with DAPI (blue). **L**, Quantification of $BrdU^+$ CMs in *col1a2:mCherry-NTR* and control hearts. Shown are individual measurements as well as median±intercuartile range; *** P=0.0004 by Mann-Whitney test, n = 23 fish per condition, from 2 different experiments. For each point, 3 whole heart sections of a ventricle were quantified. Scale bars, 10 µm (**C**,**E**,**F**,**I**), 100 µm (**B**,**D**).

DISCUSSION

DISCUSSION

I *tbx5a* as a marker for the zebrafish first heart field

In previous works, *ltbp3* (Zhou et al., 2011) and *drl* (Mosimann et al., 2015) regulatory sequences have been used as markers for the SHF and FHF, respectively, in the zebrafish. However, these markers are either not conserved (*drl*) or have not been studied (*ltbp3*) in the mouse model. In this thesis, using *tbx5a* as a maker for the FHF derived CMs, we identify for the first time that the adult zebrafish heart is derived from two different fields that are analogous to those previously described in mammals (Fig. 40 A). Of note, in mammals, *Tbx5* expression labels the derivatives of the FHF in the ventricle and also the boundary with the SHF (Devine et al., 2014; Steimle and Moskowitz, 2017); thus, we cannot exclude that the contribution of the SHF is slightly greater than that described in this thesis. When comparing the patterns of *tbx5a*:GFP and *drl*:mCherry expression, we found that although they are largely overlapping, the *tbx5a*:GFP pattern is slightly broader than that of *drl*:mCherry. One explanation is that *tbx5a*:GFP labels a region slightly wider than that of the FHF-derived cells, as it occurs in mammals. An alternative explanation is that *drl*:mCherry gets downregulated rapidly during development, and is not detected in that area at the analysed stages.

Importantly, the limit between the $Tbx5^{+}$ and $Tbx5^{-}$ CMs triggers the position of the septum in mammals (Koshiba-Takeuchi et al., 2009). Before this thesis was initiated, it was thought that the some non-mammalian vertebrates do not develop a septum because there is homogeneous *Tbx5* expression in these animals (Koshiba-Takeuchi et al., 2009), and thus there is no signal for the position of the septum. However, our finding of $tbx5a^{+}$ and $tbx5a^{-}$ ventricular domains changes this interpretation. The reason why zebrafish do not develop a septum is not the absence of a $Tbx5^{+}/Tbx5^{-}$ boundary, but instead it appears that this signal does not trigger septum formation. It is fascinating that an expression pattern that reflects initial heart development (FHF and SHF, that is $tbx5a^{+}$ and $tbx5a^{-}$) and does not seems to have major functional or morphological implications in the zebrafish, was further evolved in mammals to divide the ventricle in two chambers and provide the two circuits for blood circulation.

II *tbx5a* expression in the trabeculae

Before this thesis was conducted, transcriptional differences between the different layers in the heart had not been studied in depth. *nppa* was the only gene specifically detected in trabecular CMs (González-Rosa et al., 2014; Jensen et al., 2012). Very recently, however, enhancers specific to the primordial and trabecular layer have been described. A *ctgf* enhancer element named *careg* that does not reproduce the endogenous expression pattern and a *tbx20* enhancer are specific for

the primordial layer (Goldman et al., 2017; Pfefferli and Jaźwińska, 2017). Consistent with our own findings, a *tbx5a* enhancer was found for the trabeculae (Goldman et al., 2017) and our own studies shows that it recapitulates the endogenous *tbx5a* expression pattern.

It remains to be further explored whether trabeculae-specific *tbx5a* expression has a role in the function of trabecular CMs. In mammalian models, Tbx5 directly regulates the expression of connexin *Cx40*, and the sodium channels *Scn5*a and *Scn10a* (Arnolds et al., 2012; Bruneau et al., 2001; Moskowitz et al., 2004; van den Boogaard et al., 2012; van Weerd et al., 2014). The expression of these genes has a functional impact on CMs, making them more contractile and faster-conducting. Surprisingly, they do not have orthologs in zebrafish. Furthermore, unexpectedly we did not find any other calcium, potassium or sodium channel enriched in the *tbx5a*:GFP^{+} CMs. These data indicated that the best known function for Tbx5 in the mammalian trabeculae is not conserved in the zebrafish, opening the question of which is the role of *tbx5a* in the adult zebrafish heart, and why it is switch off specifically in the cortical layer during development.

The absence of *tbx5a* expression in a small number of trabeculae at the basal region of the ventricle warrants attention. We did not detect morphological differences between *tbx5a*$^{+}$ and *tbx5a*$^{-}$ trabecular CMs. Moreover, in some cases, a single trabecule contained morphologically perfectly-coupled *tbx5a*$^{+}$ and *tbx5a*$^{-}$ CMs. This is consistent with the possibility that *tbx5a* does not play an important role in zebrafish heart homeostasis, opposite to its very important role during heart development (Garrity et al., 2002).

Using the tools generated during this thesis, it should be possible to analyse in more depth the gene expression profile of different the trabecular, primordial and cortical CM subtypes. For example, currently, there is no cortical layer specific maker. Crossing the primordial reporter line *careg:KuO* (Pfefferli and Jaźwińska, 2017) to *tbx5a:GFP* and a myocardial specific line would enable the comparison of primordial versus cortical layer CMs.

III Cardiomyocyte plasticity in the zebrafish embryo

In a previous report, atrial CMs were shown to transdifferentiate into ventricular CMs upon cardiac ventricle ablation in the zebrafish embryo (Zhang et al., 2013). However, we observed that FHF-derived ventricular CMs ablated at 4–7 dpf, are compensated by the 10-20% SHF-derived remaining ventricular CMs, with a minor, if any, contribution from atrial CMs (Fig. 40 B).

The contribution of atrial CMs can be ruled out because *tbx5a* is expressed in these CMs. (Fig. 4). Atrial recombination cannot be evaluated in the *tbx5a:CreER^{T2};vmhcl:loxP-tagBFP-loxP-*

mCherry-NTR line, since the *vmhcl* BAC regulatory regions are ventricular specific. However, we show that *tbx5a* driven expression of CreER^{T2} is able to recombine the DNA of atrial CMs, as shown in *tbx5a:mCherry-p2a-CreER^{T2};ubb:loxP-lacZ-loxP-GFP* double transgenic fish (Fig. 9 C–E). If atrial CMs contributed to ventricular CMs, they would activate the *vmhcl* regulatory regions, and as the switch from tagBFP to mCherry would have occurred at the DNA level, they would start expressing mCherry. The low amounts of mCherry^{+} CMs detected in the regenerated ventricle rule out an important contribution from the atria.

There are different possibilities that might explain why we do not see any contribution from the atrium in our experiments:

1. We performed the ablation at a later time point than Zhang *et al*. and it is possible that atrial CMs lose their plasticity at 4–7 dpf. This possibility fits with the fact that the atrial-to-ventricle plasticity is no longer observed in the adult (Zhang et al., 2013). It will be very interesting to study whether FHF- and SHF-derived CM plasticity remains in the adult.
2. It is possible that if there are few ventricular CMs available it will be these cells that regenerate the ventricle, whereas atrial CMs would be only a last resource, if no ventricular CMs remain.

It would be interesting to explore in more detail the mechanisms of this embryonic heart regeneration. One possibility is that because the endocardium, epicardium, and the ECM are not directly damaged, they could act as a scaffold to guide CMs migration while they proliferate. This hypothesis is supported by the fact that de-cellularised zebrafish cardiac ECM induces mammalian heart regeneration (Chen et al., 2016), and by the results reported here on the role of fibroblasts for adult heart regeneration.

Our results on the compensation of the FHF by few SHF-derived ventricular CM suggest that although during normal development each progenitor gives rise to a defined area of the ventricle, the zebrafish ventricle is not functionally and morphologically compartmentalised. Different CMs have the ability to contribute to different areas of the ventricle than they would otherwise have. As the SHF-derived CM contribute mainly to the mammalian right ventricle, the hearts SHF-derived ventricles reported here could be considered equivalent to a right-ventricle mammalian heart. Surprisingly, we show that these ventricles recover their function. The only observed difference was that the SHF-derived ventricles have a slightly more rounded shape. It would be very interesting to test the regenerative capabilities of these fully SHF-derived ventricles upon cryoinjury.

Our transgenic lines would also allow to ablate the FHF-derived cardiomyocytes at different stages of development to test if the FHF- and SHF-derived CM plasticity remains in the adult.

Finally, the here reported *vmhcl:loxP-tagBFP-loxP-mCherry-NTR* transgenic constitutes a valuable tool to the research community. It opens many possibilities of future research, allowing specific cell ablation of ventricular CM subpopulations without affecting any other tissue. The possibility of crossing this line to any Cre line, as well as the uncoupling of cell labelling and ablation offers different possibilities, among them to ablate FHF-derived CMs in the adult, or to ablate the trabeculae in the adult. Additionally, it could be crossed into the *careg:CreER*^{T2} line to ablate the primordial layer, allowing its study in the adult zebrafish heart.

IV Cardiomyocyte progenitor sources during adult heart regeneration

In contrast to development, CM plasticity seems to be reduced in the regenerating adult heart (Zhang et al., 2013) as conversion of atrial CMs to ventricular CMs has not been conclusively reported (Bloomekatz et al., 2016). In this thesis, we describe cell plasticity for the first time in the adult, whereby some adult ventricular CMs lose their trabecular identity and become cortical CMs (Fig. 40 C).

Our findings are at odds with previous studies in which no contribution of the trabeculae to the cortical layer was detected (Gupta and Poss, 2012; Tekeli et al., 2017). A possible explanation for this discrepancy could be the different injury model used in these studies. Alternatively, limitations of clonal analysis in comparison with the use of a specific marker could have hindered the possibilities of detecting the here reported event. For example, in Tekeli *et al*., very few clones were analysed, lowering the chances to detect an event that does not occur at very high frequency. In addition, clonal analysis provides a snapshot of a clone at a given time. If a trabecular CM is labelled, and all its progeny converts to cortical CMs leaving no trabecular progeny, it could be interpreted as a cortical CM expansion.

Interestingly, this is a process that also occurs during development to form the cortical layer. This means that a developmental process can be repurposed in an injury context to contribute to regeneration. Even more interesting is the fact that *Oryzias latipes* (Medaka) does not have a cortical layer, and this correlates with its limited regenerative response (Ito et al., 2014). This observation, together with the here reported results showing that the newly regenerated myocardium is mainly a cortical layer, suggests the possibility that the developmental process of trabeculae to cortical layer transition is necessary for regeneration, and fish that have not evolved this mechanisms, are not able to regenerate their heart. Why some fish develop a cortical layer while other do not remains unknown. A possible explanation could be that very active fish such as zebrafish need an additional pumping force to provide sufficient nutrients.

When comparing the trabecular versus the cortical and primordial myocardium, we detected *acta2* and *myh10* as differentially expressed in the primordial and cortical myocardium. These genes encode for non-sarcomeric actin and myosin proteins that are usually located at the membrane cortex. This indicates that some of the most important differences between these types of CMs are genes usually implicated in cell contractility, motility and mechanosensing. It remains to be explored whether the trabecular to cortical layer transition could be triggered by specific mechanical properties of the different areas.

We detected a thickened *tbx5a*$^{-}$ cortical layer in the regenerated myocardium. These results fit with the described absence of *nppa* in this cell layers (González-Rosa et al., 2014). Moreover, while the overall ventricular function is recovered upon regeneration, we noted that some regions did not fully recover their function (González-Rosa et al., 2014). Taken together, these results show that heart regeneration in the zebrafish is also not 100% perfect, in which a newly thickened cortical layer is formed at least in part from trabecular CMs.

We observed the transition from trabecular CMs to cortical myocardium, but is the reversed scenario also possible? Future research in which cortical layer CMs are lineage-traced will be needed to answer this question.

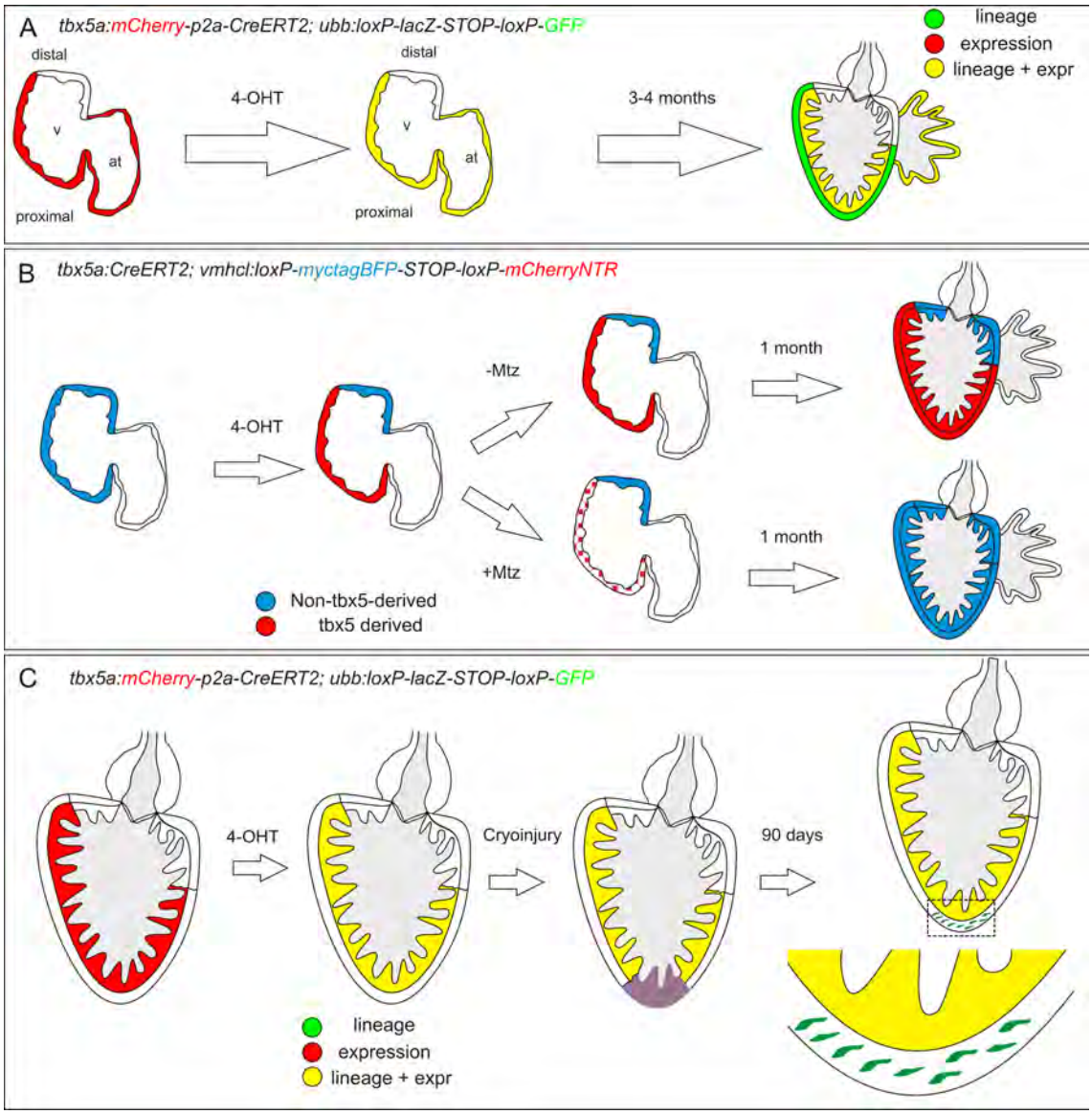

Figure 40. Summary of the contribution of *tbx5a* positive and negative myocardium during heart development and regeneration. A, Identification of *tbx5a*-expressing and *tbx5a*-derived cells in the zebrafish heart. Red: *tbx5a*$^{+}$ cells; green: *tbx5a*-derived cells not expressing *tbx5a*; yellow, *tbx5a*-expressing cells derived from embryonic *tbx5a*$^{+}$ cells. **B**, Replacement of the embryonic FHF myocardium with SHF progenitors. Blue: ventricular CMs; red: *tbx5a*-derived ventricular CMs; dotted red: ablated *tbx5a*-derived ventricular CMs. **C**, Contribution of *tbx5a*-derived cells during heart regeneration in the zebrafish. Red: *tbx5a*$^{+}$ cells; green: *tbx5a*-derived cells not expressing *tbx5a*; yellow, *tbx5a*-expressing cells derived from trabecular adult *tbx5a*$^{+}$ cells.

V Fibroblast origins

Although there are important differences between the mouse and zebrafish heart, including their capacity for regeneration, the cellular basis of fibrosis upon heart injury is similar. In both organisms, there is a resident fibroblast population that is developmentally derived from the epicardium and is the main contributor to activated fibroblasts upon injury. Moreover, there is a limited contribution from endothelial/endocardial cells (Fig. 41 A). An important difference between the two organisms, however, is that while in the zebrafish resident fibroblasts constitute a minor population restricted to a very specific location, in the mammalian model they constitute 12-13% of the cells in the heart. This could explain why the fibrotic response in the zebrafish is limited and is compatible with regeneration.

Tcf21 labels both epicardium and epicardium-derived resident fibroblasts (Fig. 41 B). While we could find a specific marker for epicardium derived fibroblasts (*wt1a*), there is no specific epicardium marker yet available. This hinders the possibility of precisely evaluating the contribution of the epicardium to fibroblasts upon injury, and to compare this to what is known in the mouse, in which epicardial cells do not contribute to cardiac fibroblasts upon pressure overload (Moore-Morris et al., 2014).

Interestingly, cells from different origins contribute to fibrosis in different ways. While the epicardium and epicardium-derived-fibroblasts express both *col1a2* and *postnb*, the endocardium activates *col1a2* expression but not *postnb*. This creates a niche with different environments that could influence regeneration, and could potentially guide CMs during heart regeneration.

Surprisingly, the endocardium is able to activate *postnb* expression during development when it gives rise to the mesenchyme of the valves (Fig. 28 F), as occurs in mammalian models (Markwald et al., 1977). Why the endocardium reacts differently during development and upon injury remains an open question, and provides an additional example of the loss of cell plasticity as development progresses.

It is very interesting that although different cell types start producing ECM proteins, they do not lose their initial identity. For example, endocardial cells activate some genes, but they do not lose *fli1a* and *kdrl* expression, and *wt1a*:GFP^{+} resident fibroblasts do not lose *wt1a*:GFP upon activation.

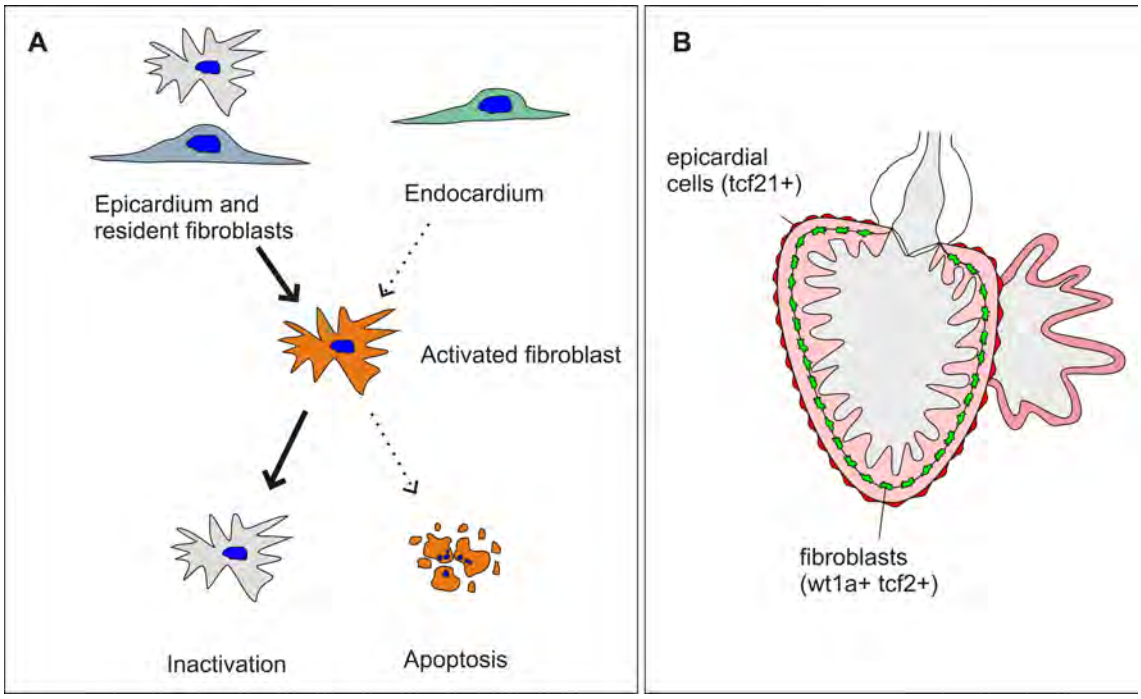

Figure 41. Fibroblast makers, origin and fate during heart regeneration in the zebrafish. A, Activated fibroblasts are derived from epicardium and resident fibroblasts, and they become inactive as regeneration progresses. **B,** *tcf21* is expressed in both epicardial cells and resident fibroblasts, while *wt1a* is specific for the resident fibroblasts.

VI Fibroblast markers

Our results support the notion that *postnb* is a very good marker for activated fibroblasts, as shown for the mouse model (Kanisicak et al., 2016). However, this marker is not quite specific when we consider the areas different from the injury area, as it is expressed in other parts of the heart such as the valves and some ventricular CMs near to the atrio-ventricular canal (Fig. 35).

According to our transcriptomics data, collagen I (coded by *col1a1a*, *col1a1b* and *col1a2* genes) is one of the most highly expressed ECM proteins. Here, we used a Col1a1 antibody and *col1a2* reporter lines to identify which cells are responsible of collagen I production. Its expression partially overlaps with *postnb* in activated fibroblasts. However, it is also expressed in the activated endocardium, although these cells cannot be considered fibroblasts. Thus, we propose the use of both markers to better characterise the fibrotic response in the zebrafish heart. Consequently, we can study not only fibroblasts, but also other ECM producing cells.

VII Fibroblast fate

The number of fibroblasts decreases as the heart regenerates, but the majority of fibroblasts remains in the heart even at 60 dpi. This, together with the finding that only a few cells are eliminated through apoptosis suggests that the main mechanism of fibrosis regression is fibroblast inactivation (Fig. 41 A).

Our results provide an explanation for the previous observation of *tcf21*-derived cells detected between the regenerated myocardium (Kikuchi et al., 2011b). Likely, they represent epicardial derived inactivated fibroblasts.

Our transcriptome analysis revealed that while most of the pro-fibrotic program is downregulated, there are some ECM proteins, including *col8a2* and *col7a1l*, that upregulate their expression only in the regenerated heart. They were, however, expressed at a very low level, making it unlikely that they contribute to fibrosis. Moreover, their role remains unknown. Are they necessary to re-establish the basal lamina? Could they influence the contractile properties of the regenerated myocardium? Studies using mutant lines for these genes could shed light on their role during heart regeneration.

Finally, the fact that a regenerated heart contains more fibroblasts than an uninjured heart suggests that these hearts might respond faster to a fibrotic stimulus, as is seen in the mammalian liver (Kisseleva et al., 2012). In this regard, experiments to analyse how the regenerated zebrafish heart responds to repetitive injuries are currently under investigation.

VIII Role of fibroblasts during regeneration

While fibrosis was thought to be a possible reason why mammalian organisms are not able to regenerate (Poss et al., 2002), we found that fibroblasts do not only not actually impede regeneration, but rather, they are necessary to promote CM proliferation. The reported transcriptomic data provides two possible explanations for this result:

1) The deposited ECM is necessary as a scaffold for CMs. This possibility is supported by the finding that the ECM protein AGRIN is necessary for neonatal mouse regeneration (Bassat et al., 2017).
2) Fibroblasts produce secreted molecules that could influence regeneration. Indeed, some of the identified genes have an already proven role during regeneration such as *igf* (Huang et al., 2013a), *bmp2b* (Wu et al., 2016) and *fstl1* (Wei et al., 2015). Others, among them *wnt5a*, *wnt16*, *rspo1* and *hhip* have not yet been studied in the context of regeneration. Further studies would be important in this regard.

It is very surprising that while fibroblast ablation impaired CM proliferation, no long-term differences on heart regeneration were observed. A possible explanation could be that Mtz, the chemical used for ablation, might have an effect on regeneration itself. Thus, if Mtz impairs regeneration, those hearts are not able to regenerate, independent of fibroblast ablation and animals from the experimental condition would not be different form the controls (non transgenic Mtz treated animals). Alternatively, heart regeneration might be a very robust injury response sustained through cellular and molecular mechanisms acting in parallel. Elimination of a single cell source might only slightly impair the process and not be sufficient to abolish it completely.

IX Concluding remarks

In this thesis, a systematic lineage tracing of cells during zebrafish heart development and regeneration was performed. CMs plasticity was found to be higher than expected, not only in the embryonic heart, but also in the adult. Additionally, the origin of cardiac fibroblasts in the zebrafish was analysed, and we found that they are not only contribute to the fibrotic response after injury but they are also necessary for CM proliferation. This new knowledge on CM plasticity and how fibrosis influences myocardial proliferation in a species with endogenous regenerative potential could have important implications for regenerative medicine strategies.

CONCLUSIONS

CONCLUSIONS

1. The zebrafish heart is derived from two different heart fields; the FHF can be labelled by *tbx5a* expression.

2. *tbx5a* is expressed in the FHF-derived trabeculae of the ventricle.

3. The cortical layer of the adult ventricle does not express *tbx5a*, but is derived from *tbx5a*$^{+}$ cells.

4. Loss of FHF-derived CMs can be compensated by SHF-derived ventricular CMs.

5. CMs plasticity remains in the adult heart and trabecular CMs contribute to the regeneration of the cortical layer.

6. Epicardium and epicardium-derived-fibroblasts are the major cells contributing to activated fibroblasts in the cryoinjured heart, whereas endocardial cells only contribute to collagen production.

7. Activated *postnb*$^{+}$ fibroblasts express ECM and secreted signalling proteins upon injury.

8. Fibroblast inactivation is the main mechanism of fibrosis regression.

9. Fibroblasts promote CM proliferation during regeneration.

CONCLUSIONES

CONCLUSIONES

1. El corazón del pez cebra deriva de dos campos cardiacos, el primero de ellos puede ser marcado por la expresión de *tbx5a*.

2. *tbx5a*, en el corazón adulto se expresa en las trabéculas derivadas del campo cardiaco primario.

3. La capa cortical del ventrículo no expresa *tbx5a*, pero deriva de células *tbx5a*$^{+}$.

4. La pérdida de cardiomiocitos derivados del campo cardiaco primario puede ser compensada por cardiomiocitos del campo cardiaco secundario.

5. La plasticidad de cardiomiocitos se mantiene en el corazón adulto, siendo los cardiomiocitos de las trabéculas capaces de contribuir a la nueva capa cortical.

6. El epicardio y los fibroblastos derivados del epicardio son la principal fuente de fibroblastos en el corazón infartado, mientras que las células endocárdicas solo contribuyen a la producción de colágeno.

7. Los fibroblastos activados postnb+ producen proteínas de matriz extracelular y moléculas señalizadoras tras el infarto.

8. La inactivación de fibroblastos es el principal mecanismo de regresión de la fibrosis.

9. Los fibroblastos promueven la proliferación de cardiomiocitos durante la regeneración.

BIBLIOGRAPHY

BIBLIOGRAPHY

Abremski, K. and Hoess, R. (1984). Bacteriophage P1 site-specific recombination. Purification and properties of the Cre recombinase protein. *J. Biol. Chem.* **259**, 1509–14.

Ahn, D., Kourakis, M. J., Rohde, L. A., Silver, L. M. and Ho, R. K. (2002). T-box gene tbx5 is essential for formation of the pectoral limb bud. *Nature* **417**, 754–8.

Albalat, R., Baquero, M. and Minguillón, C. (2010). Identification and characterisation of the developmental expression pattern of tbx5b, a novel tbx5 gene in zebrafish. **10**, 24–30.

Ali, S. R., Ranjbarvaziri, S., Talkhabi, M., Zhao, P., Subat, A., Hojjat, A., Kamran, P., Müller, A. M. S., Volz, K. S., Tang, Z., et al. (2014). Developmental Heterogeneity of Cardiac Fibroblasts Does Not Predict Pathological Proliferation and Activation. *Circ. Res.* **115**, 625–635.

Anlezark, G. M., Melton, R. G., Sherwood, R. F., Coles, B., Friedlos, F. and Knox, R. J. (1992). The bioactivation of 5-(aziridin-1-yl)-2,4-dinitrobenzamide (CB1954)--I. Purification and properties of a nitroreductase enzyme from Escherichia coli--a potential enzyme for antibody-directed enzyme prodrug therapy (ADEPT). *Biochem. Pharmacol.* **44**, 2289–95.

Apschner, A., Huitema, L. F. A., Ponsioen, B., Peterson-Maduro, J. and Schulte-Merker, S. (2014). Zebrafish enpp1 mutants exhibit pathological mineralization, mimicking features of generalized arterial calcification of infancy (GACI) and pseudoxanthoma elasticum (PXE). *Dis. Model. Mech.* **7**, 811–22.

Arnolds, D. E., Liu, F., Fahrenbach, J. P., Kim, G. H., Schillinger, K. J., Smemo, S., McNally, E. M., Nobrega, M. A., Patel, V. V. and Moskowitz, I. P. (2012). TBX5 drives Scn5a expression to regulate cardiac conduction system function. **122**,.

Banerjee, I., Fuseler, J. W., Price, R. L., Borg, T. K. and Baudino, T. A. (2007). Determination of cell types and numbers during cardiac development in the neonatal and adult rat and mouse. *Am. J. Physiol. Heart Circ. Physiol.* **293**, H1883-91.

Barandon, L., Couffinhal, T., Dufourcq, P., Ezan, J., Costet, P., Daret, D., Deville, C. and Duplàa, C. (2004). Frizzled A, a novel angiogenic factor: promises for cardiac repair. *Eur. J. Cardio-Thoracic Surg.* **25**, 76–83.

Barisic, I., Boban, L., Greenlees, R., Garne, E., Wellesley, D., Calzolari, E., Addor, M.-C., Arriola, L., Bergman, J. E., Braz, P., et al. (2014). Holt Oram syndrome: a registry-based study in Europe. **9**, 156.

Bassat, E., Mutlak, Y. E., Genzelinakh, A., Shadrin, I. Y., Baruch Umansky, K., Yifa, O., Kain, D., Rajchman, D., Leach, J., Riabov Bassat, D., et al. (2017). The extracellular matrix protein agrin promotes heart regeneration in mice. *Nature* **547**, 179–184.

Basson, C. T., Cowley, G. S., Solomon, S. D., Weissman, B., Poznanski, A. K., Traill, T. A., Seidman, J. G. and Seidman, C. E. (1994). The clinical and genetic spectrum of the Holt-Oram syndrome (heart-hand syndrome). *N. Engl. J. Med.* **330**, 885–91.

Benjamin, E. J., Blaha, M. J., Chiuve, S. E., Cushman, M., Das, S. R., Deo, R., de Ferranti, S. D., Floyd, J., Fornage, M., Gillespie, C., et al. (2017). Heart Disease and Stroke Statistics—2017 Update: A Report From the American Heart Association. *Circulation* **135**, e146–e603.

Bergmann, O., Bhardwaj, R. D., Bernard, S., Zdunek, S., Barnabé-Heider, F., Walsh, S., Zupicich, J., Alkass, K., Buchholz, B. A., Druid, H., et al. (2009). Evidence for cardiomyocyte renewal in humans. *Science* **324**, 98–102.

Bergmann, O., Zdunek, S., Felker, A., Salehpour, M., Alkass, K., Bernard, S., Sjostrom, S. L., Szewczykowska, M., Jackowska, T., dos Remedios, C., et al. (2015). Dynamics of Cell Generation and Turnover in the Human Heart. *Cell* **161**, 1566–1575.

Bloomekatz, J., Galvez-Santisteban, M. and Chi, N. C. (2016). Myocardial plasticity: cardiac development, regeneration and disease. *Curr. Opin. Genet. Dev.* **40**, 120–130.

Bollig, F., Perner, B., Besenbeck, B., Kothe, S., Ebert, C., Taudien, S., Englert, C., Köthe, S., Ebert, C., Taudien, S., et al. (2009). A highly conserved retinoic acid responsive element controls wt1a expression in the zebrafish pronephros. *Development* **136**, 2883–2892.

Bruneau, B. G., Logan, M., Davis, N., Levi, T., Tabin, C. J., Seidman, J. G. and Seidman, C. E. (1999). Chamber-specific cardiac expression of Tbx5 and heart defects in Holt-Oram syndrome. *Dev. Biol.* **211**, 100–8.

Bruneau, B. G., Nemer, G., Schmitt, J. P., Charron, F., Robitaille, L., Caron, S., Conner, D. A., Gessler, M., Nemer, M., Seidman, C. E., et al. (2001). A murine model of Holt-Oram syndrome defines roles of the T-box transcription factor Tbx5 in cardiogenesis and disease. *Cell* **106**, 709–21.

Bui, A. L., Horwich, T. B. and Fonarow, G. C. (2011). Epidemiology and risk profile of heart failure. *Nat. Rev. Cardiol.* **8**, 30–41.

Cai, C.-L., Liang, X., Shi, Y., Chu, P.-H., Pfaff, S. L., Chen, J. and Evans, S. (2003). Isl1 identifies a cardiac progenitor population that proliferates prior to differentiation and

contributes a majority of cells to the heart. *Dev. Cell* **5**, 877–89.

Cai, C.-L., Martin, J. C., Sun, Y., Cui, L., Wang, L., Ouyang, K., Yang, L., Bu, L., Liang, X., Zhang, X., et al. (2008). A myocardial lineage derives from Tbx18 epicardial cells. *Nature* **454**, 104–8.

Cai, D., Cohen, K. B., Luo, T., Lichtman, J. W. and Sanes, J. R. (2013). Improved tools for the Brainbow toolbox. *Nat. Methods* **10**, 540–547.

Carmona, R., González-Iriarte, M., Pérez-Pomares, J. M. and Muñoz-Chápuli, R. (2001). Localization of the Wilm's tumour protein WT1 in avian embryos. *Cell Tissue Res.* **303**, 173–86.

Chablais, F. and Jazwinska, A. (2012). The regenerative capacity of the zebrafish heart is dependent on TGF signaling. *Development* **139**, 1921–1930.

Chablais, F., Veit, J., Rainer, G. and Jaźwińska, A. (2011). The zebrafish heart regenerates after cryoinjury-induced myocardial infarction. *BMC Dev. Biol.* **11**, 21.

Chapman, D. L., Garvey, N., Hancock, S., Alexiou, M., Agulnik, S. I., Gibson-Brown, J. J., Cebra-Thomas, J., Bollag, R. J., Silver, L. M. and Papaioannou, V. E. (1996). Expression of the T-box family genes,Tbx1-Tbx5, during early mouse development. *Dev. Dyn.* **206**, 379–390.

Chen, W. C. W., Wang, Z., Missinato, M. A., Park, D. W., Long, D. W., Liu, H.-J., Zeng, X., Yates, N. A., Kim, K. and Wang, Y. (2016). Decellularized zebrafish cardiac extracellular matrix induces mammalian heart regeneration. *Sci. Adv.* **2**, e1600844.

Curado, S., Anderson, R. M., Jungblut, B., Mumm, J., Schroeter, E. and Stainier, D. Y. R. (2007). Conditional targeted cell ablation in zebrafish: A new tool for regeneration studies. *Dev. Dyn.* **236**, 1025–1035.

Curado, S., Stainier, D. Y. R. and Anderson, R. M. (2008). Nitroreductase-mediated cell/tissue ablation in zebrafish: a spatially and temporally controlled ablation method with applications in developmental and regeneration studies. *Nat. Protoc.* **3**, 948–954.

de Pater, E., Clijsters, L., Marques, S. R., Lin, Y.-F., Garavito-Aguilar, Z. V., Yelon, D. and Bakkers, J. (2009). Distinct phases of cardiomyocyte differentiation regulate growth of the zebrafish heart. *Development* **136**, 1633–1641.

de Preux Charles, A.-S., Bise, T., Baier, F., Marro, J. and Jaźwińska, A. (2016). Distinct effects of inflammation on preconditioning and regeneration of the adult zebrafish heart. *Open Biol.* **6**, 160102.

Debeer, P., Race, V., Gewillig, M., Devriendt, K. and Frijns, J.-P. (2007). Novel TBX5 mutations in patients with Holt-Oram syndrome. *Clin. Orthop. Relat. Res.* **462**, 20–6.

Devine, W. P., Wythe, J. D., George, M., Koshiba-Takeuchi, K. and Bruneau, B. G. (2014). Early patterning and specification of cardiac progenitors in gastrulating mesoderm. *Elife* **3**,.

Di Donato, V., De Santis, F., Auer, T. O., Testa, N., Sánchez-Iranzo, H., Mercader, N., Concordet, J.-P. and Del Bene, F. (2016). 2C-Cas9: a versatile tool for clonal analysis of gene function. *Genome Res.* **26**, 681–692.

Dodou, E., Verzi, M. P., Anderson, J. P., Xu, S.-M. and Black, B. L. (2004). Mef2c is a direct transcriptional target of ISL1 and GATA factors in the anterior heart field during mouse embryonic development. *Development* **131**, 3931–3942.

Donà, E., Barry, J. D., Valentin, G., Quirin, C., Khmelinskii, A., Kunze, A., Durdu, S., Newton, L. R., Fernandez-Minan, A., Huber, W., et al. (2013). Directional tissue migration through a self-generated chemokine gradient. **503**, 285–9.

Dyer, L. A. and Kirby, M. L. (2009). The role of secondary heart field in cardiac development. *Dev. Biol.* **336**, 137–144.

Edwards, D. I. (1993). Nitroimidazole drugs--action and resistance mechanisms. II. Mechanisms of resistance. *J. Antimicrob. Chemother.* **31**, 201–10.

Ellis, K., Bagwell, J. and Bagnat, M. (2013). Notochord vacuoles are lysosome-related organelles that function in axis and spine morphogenesis. *J. Cell Biol.* **200**, 667–679.

Feil, R., Wagner, J., Metzger, D. and Chambon, P. (1997). Regulation of Cre Recombinase Activity by Mutated Estrogen Receptor Ligand-Binding Domains. *Biochem. Biophys. Res. Commun.* **237**, 752–757.

Felker, A., Nieuwenhuize, S., Dolbois, A., Blazkova, K., Hess, C., Low, L. W. L., Burger, S., Samson, N., Carney, T. J., Bartunek, P., et al. (2016). In Vivo Performance and Properties of Tamoxifen Metabolites for CreERT2 Control. *PLoS One* **11**, e0152989.

Flink, I. L. (2002). Cell cycle reentry of ventricular and atrial cardiomyocytes and cells within the epicardium following amputation of the ventricular apex in the axolotl, Amblystoma mexicanum: confocal microscopic immunofluorescent image analysis of bromodeoxyuridine-labeled nuclei. *Anat. Embryol. (Berl).* **205**, 235–44.

Galli, D., Domínguez, J. N., Zaffran, S., Munk, A., Brown, N. A. and Buckingham, M. E. (2008). Atrial myocardium derives from the posterior region of the second heart field,

which acquires left-right identity as Pitx2c is expressed. *Development* **135**, 1157–67.

Garcia, J., Bagwell, J., Njaine, B., Norman, J., Levic, D. S., Wopat, S., Miller, S. E., Liu, X., Locasale, J. W., Stainier, D. Y. R., et al. (2017). Sheath Cell Invasion and Trans-differentiation Repair Mechanical Damage Caused by Loss of Caveolae in the Zebrafish Notochord. *Curr. Biol.* **27**, 1982–1989.e3.

Garrity, D. M., Childs, S. and Fishman, M. C. (2002). The heartstrings mutation in zebrafish causes heart/fin Tbx5 deficiency syndrome. *Development* **129**, 4635–45.

Gibb, N., Lavery, D. L. and Hoppler, S. (2013). sfrp1 promotes cardiomyocyte differentiation in Xenopus via negative-feedback regulation of Wnt signalling. *Development* **140**, 1537–49.

Gibson-Brown, J. J., I Agulnik S, Silver, L. M. and Papaioannou, V. E. (1998). Expression of T-box genes Tbx2-Tbx5 during chick organogenesis. *Mech. Dev.* **74**, 165–9.

Gilbert, S. F. (2010). *Developmental biology*. Sinauer Associates.

Goldman, J. A., Kuzu, G., Lee, N., Karasik, J., Gemberling, M., Foglia, M. J., Karra, R., Dickson, A. L., Sun, F., Tolstorukov, M. Y., et al. (2017). Resolving Heart Regeneration by Replacement Histone Profiling. *Dev. Cell* **40**, 392–404.e5.

González-Rosa, J. M. and Mercader, N. (2012). Cryoinjury as a myocardial infarction model for the study of cardiac regeneration in the zebrafish. *Nat. Protoc.* **7**, 782–8.

González-Rosa, J. M., Martín, V., Peralta, M., Torres, M. and Mercader, N. (2011). Extensive scar formation and regression during heart regeneration after cryoinjury in zebrafish. *Development* **138**, 1663–74.

González-Rosa, J. M., Peralta, M. and Mercader, N. (2012). Pan-epicardial lineage tracing reveals that epicardium derived cells give rise to myofibroblasts and perivascular cells during zebrafish heart regeneration. *Dev. Biol.* **370**, 173–86.

González-Rosa, J. M., Guzmán-Martínez, G., Marques, I. J., Sánchez-Iranzo, H., Jiménez-Borreguero, L. J. and Mercader, N. (2014). Use of Echocardiography Reveals Reestablishment of Ventricular Pumping Efficiency and Partial Ventricular Wall Motion Recovery upon Ventricular Cryoinjury in the Zebrafish. *PLoS One* **9**, e115604.

Gorza, L., Schiaffino, S. and Vitadello, M. (1988). Heart conduction system: a neural crest derivative? *Brain Res.* **457**, 360–6.

Gourdie, R. G., Dimmeler, S. and Kohl, P. (2016). Novel therapeutic strategies targeting fibroblasts and fibrosis in heart disease. *Nat. Rev. Drug Discov.* **15**, 620–38.

Gupta, V. and Poss, K. D. (2012). Clonally dominant cardiomyocytes direct heart morphogenesis. *Nature* **484**, 479–484.

Haenig, B. and Kispert, A. (2004). Analysis of TBX18 expression in chick embryos. *Dev. Genes Evol.* **214**, 407–11.

Haudek, S. B., Xia, Y., Huebener, P., Lee, J. M., Carlson, S., Crawford, J. R., Pilling, D., Gomer, R. H., Trial, J., Frangogiannis, N. G., et al. (2006). Bone marrow-derived fibroblast precursors mediate ischemic cardiomyopathy in mice. *Proc. Natl. Acad. Sci. U. S. A.* **103**, 18284–9.

He, J., Lu, H., Zou, Q. and Luo, L. (2014). Regeneration of Liver After Extreme Hepatocyte Loss Occurs Mainly via Biliary Transdifferentiation in Zebrafish. *Gastroenterology* **146**, 789–800.e8.

Herrmann, B. G., Labeit, S., Poustka, A., King, T. R. and Lehrach, H. (1990). Cloning of the T gene required in mesoderm formation in the mouse. *Nature* **343**, 617–22.

Holt, M. and Oram, S. (1960). Familial heart disease with skeletal malformations. *Br. Heart J.* **22**, 236–42.

Horb, M. E. and Thomsen, G. H. (1999). Tbx5 is essential for heart development. *Development* **126**, 1739–51.

Huang, Y., Harrison, M. R., Osorio, A., Kim, J., Baugh, A., Duan, C., Sucov, H. M. and Lien, C.-L. (2013a). Igf Signaling is Required for Cardiomyocyte Proliferation during Zebrafish Heart Development and Regeneration. *PLoS One* **8**, e67266.

Huang, W.-C., Yang, C.-C., Chen, I.-H., Liu, Y.-M. L., Chang, S.-J. and Chuang, Y.-J. (2013b). Treatment of Glucocorticoids Inhibited Early Immune Responses and Impaired Cardiac Repair in Adult Zebrafish. *PLoS One* **8**, e66613.

Hudon-David, F., Bouzeghrane, F., Couture, P. and Thibault, G. (2007). Thy-1 expression by cardiac fibroblasts: lack of association with myofibroblast contractile markers. *J. Mol. Cell. Cardiol.* **42**, 991–1000.

Ieda, M., Fu, J.-D., Delgado-Olguin, P., Vedantham, V., Hayashi, Y., Bruneau, B. G. and Srivastava, D. (2010). Direct reprogramming of fibroblasts into functional cardiomyocytes by defined factors. *Cell* **142**, 375–86.

Ito, K., Morioka, M., Kimura, S., Tasaki, M., Inohaya, K. and Kudo, A. (2014). Differential reparative phenotypes between zebrafish and medaka after cardiac injury. *Dev. Dyn.* **243**, 1106–1115.

Jahangiri, L., Sharpe, M., Novikov, N., Gonzalez-Rosa, J. M., Borikova, A., Nevis, K., Paffett-Lugassy, N., Zhao, L., Adams, M., Guner-Ataman, B., et al. (2016). The AP-1 transcription factor component Fosl2 potentiates the rate of myocardial differentiation from the zebrafish second heart field. *Development* **143**, 113–122.

Jain, R., Engleka, K. A., Rentschler, S. L., Manderfield, L. J., Li, L., Yuan, L. and Epstein, J. A. (2011). Cardiac neural crest orchestrates remodeling and functional maturation of mouse semilunar valves. *J. Clin. Invest.* **121**, 422–30.

Jensen, B., Boukens, B. J. D., Postma, A. V, Gunst, Q. D., van den Hoff, M. J. B., Moorman, A. F. M., Wang, T. and Christoffels, V. M. (2012). Identifying the evolutionary building blocks of the cardiac conduction system. *PLoS One* **7**, e44231.

Jopling, C., Sleep, E., Raya, M., Martí, M., Raya, A. and Belmonte, J. C. I. (2010). Zebrafish heart regeneration occurs by cardiomyocyte dedifferentiation and proliferation. *Nature* **464**, 606–609.

Kanisicak, O., Khalil, H., Ivey, M. J., Karch, J., Maliken, B. D., Correll, R. N., Brody, M. J., J. Lin, S.-C., Aronow, B. J., Tallquist, M. D., et al. (2016). Genetic lineage tracing defines myofibroblast origin and function in the injured heart. *Nat. Commun.* **7**, 12260.

Kelly, R. G., Brown, N. A. and Buckingham, M. E. (2001). The arterial pole of the mouse heart forms from Fgf10-expressing cells in pharyngeal mesoderm. *Dev. Cell* **1**, 435–40.

Kikuchi, K., Holdway, J. E., Werdich, A. A., Anderson, R. M., Fang, Y., Egnaczyk, G. F., Evans, T., Macrae, C. A., Stainier, D. Y. R. and Poss, K. D. (2010). Primary contribution to zebrafish heart regeneration by gata4(+) cardiomyocytes. *Nature* **464**, 601–5.

Kikuchi, K., Holdway, J. E., Major, R. J., Blum, N., Dahn, R. D., Begemann, G. and Poss, K. D. (2011a). Retinoic acid production by endocardium and epicardium is an injury response essential for zebrafish heart regeneration. *Dev. Cell* **20**, 397–404.

Kikuchi, K., Gupta, V., Wang, J., Holdway, J. E., Wills, A. A., Fang, Y. Y. and Poss, K. D. (2011b). tcf21+ epicardial cells adopt non-myocardial fates during zebrafish heart development and regeneration. *Development* **138**, 2895–902.

Kim, J., Wu, Q., Zhang, Y., Wiens, K. M., Huang, Y., Rubin, N., Shimada, H., Handin, R. I., Chao, M. Y., Tuan, T.-L., et al. (2010). PDGF signaling is required for epicardial function and blood vessel formation in regenerating zebrafish hearts. *Proc. Natl. Acad. Sci.* **107**, 17206–17210.

Kirby, M. L. (2007). *Cardiac development*. Oxford University Press.

Kisseleva, T., Cong, M., Paik, Y., Scholten, D., Jiang, C., Benner, C., Iwaisako, K., Moore-Morris, T., Scott, B., Tsukamoto, H., et al. (2012). Myofibroblasts revert to an inactive phenotype during regression of liver fibrosis. *Proc. Natl. Acad. Sci.* **109**, 9448–9453.

Koibuchi, N. and Chin, M. T. (2007). CHF1/Hey2 Plays a Pivotal Role in Left Ventricular Maturation Through Suppression of Ectopic Atrial Gene Expression. *Circ. Res.* **100**, 850–855.

Kong, P., Christia, P., Saxena, A., Su, Y. and Frangogiannis, N. G. (2013). Lack of specificity of fibroblast-specific protein 1 in cardiac remodeling and fibrosis. *AJP Hear. Circ. Physiol.* **305**, H1363–H1372.

Koshiba-Takeuchi, K., Mori, A. D., Kaynak, B. L., Cebra-Thomas, J., Sukonnik, T., Georges, R. O., Latham, S., Beck, L., Beck, L., Henkelman, R. M., et al. (2009). Reptilian heart development and the molecular basis of cardiac chamber evolution. *Nature* **461**, 95–8.

Kragl, M., Knapp, D., Nacu, E., Khattak, S., Maden, M., Epperlein, H. H. and Tanaka, E. M. (2009). Cells keep a memory of their tissue origin during axolotl limb regeneration. *Nature* **460**, 60–5.

Kwan, K. M., Fujimoto, E., Grabher, C., Mangum, B. D., Hardy, M. E., Campbell, D. S., Parant, J. M., Yost, H. J., Kanki, J. P. and Chien, C.-B. (2007). The Tol2kit: a multisite gateway-based construction kit for Tol2 transposon transgenesis constructs. *Dev. Dyn.* **236**, 3088–99.

Lafontant, P. J., Behzad, A. R., Brown, E., Landry, P., Hu, N. and Burns, A. R. (2013). Cardiac myocyte diversity and a fibroblast network in the junctional region of the zebrafish heart revealed by transmission and serial block-face scanning electron microscopy. *PLoS One* **8**, e72388.

Lawson, N. D. and Weinstein, B. M. (2002). In vivo imaging of embryonic vascular development using transgenic zebrafish. *Dev. Biol.* **248**, 307–18.

Lawson, K. A., Meneses, J. J. and Pedersen, R. A. (1991). Clonal analysis of epiblast fate during germ layer formation in the mouse embryo. *Development* **113**, 891–911.

Lee, E.-C. C., Yu, D., Martinez de Velasco, J., Tessarollo, L., Swing, D. A., Court, D. L., Jenkins, N. A. and Copeland, N. G. (2001). A Highly Efficient Escherichia coli-Based Chromosome Engineering System Adapted for Recombinogenic Targeting and Subcloning of BAC DNA. *Genomics* **73**, 56–65.

Lepilina, A., Coon, A. N., Kikuchi, K., Holdway, J. E., Roberts, R. W., Burns, C. G. and

Poss, K. D. (2006). A dynamic epicardial injury response supports progenitor cell activity during zebrafish heart regeneration. *Cell* **127**, 607–19.

Li, B. and Dewey, C. N. (2011). RSEM: accurate transcript quantification from RNA-Seq data with or without a reference genome. *BMC Bioinformatics* **12**, 323.

Lindmark, D. G. and Müller, M. (1976). Antitrichomonad action, mutagenicity, and reduction of metronidazole and other nitroimidazoles. *Antimicrob. Agents Chemother.* **10**, 476–82.

Lindsey, S. E., Butcher, J. T. and Yalcin, H. C. (2014). Mechanical regulation of cardiac development. *Front. Physiol.* **5**, 318.

Mably, J. D., Mohideen, M. A. P. K., Burns, C. G., Chen, J.-N. and Fishman, M. C. (2003). heart of glass regulates the concentric growth of the heart in zebrafish. *Curr. Biol.* **13**, 2138–47.

Männer, J., Schlueter, J. and Brand, T. (2005). Experimental analyses of the function of the proepicardium using a new microsurgical procedure to induce loss-of-proepicardial-function in chick embryos. *Dev. Dyn.* **233**, 1454–1463.

Männer, J., Wessel, A. and Yelbuz, T. M. (2010). How does the tubular embryonic heart work? Looking for the physical mechanism generating unidirectional blood flow in the valveless embryonic heart tube. *Dev. Dyn.* **239**, 1035–1046.

Markwald, R. R., Fitzharris, T. P. and Manasek, F. J. (1977). Structural development of endocardial cushions. *Am. J. Anat.* **148**, 85–119.

Marro, J., Pfefferli, C., de Preux Charles, A.-S., Bise, T. and Jaźwińska, A. (2016). Collagen XII Contributes to Epicardial and Connective Tissues in the Zebrafish Heart during Ontogenesis and Regeneration. *PLoS One* **11**, e0165497.

Martin, M. (2011). Cutadapt removes adapter sequences from high-throughput sequencing reads. *EMBnet.journal* **17**, 10.

McDermott, D. A., Bressan, M. C., He, J., Lee, J. S., Aftimos, S., Brueckner, M., Gilbert, F., Graham, G. E., Hannibal, M. C., Innis, J. W., et al. (2005). TBX5 genetic testing validates strict clinical criteria for Holt-Oram syndrome. *Pediatr. Res.* **58**, 981–6.

Mercader, N., Fischer, S. and Neumann, C. J. (2006). Prdm1 acts downstream of a sequential RA, Wnt and Fgf signaling cascade during zebrafish forelimb induction. *Development* **133**, 2805–15.

Möllmann, H., Nef, H. M., Kostin, S., von Kalle, C., Pilz, I., Weber, M., Schaper, J., Hamm, C. W. and Elsässer, A. (2006). Bone marrow-derived cells contribute to infarct

remodelling. *Cardiovasc. Res.* **71**, 661–671.

Moore-Morris, T., Guimarães-camboa, N., Banerjee, I., Zambon, A. C., Kisseleva, T., Velayoudon, A., Stallcup, W. B., Gu, Y., Dalton, N. D., Cedenilla, M., et al. (2014). Resident fibroblast lineages mediate pressure overload – induced cardiac fibrosis. *J. Clin. Invest.* **124**, 2921–34.

Morales, M. O., Price, R. L. and Goldsmith, E. C. (2005). Expression of Discoidin Domain Receptor 2 (DDR2) in the Developing Heart. *Microsc. Microanal.* **11**, 260–267.

Mosimann, C., Kaufman, C. K., Li, P., Pugach, E. K., Tamplin, O. J. and Zon, L. I. (2011). Ubiquitous transgene expression and Cre-based recombination driven by the ubiquitin promoter in zebrafish. *Development* **138**, 169–77.

Mosimann, C., Panáková, D., Werdich, A. A., Musso, G., Burger, A., Lawson, K. L., Carr, L. A., Nevis, K. R., Sabeh, M. K., Zhou, Y., et al. (2015). Chamber identity programs drive early functional partitioning of the heart. *Nat. Commun.* **6**, 8146.

Moskowitz, I. P. G., Pizard, A., Patel, V. V, Bruneau, B. G., Kim, J. B., Kupershmidt, S., Roden, D., Berul, C. I., Seidman, C. E. and Seidman, J. G. (2004). The T-Box transcription factor Tbx5 is required for the patterning and maturation of the murine cardiac conduction system. *Development* **131**, 4107–16.

Münch, J., Grivas, D., González-Rajal, Á., Torregrosa-Carrión, R. and de la Pompa, J. L. (2017). Notch signalling restricts inflammation and *serpine1* expression in the dynamic endocardium of the regenerating zebrafish heart. *Development* **144**, 1425–1440.

Nag, A. C. (1980). Study of non-muscle cells of the adult mammalian heart: a fine structural analysis and distribution. *Cytobios* **28**, 41–61.

Newbury-Ecob, R. A., Leanage, R., Raeburn, J. A. and Young, I. D. (1996). Holt-Oram syndrome: a clinical genetic study. *J. Med. Genet.* **33**, 300–7.

Oberpriller, J. and Oberpriller, J. C. (1971). Mitosis in adult newt ventricle. *J. Cell Biol.* **49**, 560–3.

Oberpriller, J. O. and Oberpriller, J. C. (1974). Response of the adult newt ventricle to injury. *J. Exp. Zool.* **187**, 249–259.

Ocaña, O. H., Coskun, H., Minguillón, C., Murawala, P., Tanaka, E. M., Galcerán, J., Muñoz-Chápuli, R. and Nieto, M. A. (2017). A right-handed signalling pathway drives heart looping in vertebrates. *Nature* **549**, 86–90.

Otten, C., van der Ven, P. F., Lewrenz, I., Paul, S., Steinhagen, A., Busch-Nentwich, E.,

Eichhorst, J., Wiesner, B., Stemple, D., Strähle, U., et al. (2012). Xirp proteins mark injured skeletal muscle in zebrafish. *PLoS One* **7**, e31041.

Parrie, L. E., Renfrew, E. M., Wal, A. Vander, Mueller, R. L. and Garrity, D. M. (2013). Zebrafish tbx5 paralogs demonstrate independent essential requirements in cardiac and pectoral fin development. *Dev. Dyn.* **242**, 485–502.

Peralta, M., González-Rosa, J. M., Marques, I. J. and Mercader, N. (2014). The Epicardium in the Embryonic and Adult Zebrafish. *J. Dev. Biol.* **2**, 101–116.

Pfefferli, C. and Jaźwińska, A. (2017). The careg element reveals a common regulation of regeneration in the zebrafish myocardium and fin. *Nat. Commun.* **8**, 15151.

Pi-Roig, A., Martin-Blanco, E. and Minguillon, C. (2014). Distinct tissue-specific requirements for the zebrafish tbx5 genes during heart, retina and pectoral fin development. *Open Biol.* **4**, 140014.

Piatkowski, T., Mühlfeld, C., Borchardt, T. and Braun, T. (2013). Reconstitution of the myocardium in regenerating newt hearts is preceded by transient deposition of extracellular matrix components. *Stem Cells Dev.* **22**, 1921–31.

Pinto, A. R., Ilinykh, A., Ivey, M. J., Kuwabara, J. T., Antoni, M. L. D., Chandran, A., Wang, L., Arora, K., Rosenthal, N. and Tallquist, M. D. (2015). Revisiting Cardiac Cellular Composition.

Poss, K. D., Wilson, L. G. and Keating, M. T. (2002). Heart regeneration in zebrafish. *Science* **298**, 2188–90.

Robb, L., Mifsud, L., Hartley, L., Biben, C., Copeland, N. G., Gilbert, D. J., Jenkins, N. A. and Harvey, R. P. (1998). epicardin: A novel basic helix-loop-helix transcription factor gene expressed in epicardium, branchial arch myoblasts, and mesenchyme of developing lung, gut, kidney, and gonads. *Dev. Dyn.* **213**, 105–13.

Robinson, M. D., McCarthy, D. J. and Smyth, G. K. (2010). edgeR: a Bioconductor package for differential expression analysis of digital gene expression data. *Bioinformatics* **26**, 139–40.

Rohr, S., Otten, C. and Abdelilah-Seyfried, S. (2008). Asymmetric involution of the myocardial field drives heart tube formation in zebrafish. *Circ. Res.* **102**, e12–e19.

Ruiz-Villalba, A., Simón, A. M., Pogontke, C., Castillo, M. I., Abizanda, G., Pelacho, B., Sánchez-Domínguez, R., Segovia, J. C., Prósper, F. and Pérez-Pomares, J. M. (2015). Interacting resident epicardium-derived fibroblasts and recruited bone marrow cells form

myocardial infarction scar. *J. Am. Coll. Cardiol.* **65**, 2057–66.

Rumyantsev, P. P. (1966). Autoradiographic study on the synthesis of DNA, RNA, and proteins in normal cardiac muscle cells and those changed by experimental injury. *Folia Histochem. Cytochem. (Krakow).* **4**, 397–424.

Rumyantsev, P. P. (1973). Post-injury DNA synthesis, mitosis and ultrastructural reorganization of adult frog cardiac myocytes. An electron microscopic-autoradiographic study. *Z. Zellforsch. Mikrosk. Anat.* **139**, 431–50.

Saga, Y., Miyagawa-Tomita, S., Takagi, A., Kitajima, S., Miyazaki, J. i and Inoue, T. (1999). MesP1 is expressed in the heart precursor cells and required for the formation of a single heart tube. *Development* **126**, 3437–47.

Sallin, P., de Preux Charles, A.-S., Duruz, V., Pfefferli, C. and Jaźwińska, A. (2015). A dual epimorphic and compensatory mode of heart regeneration in zebrafish. *Dev. Biol.* **399**, 27–40.

Samsa, L. A., Yang, B. and Liu, J. (2013). Embryonic cardiac chamber maturation: Trabeculation, conduction, and cardiomyocyte proliferation. *Am. J. Med. Genet. Part C Semin. Med. Genet.* **163**, 157–168.

Schnabel, K., Wu, C.-C., Kurth, T. and Weidinger, G. (2011). Regeneration of Cryoinjury Induced Necrotic Heart Lesions in Zebrafish Is Associated with Epicardial Activation and Cardiomyocyte Proliferation. *PLoS One* **6**, e18503.

Senyo, S. E., Steinhauser, M. L., Pizzimenti, C. L., Yang, V. K., Cai, L., Wang, M., Wu, T.-D., Guerquin-Kern, J.-L., Lechene, C. P. and Lee, R. T. (2013). Mammalian heart renewal by pre-existing cardiomyocytes. *Nature* **493**, 433–6.

Showell, C., Christine, K. S., Mandel, E. M. and Conlon, F. L. (2006). Developmental expression patterns of Tbx1, Tbx2, Tbx5, and Tbx20 in Xenopus tropicalis. *Dev. Dyn.* **235**, 1623–30.

Singh, A. R., Sivadas, A., Sabharwal, A., Vellarikal, S. K., Jayarajan, R., Verma, A., Kapoor, S., Joshi, A., Scaria, V. and Sivasubbu, S. (2016). Chamber Specific Gene Expression Landscape of the Zebrafish Heart. *PLoS One* **11**, e0147823.

Smemo, S., Campos, L. C., Moskowitz, I. P., Krieger, J. E., Pereira, A. C. and Nobrega, M. A. (2012). Regulatory variation in a TBX5 enhancer leads to isolated congenital heart disease. *Hum. Mol. Genet.* **21**, 3255–3263.

Soufan, A. T., van den Berg, G., Ruijter, J. M., de Boer, P. A. J., van den Hoff, M. J. B.

and Moorman, A. F. M. (2006). Regionalized Sequence of Myocardial Cell Growth and Proliferation Characterizes Early Chamber Formation. *Circ. Res.* **99**, 545–552.

Staudt, D. W., Liu, J., Thorn, K. S., Stuurman, N., Liebling, M. and Stainier, D. Y. R. (2014). High-resolution imaging of cardiomyocyte behavior reveals two distinct steps in ventricular trabeculation. *Development* **141**, 585–93.

Steimle, J. D. and Moskowitz, I. P. (2017). TBX5. In *Current topics in developmental biology*, pp. 195–221.

Suster, M. L., Abe, G., Schouw, A. and Kawakami, K. (2011). Transposon-mediated BAC transgenesis in zebrafish. *Nat. Protoc.* **6**, 1998–2021.

Takeuchi, J. K., Ohgi, M., Koshiba-Takeuchi, K., Shiratori, H., Sakaki, I., Ogura, K., Saijoh, Y. and Ogura, T. (2003). Tbx5 specifies the left/right ventricles and ventricular septum position during cardiogenesis. *Development* **130**, 5953–5964.

Tam, P. P., Parameswaran, M., Kinder, S. J. and Weinberger, R. P. (1997). The allocation of epiblast cells to the embryonic heart and other mesodermal lineages: the role of ingression and tissue movement during gastrulation. *Development* **124**, 1631–42.

Tanaka, M. and Tickle, C. (2004). Tbx18 and boundary formation in chick somite and wing development. *Dev. Biol.* **268**, 470–480.

Taylor, J. S., Van de Peer, Y., Braasch, I. and Meyer, A. (2001). Comparative genomics provides evidence for an ancient genome duplication event in fish. *Philos. Trans. R. Soc. B Biol. Sci.* **356**, 1661–1679.

Tekeli, I., Garcia-Puig, A., Notari, M., García-Pastor, C., Aujard, I., Jullien, L. and Raya, A. (2017). Fate predetermination of cardiac myocytes during zebrafish heart regeneration. *Open Biol.* **7**, 170116.

Tessadori, F., van Weerd, J. H., Burkhard, S. B., Verkerk, A. O., de Pater, E., Boukens, B. J., Vink, A., Christoffels, V. M. and Bakkers, J. (2012). Identification and Functional Characterization of Cardiac Pacemaker Cells in Zebrafish. *PLoS One* **7**, 1–9.

Travers, J. G., Kamal, F. A., Robbins, J., Yutzey, K. E. and Blaxall, B. C. (2016). Cardiac Fibrosis. *Circ. Res.* **118**, 1021–1040.

Tu, S. and Johnson, S. L. L. (2011). Fate Restriction in the Growing and Regenerating Zebrafish Fin. *Dev. Cell* **20**, 725–732.

van Amerongen, M. J., Bou-Gharios, G., Popa, E., van Ark, J., Petersen, A. H., van Dam, G. M., van Luyn, M. J. A. and Harmsen, M. C. (2008). Bone marrow-derived

myofibroblasts contribute functionally to scar formation after myocardial infarction. *J. Pathol.* **214**, 377–86.

van den Berg, G., Abu-Issa, R., de Boer, B. A., Hutson, M. R., de Boer, P. A. J., Soufan, A. T., Ruijter, J. M., Kirby, M. L., van den Hoff, M. J. B. and Moorman, A. F. M. (2009). A Caudal Proliferating Growth Center Contributes to Both Poles of the Forming Heart Tube. *Circ. Res.* **104**, 179–188.

van den Boogaard, M., Wong, L. Y. E., Tessadori, F., Bakker, M. L., Dreizehnter, L. K., Wakker, V., Bezzina, C. R., 't Hoen, P. A. C., Bakkers, J., Barnett, P., et al. (2012). Genetic variation in T-box binding element functionally affects SCN5A/SCN10A enhancer. *J. Clin. Invest.* **122**, 2519–2530.

van Weerd, J. H., Badi, I., van den Boogaard, M., Stefanovic, S., van de Werken, H. J. G., Gomez-Velazquez, M., Badia-Careaga, C., Manzanares, M., de Laat, W., Barnett, P., et al. (2014). A large permissive regulatory domain exclusively controls Tbx3 expression in the cardiac conduction system. *Circ. Res.* **115**, 432–41.

Verzi, M. P., McCulley, D. J., De Val, S., Dodou, E. and Black, B. L. (2005). The right ventricle, outflow tract, and ventricular septum comprise a restricted expression domain within the secondary/anterior heart field. *Dev. Biol.* **287**, 134–145.

Villefranc, J. A., Amigo, J. and Lawson, N. D. (2007). Gateway compatible vectors for analysis of gene function in the zebrafish. *Dev. Dyn.* **236**, 3077–3087.

Vincent, S. D. and Buckingham, M. E. (2010). How to Make a Heart. In *Current topics in developmental biology*, pp. 1–41.

Virágh, S. and Challice, C. E. (1981). The origin of the epicardium and the embryonic myocardial circulation in the mouse. *Anat. Rec.* **201**, 157–68.

Waldo, K., Miyagawa-Tomita, S., Kumiski, D. and Kirby, M. L. (1998). Cardiac Neural Crest Cells Provide New Insight into Septation of the Cardiac Outflow Tract: Aortic Sac to Ventricular Septal Closure. *Dev. Biol.* **196**, 129–144.

Wang, Y., Huang, X., He, L., Pu, W., Li, Y., Liu, Q., Li, Y., Zhang, L., Yu, W., Zhao, H., et al. (2017). Genetic tracing of hepatocytes in liver homeostasis, injury, and regeneration. *J. Biol. Chem.* **292**, 8594–8604.

Wei, K., Serpooshan, V., Hurtado, C., Diez-Cuñado, M., Zhao, M., Maruyama, S., Zhu, W., Fajardo, G., Noseda, M., Nakamura, K., et al. (2015). Epicardial FSTL1 reconstitution regenerates the adult mammalian heart. *Nature* **525**, 479–85.

Wessels, A. and Sedmera, D. (2003). Developmental anatomy of the heart: a tale of mice and man. *Physiol. Genomics* **15**, 165–176.

Widyantoro, B., Emoto, N., Nakayama, K., Anggrahini, D. W., Adiarto, S., Iwasa, N., Yagi, K., Miyagawa, K., Rikitake, Y., Suzuki, T., et al. (2010). Endothelial Cell-Derived Endothelin-1 Promotes Cardiac Fibrosis in Diabetic Hearts Through Stimulation of Endothelial-to-Mesenchymal Transition. *Circulation* **121**, 2407–2418.

Witman, N., Murtuza, B., Davis, B., Arner, A. and Morrison, J. I. (2011). Recapitulation of developmental cardiogenesis governs the morphological and functional regeneration of adult newt hearts following injury. *Dev. Biol.* **354**, 67–76.

Wittbrodt, J., Meyer, A. and Schartl, M. (1998). More genes in fish? *BioEssays* **20**, 511–515.

Wu, C.-C., Kruse, F., Vasudevarao, M. D., Junker, J. P., Zebrowski, D. C., Fischer, K., Noël, E. S., Grün, D., Berezikov, E., Engel, F. B., et al. (2015). Spatially Resolved Genome-wide Transcriptional Profiling Identifies BMP Signaling as Essential Regulator of Zebrafish Cardiomyocyte Regeneration. *Dev. Cell* 1–14.

Wu, C.-C., Kruse, F., Vasudevarao, M. D., Junker, J. P., Zebrowski, D. C., Fischer, K., Noël, E. S., Grün, D., Berezikov, E., Engel, F. B., et al. (2016). Spatially Resolved Genome-wide Transcriptional Profiling Identifies BMP Signaling as Essential Regulator of Zebrafish Cardiomyocyte Regeneration. *Dev. Cell* **36**, 36–49.

Xu, H., Morishima, M., Wylie, J. N., Schwartz, R. J., Bruneau, B. G., Lindsay, E. A. and Baldini, A. (2004). Tbx1 has a dual role in the morphogenesis of the cardiac outflow tract. *Development* **131**, 3217–3227.

Zak, R. (1974). Development and proliferative capacity of cardiac muscle cells. *Circ. Res.* **35**, suppl II:17-26.

Zeisberg, E. M., Tarnavski, O., Zeisberg, M., Dorfman, A. L., McMullen, J. R., Gustafsson, E., Chandraker, A., Yuan, X., Pu, W. T., Roberts, A. B., et al. (2007). Endothelial-to-mesenchymal transition contributes to cardiac fibrosis. *Nat. Med.* **13**, 952–61.

Zhang, R., Han, P., Yang, H., Ouyang, K., Lee, D., Lin, Y.-F., Ocorr, K., Kang, G., Chen, J., Stainier, D. Y. R., et al. (2013). In vivo cardiac reprogramming contributes to zebrafish heart regeneration. *Nature* **498**, 497–501.

Zhou, B., Ma, Q., Rajagopal, S., Wu, S. M., Domian, I., Rivera-Feliciano, J., Jiang, D., von Gise, A., Ikeda, S., Chien, K. R., et al. (2008). Epicardial progenitors contribute to the cardiomyocyte lineage in the developing heart. *Nature* **454**, 109–13.

Zhou, Y., Cashman, T. J., Nevis, K. R., Obregon, P., Carney, S. A., Liu, Y., Gu, A., Mosimann, C., Sondalle, S., Peterson, R. E., et al. (2011). Latent TGF-β binding protein 3 identifies a second heart field in zebrafish. *Nature* **474**,.

SUPPLEMENTARY MATERIAL

Supplementary File 1. Sequence of the plasmid used for recombineering of the *tbx5a:tdTomato* BAC.

Supplementary File 2. Sequence of the plasmid containing *mCherry-p2a-CreER^{T2}-flp-kan-flp* used as a template for recombineering.

Supplementary File 3. Sequence of the plasmid containing *iTol2Amp-Cryst:RFP* used as a template for recombineering.

Supplementary File 4. Sequence of the plasmid containing *loxP_tagBFP_loxP_mCherry-NTR-flp-kan-flp* used as a template for recombineering.

Supplementary File 5. Sequence of the plasmid containing *iTol2Amp-Cryst:GFP* used as a template for recombineering.

Supplementary File 6. Sequence of the plasmid used to generate the *wt1a:CreER^{T2}* transgenic line.

Supplementary Table 1. Differentially expressed genes comparing the *tbx5a*:GFP^{+} cardiomyocytes to the *tbx5a*:GFP^{-} cardiomyocytes.

Supplementary Table 2. Differentially expressed genes comparing the *wt1a*:GFP^{+} cells to the rest of the cells in the zebrafish ventricle.

Supplementary Table 3. Differentially expressed genes comparing the *kdrl*:mCherry^{+} cells at 7 dpi to the *kdrl*:mCherry^{+} in an uninjured zebrafish ventricle.

Supplementary Table 4. Differentially expressed genes comparing the *posntb*:citrine^{+} cells at 7 dpi to the *kdrl*:mCherry^{-} *postnb*:citrine^{-} cells in the zebrafish ventricle at 7 dpi.

Supplementary Table 5. Differentially expressed genes comparing the *postnb*-lineage traced cells at 7 dpi to the same cells at 60 dpi.

Supplementary Video 1. Confocal optical sections of *tbx5a:GFP*;*myl7*:*mbmCherry* hearts at 72 hpf. GFP (green) labels *tbx5a*$^{+}$ cells and mCherry (red) marks cells expressing the panmyocardial marker *myosin light chain 7* (*myl7*). Shown are ventral views, cranial is to the top. *tbx5a*:GFP^{-} cardiomyocytes can be observed in the distal ventricle. at, atrium; v, ventricle. Scale bar 10 μm.

Supplementary Video 2. Confocal optical sections of 56 hpf *tbx5a*:*GFP*;*drl*:*mCherry* double transgenic zebrafish larvae. GFP (green) labels *tbx5a*$^{+}$ cells, mCherry (red) *drl*$^{+}$ cells and anti-myosin heavy chain (MHC) immunofluorescence all cardiomyocytes. at, atrium; v, ventricle. Scale bar 10 μm.

Supplementary Video 3. Confocal optical sections of 72 hpf *tbx5a*:*GFP*;*drl*:*mCherry* double transgenic zebrafish larvae. GFP (green) labels *tbx5a*$^{+}$ cells, mCherry (red) *drl*$^{+}$ cells and anti-myosin heavy chain (MHC) immunofluorescence all cardiomyocytes. at, atrium; v, ventricle. Scale bar 10 μm.

Supplementary Video 4. Confocal optical sections of 72 hpf *tbx5a*:*GFP* injected with an *ltbp3:mCherry* construct. GFP labels *tbx5a*$^{+}$ cells, mCherry *ltbp3*$^{+}$ cells, and MHC all cardiomyocytes.

Supplementary Video 5. Confocal optical sections of 4 dpf *tbx5a*:*CreER*^{T2};*ubb:loxP-GFP-STOP-loxP-mCherry* treated with 5 μM 4-OHT from 24 to 48 hpf. Recombined cells are shown in red and MHC in green. Note the atria completely recombined. at, atrium; v, ventricle. Scale bar 10 μm.

AGRADECIMIENTOS

AGRADECIMIENTOS

En primer lugar me gustaría agradecer a **Nadia** la posibilidad de trabajar en su laboratorio. Me ha dirigido la tesis de la mejor forma posible: siempre ha estado atenta a cualquier pequeño resultado, para discutirlo, aportar sus ideas y contactar rápidamente con quien fuese necesario. Trabaja con una eficiencia extraordinaria que ha hecho que todo avanzase lo más rápido posible. También le agradezco su preocupación por mi formación, y la oportunidad que me ha dado de conocer muchísima gente. Al mismo tiempo, me ha proporcionado la posibilidad de desarrollar muchas de mis propias ideas. Recuerdo una de nuestras primeras reuniones, cuando yo no estaba muy convencido de querer generar peces transgénicos, en la que ella argumentó lo importante que son para el proyecto. Quizás después de llenar la fish facility de nuevas líneas, aún se esté arrepintiendo de haber sido tan convincente.

Cuando llegué al laboratorio de Nadia, era un laboratorio pequeño, en el que solo estaban Juanma y Marina. Me gustaría agradecer especialmente a **Juanma**. Él puso a punto muchas técnicas que he necesitado para esta tesis, sentó las bases de mi proyecto, me transmitió sus conocimientos, discutimos ideas e hicimos muchas "cosas geniales" juntos. Pero no solo eso, él ha sido un ejemplo a seguir durante mi tesis y un gran amigo. **Marina** me enseñó a hacer *in situs*, *in vivos*, y fue un ejemplo de habilidades sociales haciendo un número increíble de amigos en el CNIC. Después, el grupo fue creciendo, dándome la oportunidad de conocer a **Andrés**, a quien ayudé a convertirse en un experto clonador, pero que finalmente está desarrollando su proyecto principal en peces no transgénicos. Cada llegada suya a Madrid era sinónimo de "scape-room" más cena de grupo.

No sé qué habría hecho sin **María Galardi**. Pocas personas he conocido más eficientes que ella. Sus inmunos, genotipados, minis... han acelerado de manera muy importante el desarrollo de esta tesis, además de ser alguien con quien he compartido muchas conversaciones. También, **Laura**, que resiste con nosotros en Madrid, me ha ayudado durante este tiempo, sobre todo cuando he trabajado con embriones. Finalmente, agradecer al resto del grupo: **Inês**, **Carol**, **María Pérez**, **Xavi, Marcos**, **Alex**, **Ricardo**, **María Lozano**, **Fabian**, **Ronja** y **Jessica**. Aunque la mayoría está en Suiza, con ellos he podido discutir sobre ciencia, me han aportado ayuda con los experimentos que he necesitado, y a la vez he tenido muy buenos momentos.

Un grupo del CNIC que ha sido especialmente importante para mí ha sido el de **Miguel Manzanares**. Entre ellos especialmente **Julio**, un gran amigo desde el máster. Con él he compartido muchos momentos y he tenido una gran discusión científica. Me ha incluido en su día a día, y me ha transmitido una forma distinta de ver la vida. También **Sergio**, quien ha contado conmigo para todos los planes, dentro y fuera del CNIC. Siempre tan amable y correcto en todo momento. **Teresa**, con quien he podido hablar de ciencia muchísimo, y discutir proyectos súper

emocionantes. Con **Melisa** también he podido compartir muchas de mis comidas en el CNIC y partidos de pádel. De **Jesús** me llamó la atención sus buenísimas preguntas en los seminarios desde el primer momento de estar en el CNIC, así como su humor y su forma de afrontar los problemas. Y a todos los demás, con los que he compartido muchísimos momentos, especialmente **Miguel**, **Alba**, **Isa**, **Claudio**, **Mariajo** y **Eva**.

Tampoco olvidaré al resto de amigos que forman parte del grupo "Cambados", con quienes espero que continúe nuestra amistad aunque estemos cada uno en un lugar del mundo. Con **Dani** he podido tener conversaciones muy interesantes de todo tipo y me ha mostrado que después de la tesis hay muchas excelentes alternativas a la investigación. Aún recuerdo la primera vez que vi a **Susana Cañón** en el CNIC justo después de ver a su hermana gemela en el CNIO. Pensaba que me estaba mareando. A ella incluso tengo que agradecerle que antes de conocernos, me diese sus valiosísimos consejos sobre los diferentes grupos del CNIC. En ese momento aún no sabía que se convertiría en una amiga. Y **Cris**, que a pesar de que está lejos ahora, seguro que nos seguiremos viendo y pasándonoslo tan bien como cada vez que organizaba algo en su casa.

También me gustaría agradecer al resto del departamento, en el que todos me han aportado todos los consejos y materiales que he necesitado. Muy especialmente a **Lao** y **Gaetano**, que han generado un muy buen ambiente italiano en el laboratorio. A **Lao**, por hacerme dudar de la señal de cada in situ, aunque la señal fuese clarísima. Y a **Gaetano**, porque podré poner en el currículum que mi bench estaba enfrente del suyo, y que una vez hasta usé su pipeta. A **Irene**, a quien introduje en el mundo del zebrafish durante su Cicerone, y con quien pude tener conversaciones muy interesantes. A la "zebrafish community" del CNIC, entre los que están **Dimitris**, **Bea**, **Juli**, **Dorota** y **Alex**, han compartido conmigo su experiencia, protocolos, y con ellos he podido discutir las mejores formas de realizar los experimentos. Con **Carlos López** pude hablar de temas diferentes a la ciencia. Agradezco muchísimo a **Rui** sus consejos sobre clonajes, y a tantos otros, como **Miguel Torres**, **Silvia**, **Macarena**, **José Antonio**, **Rebeca**, **Briane**, **Patricia Martínez**, **Jesús Gómez Salinero**, **Alberto Roselló**… a quienes siempre recordaré.

Estoy agradecidísimo al servicio de histología, entre ellos **Roisin**, **Antonio de Molina**, **Pedro**, **Noelia**, **Ana**, **Brenda**, **Ainoa**… Sin su apoyo para cortar todos los corazones de esta tesis probablemente aún estaría cortando bloques. A **Edu** y **Antonio**, por ponerme a crecer "peces súper importantes" y cruzarme "peces de líneas super urgentes", sin ellos, no habría podido generar y mantener todas las líneas de peces que he usado en esta tesis. A la unidad de microscopía: **Elvira**, **Antonio**, **Helio** y muy especialmente a **Vero**, quien me ha solucionado todos mis problemas con ImageJ. A **Fátima**, **Carlos** y **Manuel** por enseñarme cómo resolver los diferentes problemas bioinformáticos. A **Gabriela**, **Ana Vanesa**, **Lorena** y **María Villalba** por organizar ecos en poquísimo tiempo. También agradezco a todas las personas que aunque su

trabajo no es hacer experimentos, su labor organizativa es muy importante para nuestro trabajo, entre ellos, **Teresa Casaseca**, **Beatriz Ferreiro**, **Marta Ramón**, **Sandra Cillero**, **Cristina Giménez** y **Susana Negrete**. Y a **Juan Carlos** y **Alicia** por conseguir que mis ordenadores tuviesen todo lo que he necesitado. A **Antonio Ureña** le agradezco su gran preocupación por solucionar los problemas laborales del CNIC de la mejor manera posible. También el resto de unidades del CNIC, incluyendo a **Genómica** y **Celómica**, han sido muy importantes para el desarrollo de esta tesis.

Durante mis dos estancias he sido tratado de una forma excepcional, tanto científicamente como personalmente. **Francisco Azuaje**, me acogió en Luxemburgo, preocupándose totalmente por mí y por mi formación. Y a **Federico Tessadori** le agradezco mucho su ayuda para solucionar mis problemas con las inyecciones, y las discusiones sobre las estrategias más eficientes para modificar genéticamente peces.

A **Luis Torres**, cuyas excelentes clases en la Universidad de Valencia despertaron mi interés por la investigación en Biología y Biología Molecular. A **Juan Carbonell**, **Miguel Ángel Pérez Amador, MD** y **Carolina**, con quien pude tener una primera experiencia en investigación, aunque en este caso fuese de plantas. Se preocuparon de una manera excepcional de que recibiese la mejor formación posible durante el verano que trabajé con ellos. También a **José Horcajadas** y **Estela Cañón**, que me permitieron conocer el CNIC, y con ello, la posibilidad de hacer la tesis en este centro.

También querría recordar a mis amigos de Farmacia, con los que he podido tener conversaciones que no tengan nada que ver con el laboratorio. **Manolo**, **Javi**, **Antonio**, y nuestro "Comunio" en el que siempre pierdo. **Sania** y sus interminables conversaciones por teléfono. Y los "infiltrados" que no estudiaron Farmacia: **Carmen**, **Raúl** y **Juanma**. Y finalmente, a mis amigas de Bioquímica **Blanca**, **Vero** y **Mila**, gracias a quienes me empecé a enterar de cómo funciona la investigación.

Mis amigos de Utiel: **Diego**, **Carlos**, **Víctor** y **José**, que me han acompañado desde que entré en la Universidad. Y a pesar de la distancia, siempre han estado disponibles cada "Low Festival" y cada vez que nos hemos podido ver en Utiel.

Muchas gracias a **Rocío**, por su apoyo durante toda la tesis, desde discutir los proyectos hasta quitar huevos muertos. Por su apoyo incondicional, ayudándome a tomar las decisiones, por preocuparse de mi futuro profesional tanto o más que del suyo. Por preocuparse de las pequeñas cosas a las que no doy importancia, pero que a veces la tienen. Creo que es la única persona del CNIC que entiende los papeles que hay que preparar y entregar para defender una tesis.

A mi hermana **Hortensia**, con quien he podido hablar y pedirle consejo sobre cualquier tema, y a la vez ser una más del grupo de amigos.

Mis **padres** y **abuelos** también han sido muy importantes, al haberme enseñado actitudes que son necesarias para una tesis, entre ellas las de tener paciencia, y a no rendirse fácilmente cuando las cosas no salen bien, en este caso los experimentos. Pero además, por darme su apoyo constante en todos los momentos.

The zebrafish is an established model organism to study heart regeneration, in which pre-existing cardiomyocytes (CMs) proliferate to replace the lost myocardium. During development, mesodermal progenitors from the first heart field (FHF) form a primitive cardiac tube, to which cells from the second heart field (SHF) are added. Here we investigated whether FHF and SHF derivatives in the zebrafish give rise to distinct CM populations, and examined the degree of cell fate plasticity of SHF derivatives during heart regeneration. Using *tbx5a*-lineage tracing we found that the adult zebrafish heart is also composed of CM populations from the FHF and SHF. Furthermore, ablation of FHF-derived CMs in the embryo is compensated by expansion of SHF-derived cells. *tbx5a* lineage-tracing was also employed to investigate the fate of trabecular CMs during adult heart regeneration. While previous clonal analysis suggested that the different myocardial layers are rebuilt by CMs within each layers, we describe that trabecular CMs can switch their fate and differentiate into cortical myocardium. Heart regeneration is preceded by a fibrotic response. Thus, fibrosis and regeneration are not mutually exclusive responses. Upon cardiac cryoinjury, collagen and other extracellular matrix (ECM) components accumulate at the injury site. Unlike the situation in mammals, fibrosis in zebrafish is transient and its regression is concomitant with regrowth of the myocardial wall. We describe that during fibrosis regression, fibroblasts are not fully eliminated and become inactivated. Unexpectedly, limiting the fibrotic response by genetic ablation of *col1a2*-expressing cells not only failed to enhance regeneration but also impaired CMs proliferation. We conclude that zebrafish regeneration is a process that requires CM plasticity, and involves ECM-producing cells that become inactive and promote CMs proliferation.

UAM
UNIVERSIDAD AUTONOMA
DE MADRID

cnic